UNIVERSITÀ
DEGLI STUDI
DI PADOVA

Head Office: Università degli Studi di Padova

Department: Biomedical Sciences

Ph.D. COURSE IN: BIOMEDICAL SCIENCES
SERIES: 36

# INVESTIGATION OF NEURAL CONTROL IN DISUSE AND DISEASE AND DEVELOPMENT OF THE NECESSARY TOOLS

Thesis written with the financial contribution of: Fondazione Cariparo

**Coordinator:** Prof. Fabio Di Lisa
**Supervisor**: Prof. Giuseppe De Vito
**Co-Supervisor**: Prof. Marco V. Narici

**Ph.D. student**: Giacomo Valli

# Contents


Summary ..... 5

1. **Introductory Chapter 1**: Anatomy and Physiology of the Motor Unit ..... 6

1.1. Different Populations of Motoneurons ..... 9

1.2. The Alpha Motoneuron ..... 10

1.3. The Discharge Activity of the Alpha Motoneuron ..... 15

1.4. The Muscle Unit ..... 19

1.5. Motoneuron Electrophysiological Properties Reflect those of the Muscle Unit ..... 22

1.6. The Neuromuscular Junction ..... 24

1.7. The Muscle Action Potential ..... 26

1.8. Plasticity of the Neuromuscular System ..... 28

2. **Introductory Chapter 2**: High-Density Surface Electromyography ..... 30

2.1. Development of High-Density surface Electromyography as a Non-Invasive Tool to Study the Activity of Single Motor Units ..... 31

2.2. Generation of the Interference Electromyography Signal ..... 35

2.3. Decomposition of the Interference Electromyography Signal ..... 38

2.4. Considerations for the Analysis of High-Density Electromyography Recordings ..... 41

2.5. Bipolar Surface Electromyography: Use Cases in the High-Density Electromyography Era. ..... 43

3. **Experimental Chapter 1**: Lower Limb Suspension Induces Threshold-Specific Alterations of Motor Units' Properties that are Reversed by Active Recovery ..... 45

3.1. Background ..... 46

3.2. Abstract ..... 47

3.3. Highlights ..... 48

3.4. Abbreviations ..... 49

3.5. Introduction ..... 50

3.6. Methods ..... 52

3.6.1. Participants and experimental protocol ..... 52

3.6.2. Unilateral lower limb suspension ..... 52

3.6.3. Active recovery ..... 53

3.6.4. Maximal voluntary isometric contraction ..... 53

3.6.5. HD-EMG matrix placement ..... 54

3.6.6. HD-EMG recordings ..... 55

3.6.7. Force and HD-EMG signal analyses ..... 55

3.6.8. MUs tracking and duplicates removal ..... 56

3.6.9. Statistical analysis ..... 59

3.7. Results ..... 60

3.7.1. Participants ..... 60
3.7.2. Maximal voluntary isometric contraction and force control ..... 60
3.7.3. MUs Decomposition and Tracking ..... 61
3.7.4. Total pool of MUs ..... 61
3.7.5. Correlations ..... 65
3.7.6. DR modulation ..... 66
3.7.7. Pool of tracked MUs ..... 66
3.7.8. Summary of MUs properties ..... 68
3.8. Discussion ..... 69
3.8.1. MUs DR is affected by ULLS ..... 69
3.8.2. Reduced DR, but not DR modulation, might be responsible for reduced muscle force ..... 71
3.8.3. Neural control is restored by an active recovery period ..... 72
3.8.4. Methodological considerations ..... 72
3.9. Conclusion ..... 74
3.10. Supplementary Material ..... 75
4. **Experimental Chapter 2**: Non-invasive motor unit analysis reveals distinct neural strategies of muscle force production in young people with uncomplicated type 1 diabetes ..... 84
4.1. Background ..... 85
4.2. Abstract ..... 86
4.3. Highlights ..... 87
4.4. Abbreviations ..... 88
4.5. Introduction ..... 89
4.6. Methods ..... 91
4.6.1. Participants and experimental protocol ..... 91
4.6.2. Body composition, maximal oxygen consumption and voluntary isometric torque ..... 91
4.6.3. High-Density EMG recordings ..... 92
4.6.4. Torque and High-Density EMG analysis ..... 93
4.6.5. Muscle sampling, myosin heavy-chain isoforms and gene expression analysis ..... 94
4.6.6. Statistical analysis ..... 95
4.7. Results ..... 97
4.7.1. Participants characteristics ..... 97
4.7.2. Motor units' properties ..... 98
4.7.3. MyHC proteins and mRNAs ..... 101
4.8. Discussion ..... 103
4.8.1. Neural control of force production ..... 103
4.8.2. Differences in neural control are detectable before functional manifestation ..... 106

4.8.3. Methodological considerations ..... 107
4.8.4. Final considerations and future perspectives ..... 107
5. **Experimental Chapter 3**: Tutorial: a step-by-step guide to the analysis of central and peripheral motor unit properties from High-Density Electromyography with *openhdemg* ..... 109
5.1. Background ..... 110
5.2. Abstract ..... 111
5.3. Highlights ..... 112
5.4. Abbreviations ..... 113
5.5. Introduction ..... 114
5.6. Lowering the barriers to the use of HD-sEMG with *openhdemg* ..... 116
5.7. Fundamentals of HD-sEMG signal acquisition and decomposition ..... 119
5.7.1. Signal acquisition ..... 119
5.7.2. Signal decomposition ..... 120
5.8. Load the decomposed HD-sEMG file in a working environment ..... 123
5.9. Visualization, inspection and processing of decomposition outcome ..... 125
5.10. Discard unwanted MUs based on objective criteria ..... 128
5.11. Track MUs within and between recording sessions ..... 131
5.12. Analyse central MUs properties. ..... 134
5.13. Analyse peripheral MUs properties ..... 136
5.14. Final remarks and conclusions ..... 139
6. **General discussion** ..... 140
6.1. Altered neuromuscular function: a common outcome of Muscle disuse and type 1 diabetes ..... 141
6.2. Discharge rate as an indicator of the neural condition ..... 142
6.3. Challenges and solutions for the widespread adoption of HD-EMG ..... 144
7. **Future perspectives** ..... 146
7.1. Muscle disuse ..... 146
7.2. Type 1 diabetes ..... 148
7.3. openhdemg ..... 149
Glossary ..... 151
References ..... 154

## Summary

The motor unit (MU) is the basic functional component of the neuromuscular system and consists of an alpha motoneuron, its axon, and all the muscle fibres it innervates (Sherrington, 1925). The MU acts as a neuromechanical transducer and plays a pivotal role in generating muscle contractions by converting descending neural inputs into muscle forces (Heckman & Enoka, 2012). The conversion of the electrical current traveling in the motoneuron into a depolarisation stimulus in the muscle fibres is performed at the level of the neuromuscular junction that, given its functional stability (safety factor), usually results in a one-to-one relationship between the discharges of a motoneuron and the transduced signal that propagates into the muscle (Wood & R. Slater, 2001; Duchateau & Enoka, 2011). Therefore, a motoneuron and the innervated muscle fibres normally function as a single entity, with the motoneuron's action potentials directly reflected in muscle fibres' action potentials. This fundamental principle made of the motoneuron the only neural cell that can be studied in humans with non-invasive techniques (Farina *et al.*, 2004). Currently, High-Density surface Electromyography (HD-EMG) is considered the preferred non-invasive tool for the investigation of how the CNS controls voluntary movements in humans (Farina *et al.*, 2016) and how it adapts to different conditions (Gallego *et al.*, 2015*a*; Martinez-Valdes *et al.*, 2018*a*; Valli *et al.*, 2023).

In the two introductory chapters of this thesis, I will discuss the anatomical and physiological fundamentals of the MU and its components, as well as the principles and evolution of the HD-EMG technique. This comprehensive understanding will lay the groundwork for the following three experimental chapters investigating the physiological adaptation of neural control to disuse and disease, and proposing technical advancements to the HD-EMG technique.

## 1. **Introductory Chapter 1**: Anatomy and Physiology of the Motor Unit

At the beginning of the 20th century, Sir Charles Sherrington introduced the concept of the "motor unit" (MU) as a fundamental functional element in muscular action (Sherrington, 1925). Sherrington defined the MU as the "motoneuron axon and its adjunct muscle-fibres," emphasizing the inseparable link between the alpha motoneuron and the muscle fibres it innervates (Liddell & Sherrington, 1925). This notion became a cornerstone in understanding the organization of the motor system and the neural control of movement.

Within the muscle, each alpha motoneuron branches out and forms synapses with multiple muscle fibres distributed over the muscle area. This intricate network of connections ensures even force distribution throughout the muscle and serves as a protective mechanism to reduce the risk of significant muscle impairment in case of damage to a single or few motoneurons (Purves *et al.*, 2001*a*).

Originally, Sherrington assumed that each motor axon spike would result in the activation of every muscle fibre within a MU, resulting in uniform mechanical action. He also postulated that a given muscle fibre belongs to only one MU, with little or no polyneuronal innervation (Sherrington, 1925). Subsequent research has supported these assumptions, demonstrating that neuromuscular transmission is generally reliable, albeit occasional activation failures have been observed in vitro (Burke, 1981). Similarly, adult healthy muscles typically exhibit little or no polyneuronal innervation of individual muscle fibres (Feindel *et al.*, 1952; Brown & Matthews, 1960). Thus, the coupling between motoneuron and the innervated muscle fibres is functionally reliable and anatomically exclusive in healthy adult muscles. However, exceptions to these principles can be observed during the innervation/reinnervation processes typically occurring during development (Redfern, 1970; Bagust *et al.*, 1973) or during aging and in some neuromuscular diseases (Slack *et al.*, 1979; Gordon *et al.*, 2004).

MUs can be categorized based on size and functional properties. In a simplistic view, small alpha motoneurons innervate relatively few muscle fibres, forming slow MUs composed of small "red" muscle fibres that contract slowly and are resistant to fatigue (Purves *et al.*, 2001*a*, 2001*b*). In contrast, larger alpha motoneurons innervate larger, pale muscle fibres, forming fast fatigable MUs. These MUs generate greater force but are prone to fatigue (Purves *et al.*, 2001*a*). A third category, fast fatigue-resistant MUs, lies between slow and fast fatigable units, exhibiting intermediate properties (Purves *et al.*, 2001*a*).

The different characteristics of various motoneurons and muscle fibres suggest that different tasks will involve different MUs. Indeed, slow MUs are more suitable for long-lasting low intensity tasks, as these MUs are capable of maintaining their discharge activity over long periods, although they cannot produce elevated force. Differently, when faster and more intense contraction tasks are required, it is necessary to recruit fast fatigue-resistant and fast fatigable MUs that are capable of greater speed of contraction and force generation capacity.

The physiological rules defining the strategy used by the nervous system to take advantage of the specific properties of the different MUs were depicted by Henneman and Mendell in the 1960s with a series of articles introducing and explaining the so called 'Size principle' (Mcphedran *et al.*, 1965; Wuerker *et al.*, 1965; Henneman & Olson, 1965; Henneman *et al.*, 1965*a*, 1965*b*).

According to the size principle, small MUs, which consist of smaller alpha motoneurons and innervating slow-twitch muscle fibres, are recruited first during low-intensity tasks. That is because slow-twitch muscle fibres are resistant to fatigue and are suited for sustained, low-force activities. As the force requirements of a task increase, larger MUs, which consist of larger alpha motoneurons and innervate fast-twitch muscle fibres, are progressively recruited. Fast-twitch muscle fibres can generate more force but fatigue more quickly than slow-twitch fibres (Mendell, 2005*a*).

The size principle ensures that MUs are activated in a graded and sequential manner, allowing for smooth and coordinated muscle contractions. This recruitment pattern is grossly managed by the central nervous system via modulation of the synaptic input (Enoka & Duchateau, 2017) to match the force requirements of different motor tasks but, as described in the next paragraphs, it is fine-tuned by the intrinsic properties of the motoneurons membrane (Heckman & Enoka, 2012).

By adhering to the size principle, the nervous system optimizes muscle performance, minimizes unnecessary energy expenditure, and allows for precise control over muscle force production during various activities.

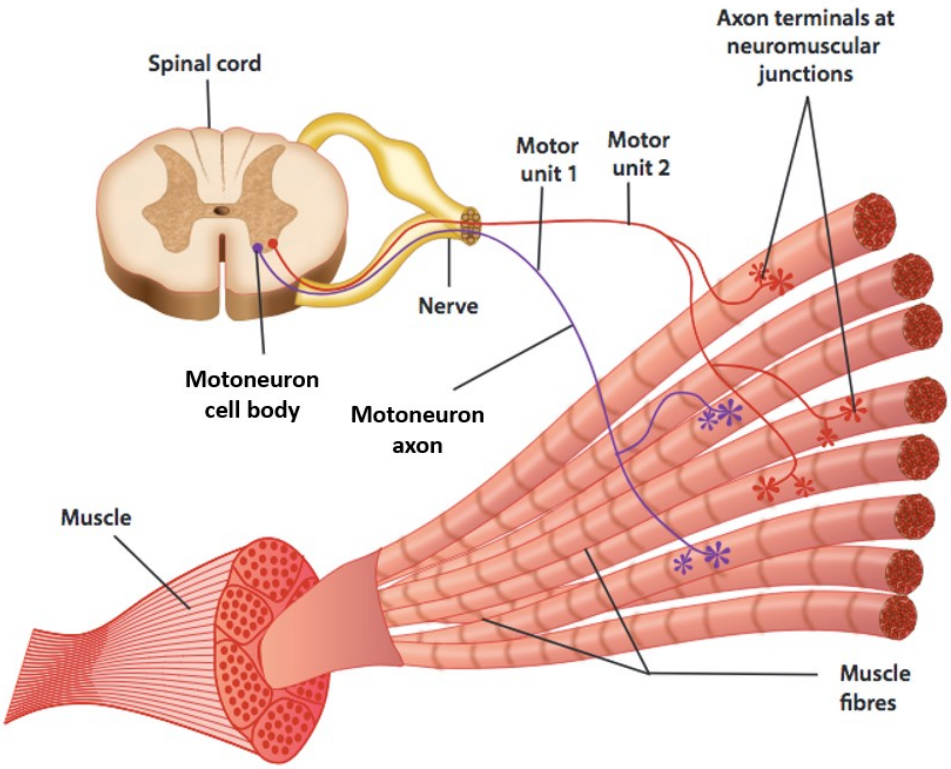


*Figure 1-1: The motor unit, the functional unit of the neuromuscular system, comprises an alpha motoneuron and the muscle fibres it innervates. The alpha motoneuron originates from the spinal cord and extends its axon through the peripheral nerves to reach the target muscle. At the neuromuscular junction, the axon terminal forms specialized synapses with individual muscle fibres. Each motor unit consists of a single alpha motoneuron branching to innervate multiple muscle fibres, forming a precise and coordinated neuromuscular interface.*
*Figure adapted from https://github.com/iandanforth/pymuscle*

## 1.1. Different Populations of Motoneurons

The motoneuron should not be considered as a standard cell or structure. Indeed, different types of motoneurons have been identified over the years and have been categorised in at least two distinct populations, the alpha and gamma motoneurons (Manuel & Zytnicki, 2011). Although today we distinguish these motoneurons based on their function, their discovery was based on the observation of different structural and functional aspects.

The journey to uncovering alpha and gamma motoneurons can be traced back to the discovery of muscle spindles in frogs (Kolliker A, 1862) and mammals (Kuhne, 1863) in the 19$^{th}$ century. These muscle spindles presented a bundle of thin muscle fibres, distinct from the ordinary muscle fibres. Further investigation revealed that the largest motor axons innervate the ordinary muscle fibres, while the smallest axons are specifically innervating intrafusal muscle fibres within the muscle spindle. Additionally, electrophysiological investigations demonstrated that smaller motor axons with high electrical threshold conduct action potentials at slower velocities than large motor axons with low electrical threshold (Manuel & Zytnicki, 2011).

These smaller motoneurons, innervating the muscle spindle were named gamma motoneurons (Leksell, 1945). Gamma motoneurons maintain the sensitivity of muscle spindles, which are specialized sensory receptors embedded within the muscle. The muscle spindles provide essential proprioceptive feedback, informing the nervous system about muscle length and changes in muscle length during movement (Santuz & Akay, 2023).

Differently, the large motoneurons innervating muscle fibres were named alpha motoneurons (Erlanger *et al.*, 1926). Alpha motoneurons are responsible for directly controlling the contraction of skeletal muscles. When activated, alpha motoneurons send signals to the extrafusal muscle fibres, causing them to contract and generate force. These muscle contractions are what produce the voluntary movements and actions of the body.

As a final note, experiments in animals identified also a third population of motoneurons, the beta motoneurons, which innervate both the intrafusal and extrafusal muscle fibres. However, their presence and relevance in humans is not well known (Manuel & Zytnicki, 2011).

Given the topic of this thesis, we will only focus on the alpha motoneuron from now on, as this is the only population of motoneurons that can be investigated with High-Density surface Electromyography (HD-EMG).

## 1.2. The Alpha Motoneuron

The alpha motoneuron is also referred to as the final common pathway in the nervous system because it is the ultimate connection point where voluntary motor commands from the brain converge to produce muscle contractions (Heckman & Enoka, 2004). As the ultimate convergence point for voluntary motor commands from the brain, the alpha motoneuron integrates and processes various inputs before transmitting the resulting signals to the muscles it innervates. Far from being a simple signal conduit, the alpha motoneuron is a sophisticated structure with multiple mechanisms that enable it to finely tune and modulate incoming signals (Manuel & Zytnicki, 2011). This intricate integration of inputs allows for precise and coordinated muscle responses, making of the alpha motoneuron an essential component of motor control.

The activity of the alpha motoneuron is governed by the all-or-none principle, which means that it either fires at its full potential or not at all (Rosenblueth, 1935). When the motoneuron receives a strong enough signal from the brain or other neural circuits, it generates an action potential that propagates along its axon to the neuromuscular junction, where it releases neurotransmitters, specifically acetylcholine, leading to muscle contraction (Tintignac *et al.*, 2015). The all-or-none concept in motoneurons contrasts with the graded response observed in the entire muscle. Unlike the motoneuron, which either fires maximally or remains silent, the force produced by the entire muscle can vary and be finely adjusted. This graded response is achieved through the recruitment of multiple selected motoneurons and by modulation of their discharge frequency (Mendell, 2005*a*).

The integration of all the inputs received by the motoneuron and the transmission of the resulting signal to the muscle depend on the activity of various ion channels that regulate the membrane potential of the motoneuron and govern the generation of action potentials. These ion channels are critical components distributed throughout the motoneuron's three distinct regions, each characterised by unique properties and functions (Heckman & Enoka, 2012).

1- Dendrites: The dendrites constitute the larger portion of the motoneuron and are responsible for receiving numerous synaptic inputs from other neurons. These inputs arrive at synapses distributed throughout the dendritic tree, allowing the motoneuron to integrate information from multiple sources. Dendritic ion channels play a crucial role in shaping the incoming signals, enhancing synaptic currents, and contributing to the overall excitability of the cell (Cullheim *et al.*, 1987).

2- Soma: The soma, or cell body, and the axon initial segment are involved in the generation of action potentials. Here, a dense concentration of voltage-gated ion channels, such as sodium ($Na^+$), potassium ($K^+$) and calcium ($Ca^{2+}$) channels, enables the initiation and propagation of action potentials along the axon. The unique arrangement of these ion channels allows for the rapid and efficient transmission of electrical signals from the cell body to the axon terminals (Rekling *et al.*, 2000).

3- Axon: The axon serves as the communication channel, transmitting action potentials over long distances from the motoneuron's cell body to the neuromuscular junction. Along the axon, voltage-gated ion channels, predominantly Na and K channels, play a fundamental role in the action potential's propagation. The myelination of the axon facilitates saltatory conduction, increasing the speed of signal transmission and conserving energy (Black *et al.*, 1990).

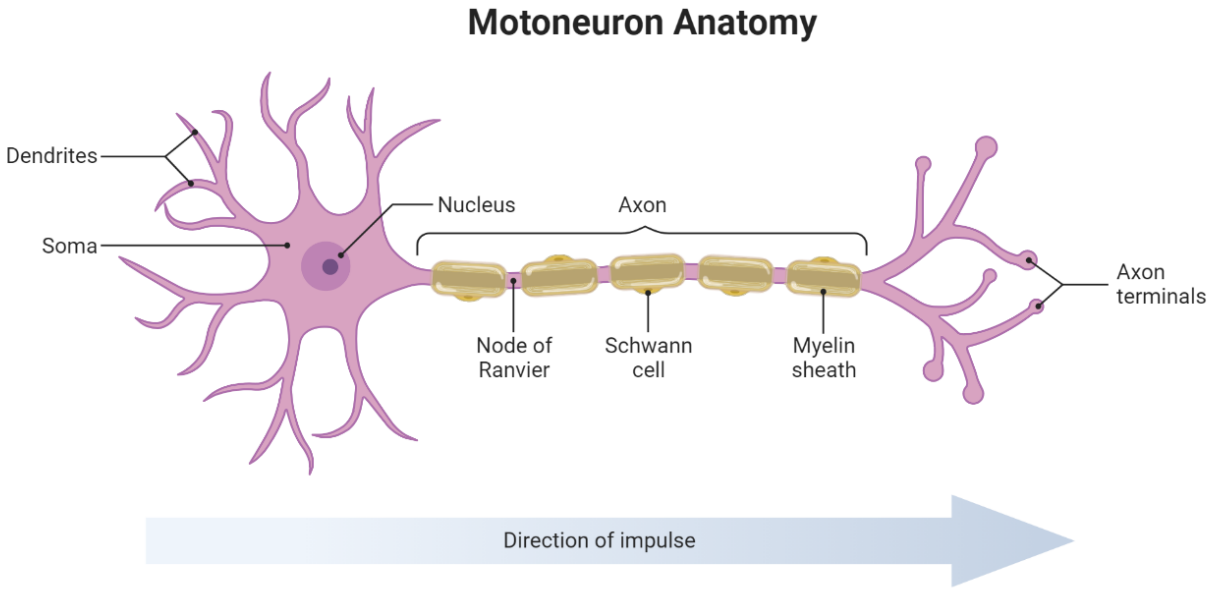


*Figure 1-2: This figure illustrates the structure of a motoneuron, the specialized nerve cell responsible for transmitting motor commands from the central nervous system to muscle fibres. The motoneuron comprises three main regions: the dendrites that receive incoming signals, the cell body (soma) that integrates these signals, and the axon, which transmits the processed signals to the muscle fibres. Along the axon, Schwann cells provide myelin sheaths, facilitating saltatory conduction, a process where action potentials "jump" from one node of Ranvier to another, allowing for faster and more efficient signal transmission.*
*Figure from https://www.biorender.com*

The channels present on the motoneurons' membrane can be classified in four major types based on their function and, consequently, on their distribution over the motoneuron membrane (Hille, 2001). These major types are i) leak channels, ii) Ionotropic synaptic channels, iii) voltage-gated channels and iv) metabotropic receptors (Grillner, 2003).

At rest, the membrane potential of motoneurons is primarily regulated by the leak channels present on the motoneuron's dendrites, which allow the passage of $K^+$ ions. This sets the membrane resting potential very close to the equilibrium potential of $K^+$ ions to around -70 mV. However, the resting potential is not a fixed parameter, as it can be modified by tonic synaptic input. Neuromodulators, such as serotonin and norepinephrine, play a crucial role in this process via metabotropic receptors by depolarizing the resting potential and increasing the motoneuron's input resistance (Heckman & Enoka, 2004). In neurons, the input resistance refers to how easily the cell's membrane potential changes in response to incoming electrical signals (current) (Hille, 2001). When the input resistance is high, the membrane is less permeable to ions and small amounts of current can cause larger changes in the membrane potential. Conversely, when the input resistance is low, the membrane is more permeable to ions and larger amounts of current are needed to produce significant changes in the membrane potential (Heckman *et al.*, 2009). These neuromodulatory actions fine-tune the excitability of motoneurons and adapt them to different physiological contexts (Heckman & Enoka, 2012).

Ionotropic synaptic channels play a crucial role in the alpha motoneuron by mediating synaptic transmission from other neurons onto the motoneuron. These channels are also known as ligand-gated channels because their activation depends on the binding of specific neurotransmitters, such as glutamate (excitatory) and glycine or GABA (inhibitory), to their corresponding receptors on the motoneuron's membrane (Grillner, 2003). Obviously, the alpha motoneuron receives inputs from various sources, including sensory neurons, interneurons, and higher brain centres, that converge onto its dendrites. When a presynaptic neuron releases neurotransmitters, they diffuse across the synaptic cleft and bind to the ligand-gated channels on the postsynaptic alpha motoneuron. The binding of neurotransmitters causes these ionotropic channels to open or close, leading to changes in the motoneuron's membrane potential, which might reach a critical threshold. The change in the membrane potential leading to depolarization is termed the excitatory post-synaptic potential, and the resulting current flow is known as the excitatory post-synaptic current. On the other hand, the change in the membrane potential leading to hyperpolarization is termed inhibitory post-synaptic potential, and the resulting current flow is known as the inhibitory post-synaptic current. Inhibitory channels are selective for chloride and $K^+$ ions, with a reversal potential around -80 mV, which makes them responsible for the motoneuron hyperpolarization (Coombs *et al.*, 1955).

Voltage-gated channels respond to changes in the membrane potential of the motoneuron and play a fundamental role in generating and propagating action potentials. When the alpha motoneuron receives excitatory inputs from other neurons through ionotropic synaptic channels, the net depolarization of the membrane may reach a critical threshold. This threshold potential is the minimum voltage required to activate the voltage-gated channels and trigger an action potential. There are several types of voltage-gated channels in the alpha motoneuron, including (Grillner, 2003):

- Voltage-gated $Na^+$ channels: These channels open rapidly in response to a depolarization above the threshold. When they open, they allow an influx of $Na^+$ ions into the cell, causing a rapid and massive depolarization responsible for the rising phase of the action potential. This depolarization propagates along the axon of the motoneuron.
- Voltage-gated $K^+$ channels: These channels also respond to depolarization, but they open more slowly than sodium channels. Once open, they allow an efflux of $K^+$ ions out of the cell, leading to repolarization of the membrane potential. This is the falling phase of the action potential. The channels involved in the efflux of $K^+$ ions to repolarise the cell are named Hodgkin–Huxley K channels (Schwiening, 2012), which differentiate from $Ca^{2+}$-mediated $K^+$ channels that are instead responsible for the long-lasting afterhyperpolarization that occurs after each action potential (in this case, the $Ca^{2+}$ that enters the cell via voltage-sensitive $Ca^{2+}$ channels during the action potential activates the $Ca^{2+}$-sensitive $K^+$ channels, which hyperpolarise the cell) (Barrett *et al.*, 1980).
- Voltage-gated $Ca^{2+}$ channels: These channels are primarily found in the axon terminal of the alpha motoneuron, where they play a critical role in neurotransmitter release. When the action potential reaches the axon terminal, voltage-gated $Ca^{2+}$ channels open, allowing $Ca^{2+}$ ions to enter the cell. This influx of $Ca^{2+}$ triggers the fusion of synaptic vesicles containing neurotransmitters with the presynaptic membrane, leading to the release of neurotransmitters into the synaptic cleft.

The opening and closing of these voltage-gated channels create a rapid change in the alpha motoneuron's membrane potential, leading to the generation and propagation of action potentials along the axon. Once initiated, the action potential travels down the axon to the neuromuscular junction, where it triggers the release of acetylcholine, a neurotransmitter that activates the muscle fibres and leads to muscle contraction (Tintignac *et al.*, 2015).

Unlike ionotropic synaptic channels that directly regulate ion flow through the cell membrane upon neurotransmitter binding, metabotropic receptors exert their effects indirectly through intracellular signalling pathways. When neurotransmitters bind to metabotropic receptors on the alpha motoneuron's membrane, it initiates a series of intracellular signalling events mediated by G proteins. These signalling pathways can modulate the activity of ion channels, including both ionotropic synaptic channels and voltage-gated channels, as well as other cellular processes. Metabotropic receptors provide a mechanism for neuromodulation, allowing the alpha motoneuron to fine-tune its response to synaptic inputs and adapt its excitability based on the overall state of the nervous system. This modulation can occur in various ways (Heckman & Enoka, 2012):

- Potentiation or Inhibition of Synaptic Inputs: Activation of metabotropic receptors can enhance or suppress the effects of ionotropic synaptic channels. For example, activation of certain metabotropic receptors may lead to increased neurotransmitter release from presynaptic terminals, resulting in stronger excitatory or inhibitory synaptic responses in the alpha motoneuron.
- Modulation of Voltage-Gated Channels: Metabotropic receptors can also influence the activity of voltage-gated channels, altering the threshold for action potential generation or affecting the kinetics of channel opening and closing. This modulation can impact the firing properties of the alpha motoneuron and its responsiveness to incoming signals.
- Long-Term Effects on Synaptic Plasticity: Activation of metabotropic receptors can initiate signalling cascades that lead to changes in the strength and efficacy of synaptic connections over time. These long-term effects on synaptic plasticity play a crucial role in learning and memory processes within the motor system.
- Regulation of Cellular Excitability: The activation of metabotropic receptors can lead to the opening or closing of ion channels that regulate the resting membrane potential of the alpha motoneuron. This can affect the overall excitability of the cell and its ability to generate action potentials in response to synaptic inputs.

## 1.3. The Discharge Activity of the Alpha Motoneuron

Once the membrane potential of the alpha motoneuron reaches the critical threshold (usually around -50/-55 mV), the opening of the voltage-gated Na+ channels causes a rapid depolarization that originates the action potential. The stimulus that drives the depolarisation of the membrane can be summarised as the current flow from the dendrites to the soma, which is also named synaptic input (Farina & Negro, 2015). Increasing the synaptic input (represented by the current intensity in Fig. 1-3), the frequency of generation of the action potential increases, more or less linearly, with the magnitude of the synaptic input. This relationship between the magnitude of the synaptic input and the discharge rate (DR) has been defined as the input-output functions of mammalian motoneurons, which describes the basic behaviour of the motoneuron discharge activity (Powers & Binder, 2001) (Fig. 1-3).

This increase in discharge frequency is driven by the mounting synaptic input, which heightens the excitability of the motoneuron by bringing its membrane potential closer to the action potential firing threshold (Heckman & Enoka, 2004). It is important to note that the afterhyperpolarization phase remains a part of this process. However, due to the proximity of the membrane potential to the firing threshold, the resulting afterhyperpolarization phase exhibits a diminished magnitude and duration (Heckman & Enoka, 2004). Consequently, the afterhyperpolarization does not limit the increase in motoneuron DR (at least in healthy people), becoming less and less relevant at higher levels of synaptic input, where also random synaptic noise might be sufficient to initiate motoneuron action potentials (Matthews, 1996).

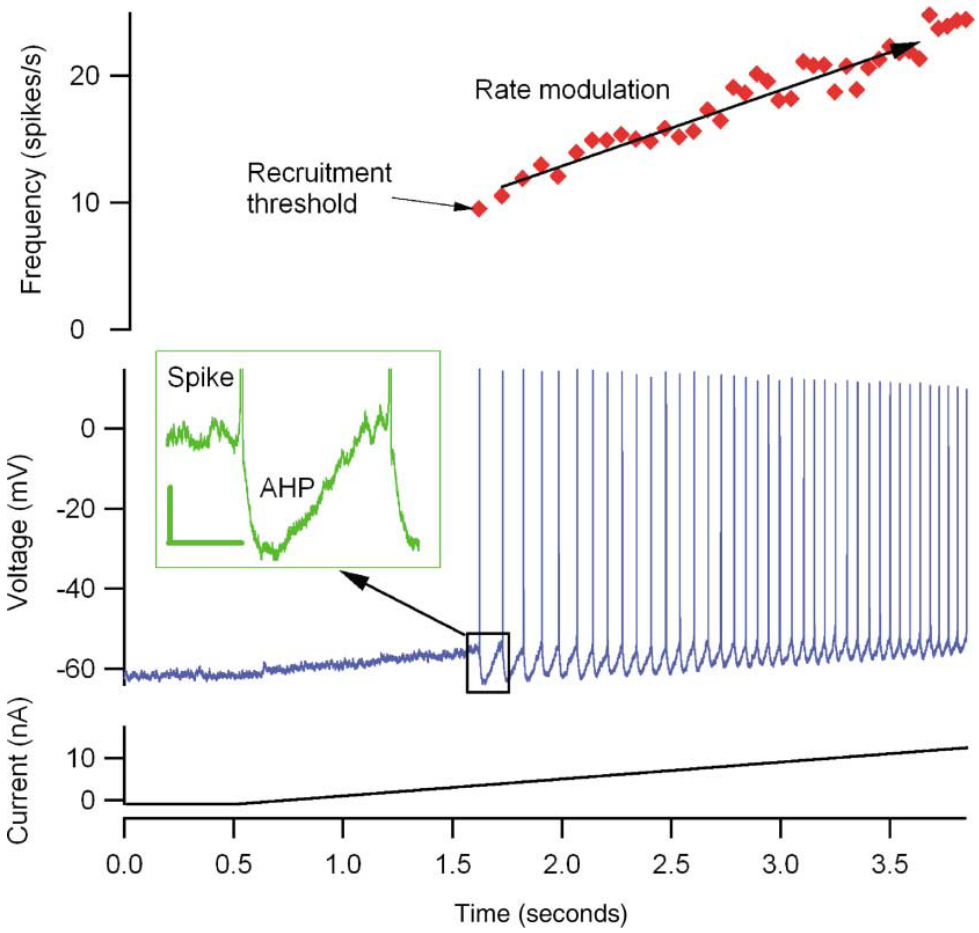


*Figure 1-3: Increasing current in a motoneuron above its threshold (recruitment) generates progressively increasing frequencies of firing (rate modulation). The bottom trace shows the current injected into the motor neuron via the microelectrode. The middle trace shows the firing response of the cell, with the inset illustrating that the afterhyperpolarization determines the time of occurrence of each action potential (spike). The upper panel shows instantaneous firing rate for the spikes in the middle panel. Note the overall increase is approximately linear, so that the relation between frequency and current is also linear. Figure from* (Heckman & Enoka, 2004).

Each motoneuron's input/output response is characterised by a specific slope (Fig. 1-4), which reflects the gain of the motoneuron (in terms of DR) to the synaptic input, and is associated to the electrical properties of the motoneuron membrane (Powers & Binder, 2001).

Similarly, also the recruitment threshold of a motoneuron, defined as the magnitude of net synaptic input that is necessary to induce the generation of an action potential, depends on the electrical properties of the motoneuron membrane.

The input-output function of the motoneurons is a bit more complex when compared across different types of alpha motoneurons. Indeed, motoneurons with different recruitment thresholds, present slightly different input-output functions (Fig. 1-4).

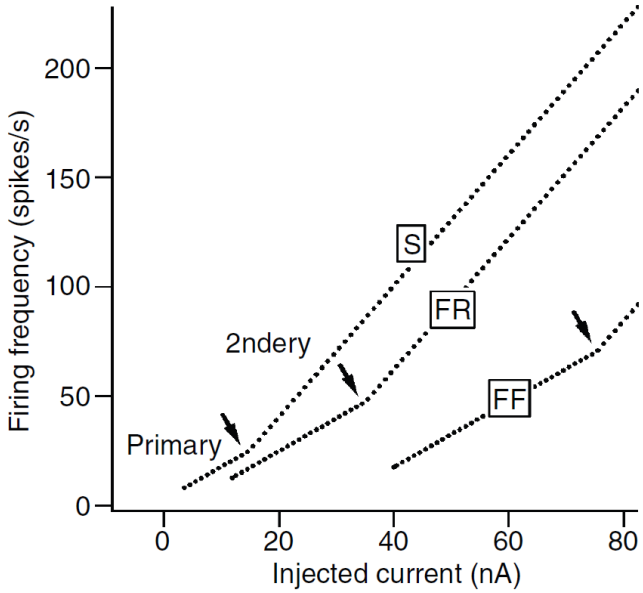


*Figure 1-4: Summary of frequency-current relations in slow (S), fast fatigue-resistant (FR), and fast fatigable (FF) motoneurons generated by linearly increasing injected currents. Different motoneurons exhibit a wide 10-fold range in recruitment threshold, primarily influenced by their size. Additionally, the input-output function displays a transition from a primary to a secondary range, attributable to persistent inward currents that enhance synaptic input and discharge response. Results are based on simulations. Figure from* (Heckman & Binder, 1991).

As shown in Fig. 1-4, the amount of current required to reach the recruitment threshold for different motoneurons has a very wide range of about 10-fold or more (Heckman & Binder, 1991), and the response of each motoneuron to the current above the critical depolarisation threshold depends on its recruitment threshold.

The 10-fold difference in recruitment threshold of different motoneurons is mainly attributable to the size of the motoneuron, which is a primary determinant of motoneuron input conductance and of the current required to reach the critical threshold (Henneman & Mendell, 1981; Binder *et al.*, 1996). This 10-fold difference in recruitment threshold allows to define the order of recruitment of the different motoneurons without the need for explicit computation by higher brain centres, thus making of the size principle a very efficient mechanism for coordinating motoneuron activation (Heckman & Binder, 1993). Together, the threshold and gain of the input-output function characterize the intrinsic excitability of the motoneuron (Heckman & Enoka, 2004).

Additionally, we can also observe that the input-output function of the motoneurons is not completely linear, but presents a transition from a primary range slope to a secondary range (Fig. 1-4). This transition is likely attributable to the activation of persistent inward currents that amplify the synaptic input and the discharge response of the motoneuron (Heckman & Enoka, 2012). The separation of two distinct range allows for precise control of muscle force, in the primary range, and

for the maximisation of muscle force production in the secondary range (Powers & Heckman, 2017; Binder *et al.*, 2020).

Persistent inward currents are a type of voltage-dependent $Na^+$ and $Ca^{2+}$ currents that inactivate slowly (Heckman *et al.*, 2008). In motoneurons, persistent inward currents are mainly generated in dendritic areas and, therefore, these can directly influence the synaptic input. Persistent inward current are particularly important for the amplification of the synaptic input and for saturation/rate limiting, and prolongation/hysteresis of the motoneuron firing (Heckman & Enoka, 2012). Persistent inward currents are mainly influenced by serotonin and norepinephrine, and can induce up to fivefold amplification of ionotropic inputs, thus having an enormous impact on input-output gain of the motoneuron (Hultborn, 2002; Binder, 2003; Heckman *et al.*, 2005).

Overall, the alpha motoneurons exhibit a wide range of electrical properties that profoundly influence their excitability and functional capabilities. To better understand these properties, researchers have categorized motoneurons into different types based on their firing characteristics. Among different classifications, the prevailing taxonomy categorizes motoneurons into three primary types: slow, fast fatigue-resistant, and fast fatigable. These categories closely align with the specific muscle unit properties (Kernell, 2006) as discussed in the paragraph 'The Muscle Unit'. This classification provides valuable insights into how motoneurons contribute to motor control and muscle performance.

## 1.4. The Muscle Unit

The group of muscle fibres innervated by a given motoneuron are commonly referred to as the muscle unit, a term indicating that all the innervated muscle fibres act as a single functional unit (Heckman & Enoka, 2004).

Muscle fibres are far from being a homogenous population. Indeed, they display a remarkable variety of biochemical and contractile properties (Bączyk *et al.*, 2022). The early observation that some muscles appeared redder than others in rabbits and other animal models, with this difference in colour correlating with contraction speed, was a crucial milestone in understanding this diversity (Ranvier, 1873; Needham, 1926). Subsequent investigations based on myosin ATPase activity and enzymatic analysis further revealed that muscle fibres could be grouped into three main categories: slow-twitch oxidative or type I fibres, fast-twitch oxidative glycolytic or type IIA fibres, and fast-twitch glycolytic or type IIB fibres (Brooke & Kaiser, 1970).

Type I fibres are characterized by their slow contraction speed and abundant oxidative enzymes, allowing them to sustain long-duration energy demands, resulting in high resistance to fatigue. In contrast, type IIA fibres, also possess good resistance to fatigue, although to a lesser extent than type I fibres but with greater contraction speed. Lastly, type IIB fibres, are characterized by a poor oxidative enzyme content, making them more prone to fatigue, but capable of high contraction speed (Schiaffino & Reggiani, 2011).

Interestingly, all muscles throughout the body consist of a mosaic of muscle fibres types, but the proportion of each type varies according to the muscle's function (Ariano *et al.*, 1973). For instance, postural muscles tend to contain a higher concentration of slow (Type I) muscle fibres, while flexor muscles tend to have more Type II fibres. This diversity is essential to generate a vast repertoire of movements and behaviours with a finite number of muscles (Bączyk *et al.*, 2022).

Importantly, Edström and Burke demonstrated that also MUs are homogenous in terms of muscle fibre types they contain and that their contractile properties match the contractile properties of the fibres (Edström & Kugelberg, 1968).

Through elegant in vivo experiments in the rat tibialis anterior, they established correlations between the physiological properties of MUs and the histochemical profiles of their muscle fibres. By stimulating a single MU and examining the depletion of glycogen in muscle fibres, three types of MUs were identified: slow MUs, comprising type I fibres and highly resistant to fatigue; fast fatigue-resistant MUs, composed of type 2A fibres and developing more force than slow MUs but less

fatigue-resistant than type slow; and fast-fatigable MUs, consisting of type 2B fibres, capable of developing the greatest amount of force but highly fatigable (Edström & Kugelberg, 1968; Burke *et al.*, 1971).

In the late 90s, a notable shift occurred in muscle fibre typing, with the adoption of monoclonal antibodies targeting various isoforms of the myosin heavy-chain protein (Bączyk *et al.*, 2022). While type I, IIA, and IIB fibres were associated with distinct myosin heavy-chain isoforms (myosin heavy-chain I, 2A, and 2B, respectively) also a new isoform, named 2X was identified (Schiaffino *et al.*, 1989). This approach has been applied across diverse vertebrates demonstrating that the diversity in muscle fibres is highly conserved (Bączyk *et al.*, 2022), with the exception that myosin heavy-chain 2B isoform is absent in humans, with expression limited to the isoforms I, IIA and 2X (Smerdu *et al.*, 1994).

As a final remark, the contractile properties of the muscle unit act as a filter on the almost linear input-output function of the motoneuron, resulting in a sigmoidal relationship between motoneuron DR and muscle force (as shown in Fig 1-5) (Heckman & Enoka, 2004). As the motoneuron's DR increases, the contractile force of the muscle unit enters a range of more or less linear increase, progressively leading to greater force output. However, this linear relationship reaches a threshold when the muscle achieves a tetanic contraction. Beyond this point, further increases in DRs do not translate into higher contractile force (Heckman & Enoka, 2004). It's important to note that the slope of this relationship varies between slower and faster muscle units, but the sigmoidal behaviour remains consistent. This fundamental concept enables us to fully understand the mechanical integration between neural signalling and muscle contraction, which becomes evident in HD-EMG recordings.

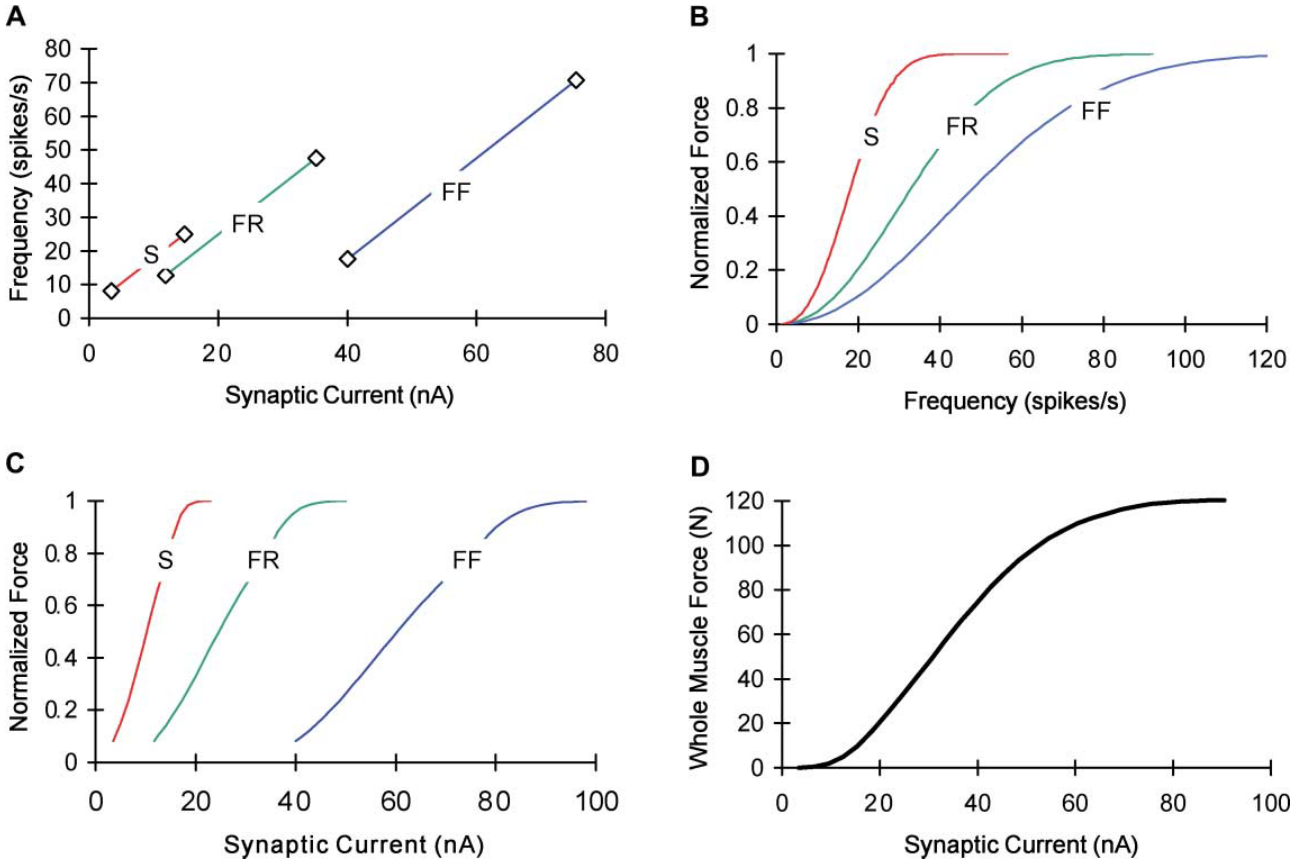


*Figure 1-5: Computer simulations of the input–output relations for the pool of motor units that innervate a single muscle. (A) The input–output relations (frequency–current) for the motor neurons. (B) The input–output relations (force–frequency) for the muscle units. (C) The input–output relations (force–current) for the motor units. (D) The input–output relation (force–current) for the entire motor unit pool. S, slow; FR, fast fatigue-resistant; FF, fast fatigable.*
*Figure and caption from* (Heckman & Enoka, 2004).

## 1.5. Motoneuron Electrophysiological Properties Reflect those of the Muscle Unit

In this introductory chapter 1, we often discussed about the relationship between the properties of the motoneuron and those of the muscle unit. In this section, we aim to further expand on this idea, explaining why the properties of the motoneuron must precisely match those of the muscle unit. This concept has fundamental implications in the use of HD-EMG, as with this technique we aim to infer the properties of the motoneuron by recording the electrical signal at the muscle level.

From the theoretical point of view, the specialisation of the muscle fibres in each muscle unit requires the innervation from motoneurons with compatible discharge characteristics. In practice, this is fundamental to take full advantage of their contraction capabilities (Bączyk *et al.*, 2022).

As previously discussed, type I fibres (in slow MUs) are most suitable during low-intensity contractions and should be recruited before type IIA and IIX fibres (in fast fatigue-resistant and fast fatigable MUs), following the Henneman's size principle (Mendell, 2005*a*). The motoneurons innervating slow MUs are small and have fewer dendrites, while those innervating faster MUs are larger and possess many long dendrites. The size of the motoneuron soma and the extension of the dendritic branches determines the input conductance, which is lower in smaller motoneurons, making them easier to recruit (Burke, 1981). In other words, larger motoneurons have a lower input resistance and a higher voltage for spiking. Typically, motoneurons with a larger soma also present larger axons, allowing for more branching and reaching a greater number of muscle fibres (faster MUs are usually composed of more fibres than slower MUs) (Cullheim & Ulfhake, 1979).

In addition to the ordered recruitment, the DR modulation plays a crucial role in the size principle, ensuring the attainment of maximum contraction in each muscle unit (Mendell, 2005*a*). Fast MUs consist of muscle fibres with shorter contraction and relaxation times compared to slow MUs. Consequently, a higher DR is required to achieve tetanic contractions in fast MUs (Burke, 1981). The DR is primarily constrained by the duration of the after-hyperpolarization period of the motoneuron, and interestingly, larger motoneurons tend to exhibit shorter after-hyperpolarization periods. This difference in after-hyperpolarization duration between smaller and larger motoneurons might be attributed to the presence of different $Ca^{2+}$ activated K+ channels in the slow and fast motoneurons, that reducing the time between consecutive action potentials, allow for the fusion of individual muscle twitches (Bączyk *et al.*, 2022).

Although large motoneurons reach high DR, these are sustainable only for a short time, in accordance with the low resistance to fatigue of fast muscle units. From the electrical point of view, this is attributable to the spike-frequency adaptation phenomenon, which is more evident for larger motoneurons (Pascoe *et al.*, 2014*a*; Enoka & Duchateau, 2017). This difference is likely attributable to the difference in persistent inward currents, which tend to inactivate faster in larger motoneurons (Heckman & Enoka, 2012). Persistent inward currents are fundamental for the bistable behaviour of the motoneuron, which allows for repetitive firing and to sustain tonic contractions (Heckman *et al.*, 2008). Indeed, their faster inactivation in larger motoneurons disfavour the amplification of tonic inputs, favouring the amplification of phasic (short) inputs (Manuel *et al.*, 2007).

## 1.6. The Neuromuscular Junction

In this chapter we will briefly introduce some basic concepts on the neuromuscular junction, as it is the fundamental interface where the neural signalling is translated into muscle contraction. Indeed, the neuromuscular junction is responsible for converting each motoneuron action potential into a MU action potential (Tintignac *et al.*, 2015).

The reliability of neuromuscular junction transmission is a critical assumption in HD-EMG studies because the technique relies on detecting the MU action potentials generated by individual MUs at the muscle surface. Therefore, if the conversion of the neural signalling at the neuromuscular junction level is unstable, we would not be able to infer on the motoneuron functioning (Del Vecchio *et al.*, 2020).

The neuromuscular junction is composed of a motor nerve terminal, a synaptic cleft, and a postsynaptic muscle fibre membrane (also called motor end plate). The motor nerve terminal contains vesicles filled with acetylcholine, a neurotransmitter critical for transmitting nerve impulses to the muscle fibre. Upon the arrival of an action potential at the motor nerve terminal, voltage-gated $Ca^{2+}$ channels are activated, leading to an influx of $Ca^{2+}$ ions. This increase in intracellular calcium triggers the fusion of acetylcholine-containing vesicles with the motor nerve terminal's membrane, releasing acetylcholine into the synaptic cleft. Acetylcholine diffuses across the synaptic cleft and binds to nicotinic acetylcholine receptors on the motor end plate. This binding event opens cation channels, predominantly allowing the influx of $Na^{+}$ ions and resulting in depolarization of the muscle fibre membrane, thus generating the MU action potential (Omar *et al.*, 2023).

Given the fundamental importance of the neuromuscular junction, many biological mechanisms ensure its stability and reliability (Bloch-Gallego, 2015). Among these, the safety factor of neuromuscular transmission is fundamental for the one-to-one correspondence between the motoneuron signalling and muscle unit action potentials. The safety factor can be defined as the "number of acetylcholine quanta actually released compared to the number which must act to generate an action potential" (Wood & Slater, 1997). In normal conditions, the amount of released acetylcholine is greater than the amount required to generate action potentials in the muscle unit, therefore allowing for a safety margin capable of compensating for fluctuations in the amount of released acetylcholine (Wood & R. Slater, 2001). Thanks to the safety factor, the neuromuscular transmission is a highly reliable process, capable of resisting to many stressors, including aging

(Robbins, 1992) and disuse (Sarto *et al.*, 2022*a*), and therefore allowing for the reliable recording of the motoneuron discharge activity at muscle level.

However, it should be noted that particular conditions might impair the neuromuscular junction transmission (Tintignac *et al.*, 2015), and this should not be overlooked when using the HD-EMG technique.

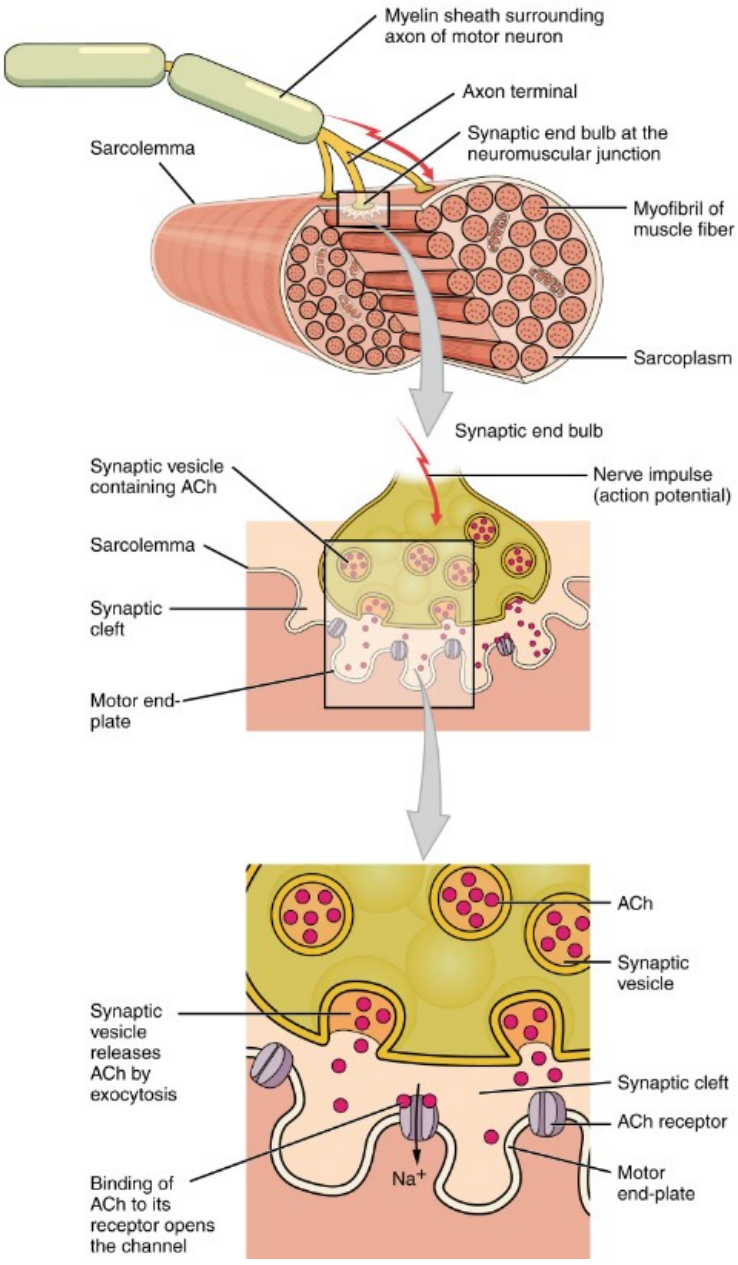


*Figure 1-6: Schematic representation of the Neuromuscular Junction. At the NMJ, the motoneuron's axon terminal releases the neurotransmitter acetylcholine (ACh). The motor end-plate, located on the muscle fibre sarcolemma, contains acetylcholine receptors. Upon release, acetylcholine molecules diffuse across the synaptic cleft, a minute space between the axon terminal and motor end-plate, where they bind to the acetylcholine receptors. This binding initiates a series of events leading to muscle fibre contraction. Figure from https://openstax.org/details/books/anatomy-and-physiology.*

## 1.7. The Muscle Action Potential

The influx of $Na^+$ ions in the muscle fibre results in the generation of a depolarizing graded potential called the end-plate potential. The end-plate potential is a local, depolarizing event that occurs at the motor end-plate and is not propagated along the entire muscle fibre. The end-plate potential needs to reach a certain threshold level for the muscle fibre to initiate an action potential (Feher, 2017). If the end-plate potential is strong enough to reach the threshold, voltage-gated $Na^+$ channels located in the adjacent regions of the sarcolemma (cell membrane of the muscle fibre) open in response to the depolarization caused by the end-plate potential. The opening of voltage-gated sodium channels allows an influx of $Na^+$ into the muscle fibre, leading to a rapid depolarization of the sarcolemma. This depolarization propagates along the sarcolemma, initiating an action potential that spreads bidirectionally throughout the entire muscle fibre (Sherwood, 2010). As the action potential travels along the sarcolemma, it enters the network of transverse tubules (T-tubules) that penetrate deep into the interior of the muscle fibre. The T-tubules play a crucial role in excitation-contraction coupling by rapidly transmitting the action potential into the core of the muscle fibre, allowing simultaneous activation of all sarcomeres (Frontera & Ochala, 2015). The action potential travels along the T-tubules and reaches the sarcoplasmic reticulum, a specialized network of membrane-enclosed compartments filled with $Ca^{2+}$. The action potential alters the conformation of dihydropyridine receptors located on the T-tubule membrane, which then activate ryanodine receptors located on the sarcoplasmic reticulum (specifically, at the level of the terminal cisternae). The activation of ryanodine receptors leads to the release of stored $Ca^{2+}$ from the sarcoplasmic reticulum into the cytoplasm (Rebbeck *et al.*, 2014). This sudden increase in cytoplasmic $Ca^{2+}$ concentration initiates the subsequent steps of the excitation-contraction coupling process, which consists in the binding and sliding of myosin to actin. This movement of myosin pulls the actin filaments towards the centre of the sarcomere, resulting in muscle contraction (Feher, 2017).

Of note, the generation and propagation of muscle action potentials is the final electrical event in the MU, and it is the event generating the electrical signal recorded via HD-EMG.

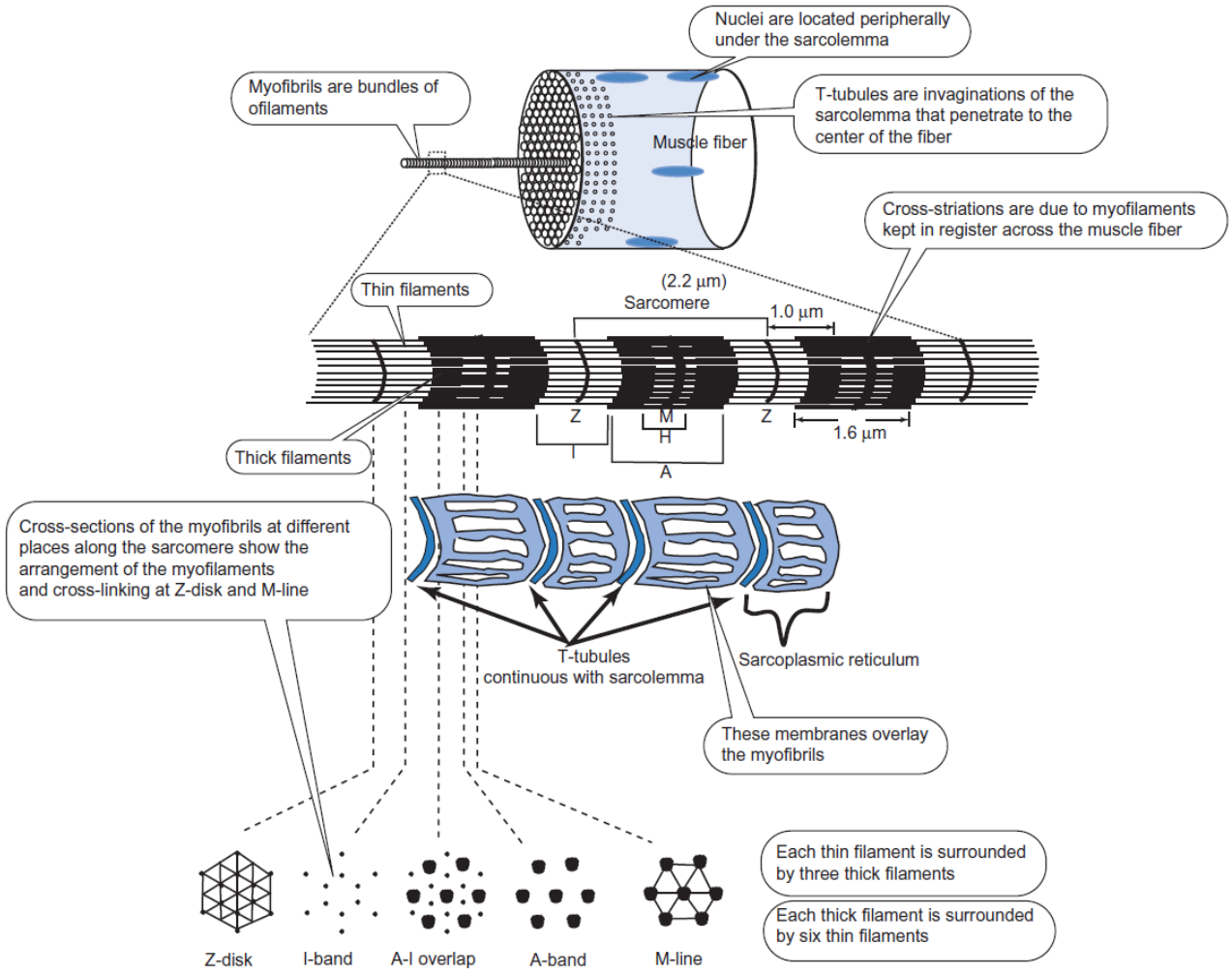


*Figure 1-7: Structure of the muscle fibre and myofibrils. The A-band corresponds to the length of the thick filaments (myosin), 1.6 µm. The I band corresponds to the thin filaments (actin) where they do not overlap with the thick filaments. Its width depends on the activation of the muscle. The Z-line or disk is where the thin filaments from opposite sarcomeres are attached. The M-line in the middle of the A-band keeps the thick filaments cantered and in register. The clear zone in the middle of the A-band is the region where thin filaments do not overlap thick filaments.*
*Figure and caption from* (Feher, 2017).

## 1.8. Plasticity of the Neuromuscular System

In physiology, the term “plasticity” summarises the ability of cells to adapt their phenotype, at any stage in their development, in response to changes in their state or environment (Winlow & McCrohan, 1987). Obviously, this concept extends to the organ and tissue level, defining the capacity of our entire body to adapt to a broad range of stressors, in both physiology and pathology (Laidler, 1994).

The neuromuscular system does not make any exception to this principle and shows high plasticity, both during development and in adulthood (Kandel *et al.*, 2012). Obviously, the maximum plasticity of the neuromuscular system manifests during the early development stages, when the connection between the brain and the muscle is formed for the first time. In this situation, new motoneurons are generated and they start establishing connections with the developing muscle. This first attempt of connection is prone to errors and most of the original connections are removed with time (in a process named pruning), leading to an exclusive and functional communication between the motoneuron and a set of muscle fibres (Winlow & McCrohan, 1987). On the muscle side, this phase is characterised by the fusion of myoblasts and the formation of myotubes, which after establishing connection with motoneurons become able to contract. In this phase, the functional demand will shape the phenotype of muscle fibres and motoneurons determining a complex and hierarchical organisation of the neuromuscular connections that tends to remain stable during adulthood (Chalif & Mentis, 2022).

During adulthood and in healthy people, the neuromuscular system adapts mainly to the external demand (e.g., loading and unloading) with its muscular component exhibiting the major structural adaptations (Campbell *et al.*, 2013; Ahtiainen, 2019; Smith *et al.*, 2023). On the neural side, motoneurons mainly respond with functional adjustments that will be reflected in a different discharge activity (Škarabot *et al.*, 2021), while the innervation pattern tends to be preserved (Inns *et al.*, 2022; Sarto *et al.*, 2022*b*). For clarity, the last statement does not intend that the innervation pattern never changes in adulthood, but rather specifies that this is a very slow and gradual adaptation, that becomes evident in advanced aging (Hepple & Rice, 2016).

Obviously, there are exceptions to the general stability of the innervation pattern. Indeed, two extreme cases stimulate the acute plasticity of the innervation pattern in adulthood, the severance of the motoneuron’s own axon and the severance of the axons of neighbouring motoneurons (Winlow & McCrohan, 1987). While these scenarios are infrequent occurrences in the

context of healthy adults, they can emerge as responses to traumatic injury, pathological conditions (Chalif & Mentis, 2022), or even as a natural consequence of the advanced aging process (Piasecki *et al.*, 2016; Jones *et al.*, 2022). When the motoneuron's axon is damaged or axotomized (physically interrupted), many molecular changes take place in the motoneuron body, which are primarily aimed at driving the restoration of the original innervation pattern. This reinnervation process is often successful, allowing for the preservation of function (Winlow & McCrohan, 1987). If the reinnervation process is not successful, axons of neighbouring motoneurons can create new branches and innervate the denervated muscle fibres. This phenomenon is named collateral sprouting and is fundamental to prevent death of the denervated fibres and muscle atrophy (Tam & Gordon, 2003; Udina *et al.*, 2011). However, axon sprouting is not the privileged choice of regeneration as it comes with a trade-off between the complete loss of function and the optimal function. For example, the newly formed synapses through axon sprouting may exhibit synaptic instability. Unlike the mature and well-organized synapses formed during development, these sprouted synapses might be less stable and reliable (Chalif & Mentis, 2022). Axon sprouting will also cause an enlargement of the MU with consequent loss in precision and fine regulation of force production and with increased demand on the motoneuron, which needs to supply depolarising currents to more synapsis than originally intended (Tam & Gordon, 2009).

Overall, the functional adaptation of the motoneurons, and in general of the MUs, are the preferred adaptive mechanism of the neuromuscular system as it provides a fast and reliable way to respond to external stressors and different functional demands (Škarabot *et al.*, 2021; Chalif & Mentis, 2022). While the direct investigation of the changes in the innervation profile (both during development and in adulthood) is usually performed *in vitro* or in animal models, the functional plasticity of the motoneuron and in general of the neuromuscular system can be investigated *in vivo* with non-invasive or minimally invasive techniques such as EMG recordings (Farina & Enoka, 2023). Nowadays, HD-EMG is the most widely used technique to study the plasticity of the neuromuscular system in humans and most of our knowledge on the neuromuscular functioning and adaptations in humans are derived from EMG or similar techniques (e.g., electroencephalography), which are perfectly suitable for the discovery of the physiological mechanisms regulating the functioning of the neuromuscular system or how these adapt to acute and chronic stressors (Atherton & Wilkinson, 2023).

## 2. **Introductory Chapter 2**: High-Density Surface Electromyography

In chapter 1, we presented the mechanisms that generate the MUs action potentials and we explained why the action potentials detected at muscle level can be used to estimate the motoneuron discharge activity. In this chapter, we explain how the action potentials from single MUs can be discriminated with the non-invasive technique of surface HD-EMG, and the technological advances that allowed for this.

HD-EMG is a sophisticated technique that involves recording multiple surface EMG signals using at least four closely spaced, small-diameter electrodes (Gallina *et al.*, 2022). The application of HD-EMG to study single MU behaviour is a relatively recent development that gained significant popularity over the past 15-20 years (Farina *et al.*, 2004, 2014*a*). The adoption of HD-EMG was facilitated by advancements in electrode manufacturing techniques and computational tools, which enabled researchers to achieve high spatial resolution in recording muscle activity (Farina *et al.*, 2016). This increased resolution allows for the identification of a large number of MUs and for detailed mapping of MU action potentials across the muscle surface (Del Vecchio *et al.*, 2020).

An important advantage of HD-EMG is its non-invasiveness, as it requires no invasive procedures and involves placing electrodes on the skin surface. This feature makes it suitable for various research applications, including the basic study of the physiological mechanisms of neural control of muscle force production (Del Vecchio *et al.*, 2019*b*) up to neuromuscular disorders (Nishikawa *et al.*, 2022). Furthermore, the spatial resolution of this technique allows for the recognition of the same MU across different data collection points and increases the precision in monitoring changes in MUs properties across interventions (Martinez-Valdes *et al.*, 2017).

Continued advancements in HD-EMG technology, such as extended multi-channel systems with hundreds of electrodes, enable simultaneous recording from large muscle regions or from different muscles, enabling researchers to investigate muscle synergies and complex motor tasks (Del Vecchio *et al.*, 2023). Additionally, machine learning algorithms applied to HD-EMG data hold promise for automating motor unit identification, accelerating the time consuming process of MUs decomposition and editing (Wen *et al.*, 2021).

Overall, the exponential evolution and application of the HD-EMG technique has the potential to transform our understanding of the neural control of muscle force production.

## 2.1. Development of High-Density surface Electromyography as a Non-Invasive Tool to Study the Activity of Single Motor Units

The first ever successful attempts to record the activity of single MUs in humans were performed with wire intramuscular electrodes in the first half of the 20th century. This primacy is usually attributed to Kurt Wachholder (Wachholder, 1928) and to Edgar Adrian and Detlev Bronk (Adrian & Bronk, 1928, 1929). Adrian and Bronk are recognised as those who discovered that neural impulses arrive at the muscle following the all-or-none principle and that graded force production is achieved through modulation of impulse frequency and recruitment of additional MUs.

During the 20th century, the effort of many researchers allowed for the design of new intramuscular recording systems that reduced the discomfort for the participant and increased the quality of the recorded signal (Duchateau & Enoka, 2011). In this framework, Elwood Henneman made one of the largest contribution in unveiling the mechanisms of neuromuscular functioning, although in animal models, with the definition of the "size principle" (Mcphedran *et al.*, 1965; Wuerker *et al.*, 1965; Henneman & Olson, 1965; Henneman *et al.*, 1965*a*, 1965*b*). Indeed, Henneman was able to demonstrate that in cat muscles new MUs are recruited with increased intensity of electrical stimulation to the sciatic nerve, and that are derecruited following the same order. Additionally, the ability to detect the MUs firing behaviour allowed him to identify that increased force production is associated to increased DR and that higher impulses are usually coming from larger motoneurons.

Soon after, many researchers took advantage of the advances in intramuscular EMG for the validation of the size principle in humans (Milner-Brown *et al.*, 1973) and for the identification of other physiological aspects of neural control. For example, it was demonstrated that although the recruitment order is usually preserved, the force intensity at which the MUs are recruited is strictly dependent on the speed of contraction, with explosive contractions resulting almost in the simultaneous recruitment of all the MUs (Freund, 1983). In this extreme situation, it is also possible that faster MUs are recruited before slower ones, given the higher conduction velocity of the larger motoneuron's axon. However, given the minimal differences in recruitment time, it is virtually impossible to experimentally demonstrate the fact. Additionally, in the late '80s it was demonstrated that the recruitment of new MUs continues up to some percentage of the maximum force production range, after which the modulation of MUs DR is the only possible mechanism to increase force production (De Luca, 1985). Of note, the upper limit for the recruitment of additional MUs (full MUs recruitment) is muscle specific, and it is usually lower for smaller, compared to larger

muscles, and grossly ranging between 50 and 90% of maximum force (Kukulka & Clamann, 1981; de Luca *et al.*, 1982).

Overall, intramuscular EMG recordings have the undoubtful recognition of the first tool for the investigation of neural control in humans and provided a way to define most of the fundamental physiological mechanisms governing neuromuscular control (Duchateau & Enoka, 2011).

The technological advancements of intramuscular EMG were driven both by advanced needle manufacturing techniques and decomposition techniques. Indeed, the discrimination of single MUs was originally performed visually by manually classifying the prominent impulses in the intramuscular EMG signal. This technique, although effective, was extremely time consuming and prone to error. To overcome these limitations, different research groups proposed semi-automated spike sorting methods, which provided the possibility to accurately identify a few concurrently active MUs from voluntary contractions at low and moderate force levels (LeFever & De Luca, 1982; Mcgill *et al.*, 1985; Stashuk, 1999).

The possibility of automatic or semi-automatic decomposition of EMG signals made possible to experiment with new recording techniques and drove the development of multi-channel intramuscular recording systems capable of resolving partially superimposed MU action potentials (LeFever & De Luca, 1982). The introduction of multi-channel recording systems paved the way for the development of surface EMG techniques oriented at the identification of single MUs activity (Merletti *et al.*, 2008).

The detection of single MUs from surface EMG systems became reality in the early 2000s (Blok *et al.*, 2002; Lapatki *et al.*, 2004), when large grids of multiple recording electrodes were developed (Lapatki *et al.*, 2004). One problem of EMG recordings from the muscle surface is that the volume conductor acts as a low-pass filter on the EMG signal, therefore smoothing the resulting signal and reducing the possibility to discriminate the contribution of single MU action potentials in the generation of the interference EMG signal. In this situation, the high spatial sampling of large grids with multiple recording electrodes increases the likelihood of observing unique MU action potentials at least in some electrodes and increases the chances to discriminate the contribution of single MUs.

With time, electrodes manufacturing moved from dry grids attached directly to the skin to flexible grids firmly attached to the skin with adhesive foam and in contact with the skin via conductive paste. This system allowed to reduce the electrode-skin contact impedance, to make it similar across the different channels and to reduce/remove movement artefacts (Merletti *et al.*,

2008). This technological advancement allowed to reduce the disturbing/noisy component in the recorded EMG signal and enhanced the representation of MU action potentials.

Given the high number of recording channels and the complexity of the surface EMG signal (in comparison to the intramuscular one), it is practically impossible to manually discriminate the contribution of single MUs from HD-EMG recordings. Therefore, the advances in manufacturing techniques were accompanied by the development of sophisticated algorithms specifically designed to identify single MUs from the interference HD-EMG signal (Gazzoni *et al.*, 2004; Kleine *et al.*, 2007; Holobar & Zazula, 2007; Negro *et al.*, 2016; Chen & Zhou, 2016).

Thanks to the high spatial sampling, specialised grids and decomposition algorithms, it is now possible to decompose a high number of single MUs from HD-EMG recordings in different muscles and up to moderate to high intensities of contraction (Del Vecchio *et al.*, 2019*b*). Additionally, MUs behaviour can now be investigated both in the time and space domain, allowing researchers for novel analyses and to acquire additional knowledge in the mechanisms of neural control of muscle force production (as explained in the next paragraphs).

All the advances of the HD-EMG technique opened a new era in the study of MUs physiology and activity in response to different stimuli (Martinez-Valdes *et al.*, 2018*a*; Casolo *et al.*, 2021), in health and pathology (Drost *et al.*, 2001; Gallego *et al.*, 2015*b*), to injury (Nuccio *et al.*, 2021) and for man-machine interface applications (Farina *et al.*, 2017).

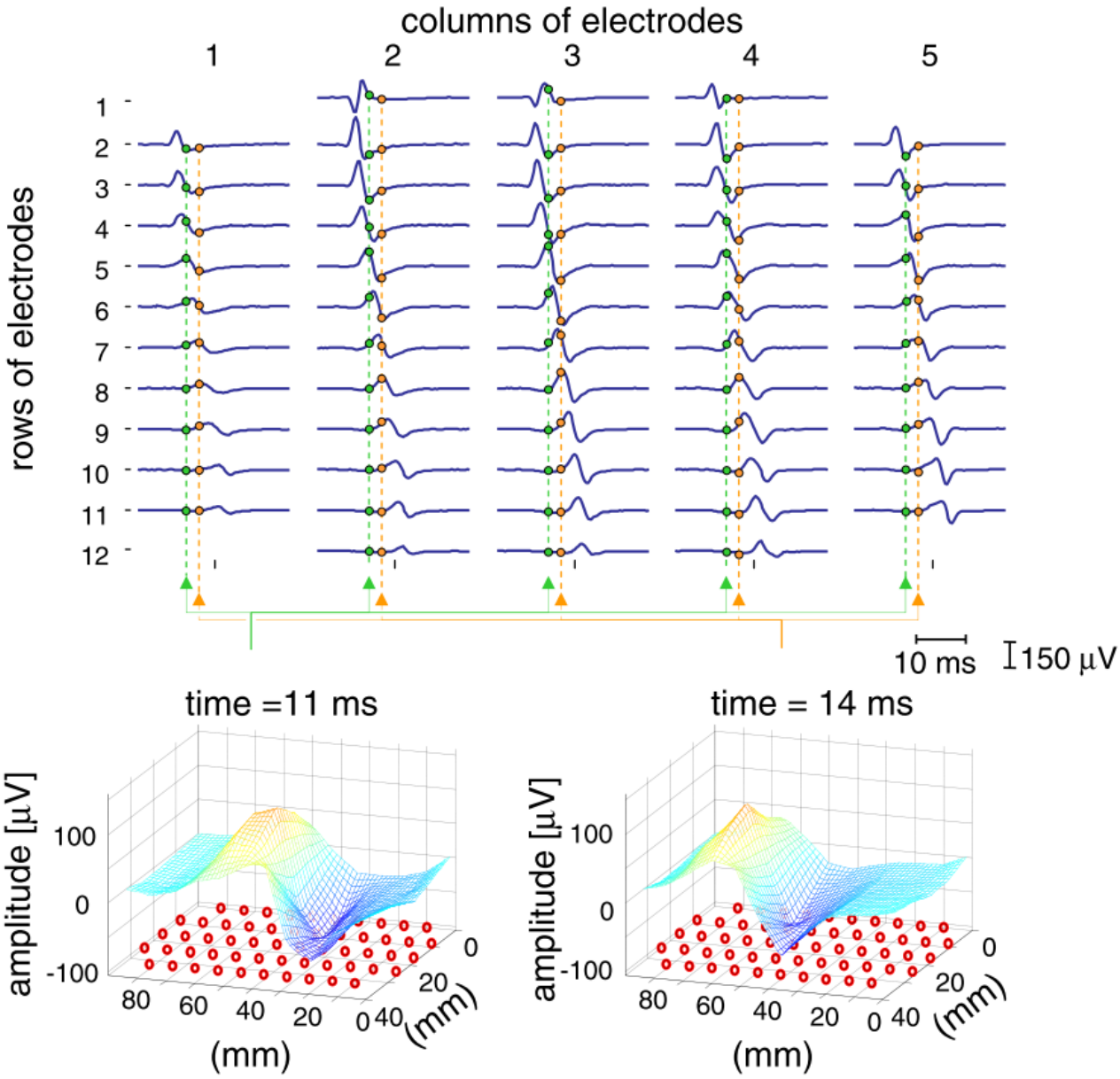


*Figure 2-1: Motor unit activity in space and time. Motor unit action potential recorded with a grid of 61 electrodes (13 by 5 electrodes, inter-electrode distance 5 mm) from the biceps brachii muscle during an isometric contraction at 10% of the maximal force. The bipolar signals derived along the direction of the muscle fibres are shown in the top panel. The electrode grid was placed distal with respect to the innervation zone of the motor unit. The signals detected along the rows show similar action potential shapes with a delay corresponding to the propagation along the muscle fibres. The multi-channel action potential is a three-dimensional signal in time and space. The two-dimensional spatial representations for two-time instants (11 ms and 14 ms after the generation of the action potential) are shown (bottom panel). The circles on the plane representing the spatial coordinates represent the locations of the electrodes of the grid. The spatial distributions have been interpolated for the graphical representation. The values reported for each location of the grid correspond to the amplitude of the action potential, indicated by circles in the multi-channel signal shown in the top panel.*
*Figure and caption from* (Merletti *et al.*, 2008).

## 2.2. Generation of the Interference Electromyography Signal

Although the mathematical component of the models used to describe the HD-EMG signals is outside the scope of this thesis, the theoretical concepts behind the generation of the recorded signal are fundamental to understand the remaining of this introductory chapter and the methodological rationale of the experimental chapters.

The surface HD-EMG technique records the electrical activity of the contracting muscle from a large area of the skin with a high number of electrodes (Gallina *et al.*, 2022). This basic concept implies at least 3 fundamental assumptions (Farina & Merletti, 2001; Merletti & Farina, 2016):

1- The recording signal is generated by the summation of the action potentials of each MU active in the area below the recording grid. The summation of the action potentials increases the complexity of the signal and hides the contribution of single action potentials.

2- The recorded signal is a filtered version of the electrical activity of single muscle fibres. The filtering effect is due to the conductivity of the volume conductor, which can be described as all the tissue located between muscle fibres and skin.

3- The geometry of the muscle fibres and the distance from the innervation zone alters the shape and synchronisation of the MU action potentials.

Point 1 is common for any system of EMG recording (e.g., intramuscular and surface) while points 2 and 3 are specific of surface HD-EMG. As a consequence of point 2, the signal recorded with HD-EMG is more complex and difficult to dissociate in the contribution of single MUs.

The generation of the action potential has been described in chapter one from the physiological point of view. In this context, it is important to understand the implications of MU action potentials summation. When few MUs are simultaneously active, there are small chances that their action potentials will happen in overlapping time windows and their summation will be minimal. Increasing the intensity of the contraction, and therefore the number of recruited MUs, many action potentials will happen in overlapping windows and the summation of their contribution will alter the shape of the resulting MU action potentials. Furthermore, the action potentials of larger MUs will exceed those of smaller MUs, hiding their contribution (Del Vecchio *et al.*, 2020). With these considerations, it is understandable that the contribution of larger MUs will be easier to discriminate than that of smaller MUs, and that increasing contraction intensity, it will become

progressively more difficult to identify the contribution of small MUs. This concept is fundamental in the interpretation of MU properties when recording at different intensities. Indeed, increasing contraction intensity, the identification of single MUs in HD-EMG recordings will be biased toward higher-threshold (and larger/faster) MUs (Del Vecchio *et al.*, 2019*a*; Nuccio *et al.*, 2021). At the same time, the simpler EMG signal at low intensity of contraction will allow for the identification of a greater number of MUs. In practical terms, the understanding of EMG signal generation will guide the researcher in the design of recording protocols that maximise both the number of identified MUs and their representation across the recruitment range. It must be noted that an excessive superimposition of action potentials greatly reduces the chances of discriminating the MU action potentials of different MUs, therefore making it extremely challenging to detect single MUs at maximum contraction intensity (Del Vecchio *et al.*, 2019*b*).

The volume conductor acts as a filter on the EMG signal, altering the shape of the MU action potentials and increasing their similarity (Farina & Merletti, 2001). To a larger volume conductor corresponds a greater filtering effect and similarity between MU action potentials. This is one of the greatest limitations in the HD-EMG technique as the number of identifiable MUs greatly differs between anatomical locations in the same subject or within subjects (Oliveira *et al.*, 2022). Indeed, the most commonly investigated muscles are those located closer to the surface and with reduced volume conductor, such as the *tibialis anterior* (Cudicio *et al.*, 2022), the *biceps brachii* (Casolo *et al.*, 2023) and the distal portion of the *vastus lateralis* (Nuccio *et al.*, 2021).

After the MU action potential is generated in the innervation zone, it propagates through the muscle fibre to the end of the fibre. This process can be observed in HD-EMG recordings thanks to the spatial resolution of the grid. The innervation zone can be identified as the point of inversion in the propagation direction of action potentials and the extinction of the action potential can be observed in the electrodes with greater distance to the innervation zone (Casolo *et al.*, 2020). The process of generation, propagation and extinction of the action potential is accompanied by a modification in the amplitude (and observed shape) of the action potential (Farina & Merletti, 2001). The ability to discriminate the propagation of action potentials depends on the anatomical characteristics of the muscle and it is easier to observe in pennate muscles (Mesin *et al.*, 2007).

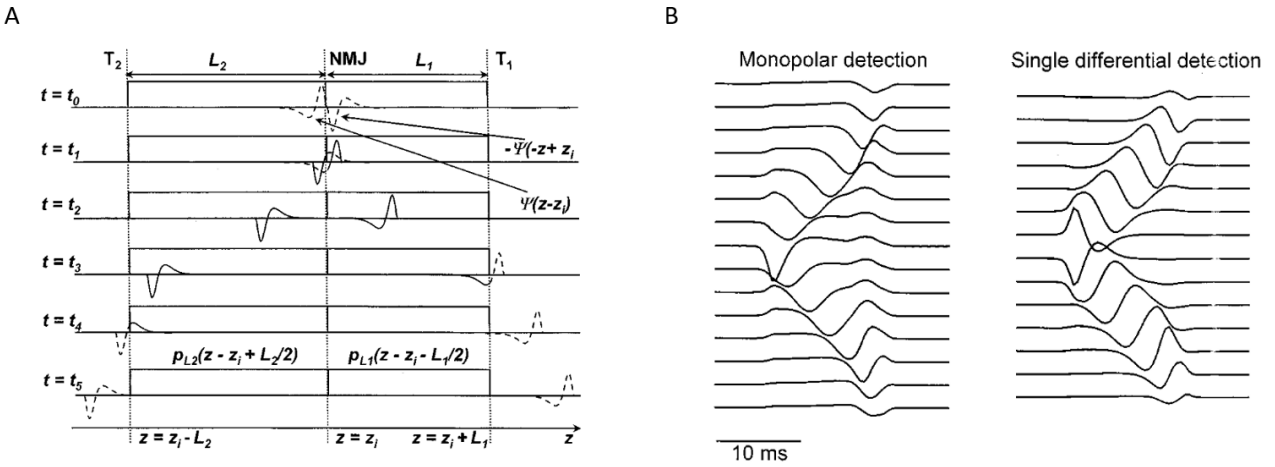


*Figure 2-2: Generation and propagation of the motor unit action potential. The action potential originates at the level of the neuromuscular junction (NMJ) and propagates in opposite directions in the muscle fibre. The area in which the action potential starts propagating in different directions identifies the innervation zone. The action potential travels along the fibres until its progressive extinction at the fibre end plate and at the tendons. Panel A is a theoretical representation of the action potential generation and propagation while Panel B is the resulting simulation in a surface high-density grid with different spatial filtering approaches.*
*Figure adapted from* (Farina & Merletti, 2001).

## 2.3. Decomposition of the Interference Electromyography Signal

The identification of the discharge activity of single MUs from the interference EMG signal is achievable via a process called decomposition. HD-EMG decomposition can be performed with different computational methods (Gazzoni *et al.*, 2004; Kleine *et al.*, 2007; Holobar & Zazula, 2007; Negro *et al.*, 2016; Chen & Zhou, 2016) but for the scope of this thesis, we will only focus on the convolutive blind-source separation approach proposed by Francesco Negro in 2016 (Negro *et al.*, 2016).

To facilitate effective decomposition, preliminary steps of signal transformation must be executed. These entail both extension and whitening of the HD-EMG signals. Extension incorporates delayed replicas of the original signals, converting the convolutive model into an instantaneous one (Negro *et al.*, 2016). Whitening, on the other hand, serves to decorrelate the extended measurements, mitigating the impact of volume conductor filtering and enhancing the spatial-temporal representation of the signals (Martinez-Valdes & Negro, 2023). The result is a more localized and temporally precise delineation of motor unit action potentials. The combination of extension and whitening is also referred to as 'convolutive sphering' (Thomas *et al.*, 2006).

At the core of the decomposition process lies an iterative optimization procedure based on independent component analysis. This involves applying the optimization algorithm to the whitened and extended measurements, initializing from an appropriate estimate and converging to a local maximum of the chosen contrast function. The main goal of independent component analysis is to estimate the mixing matrix and the original sources. The algorithm aims to find a set of filters that, when applied to the mixed signals, produce statistically independent output signals. These output signals are the estimated source signals (Thomas *et al.*, 2006). The culmination of this step yields a pulse train that describes the probability of motor unit discharges at distinct time points (Martinez-Valdes & Negro, 2023).

The technical terms used in this paragraph are well explained in the glossary section at the end of the thesis.

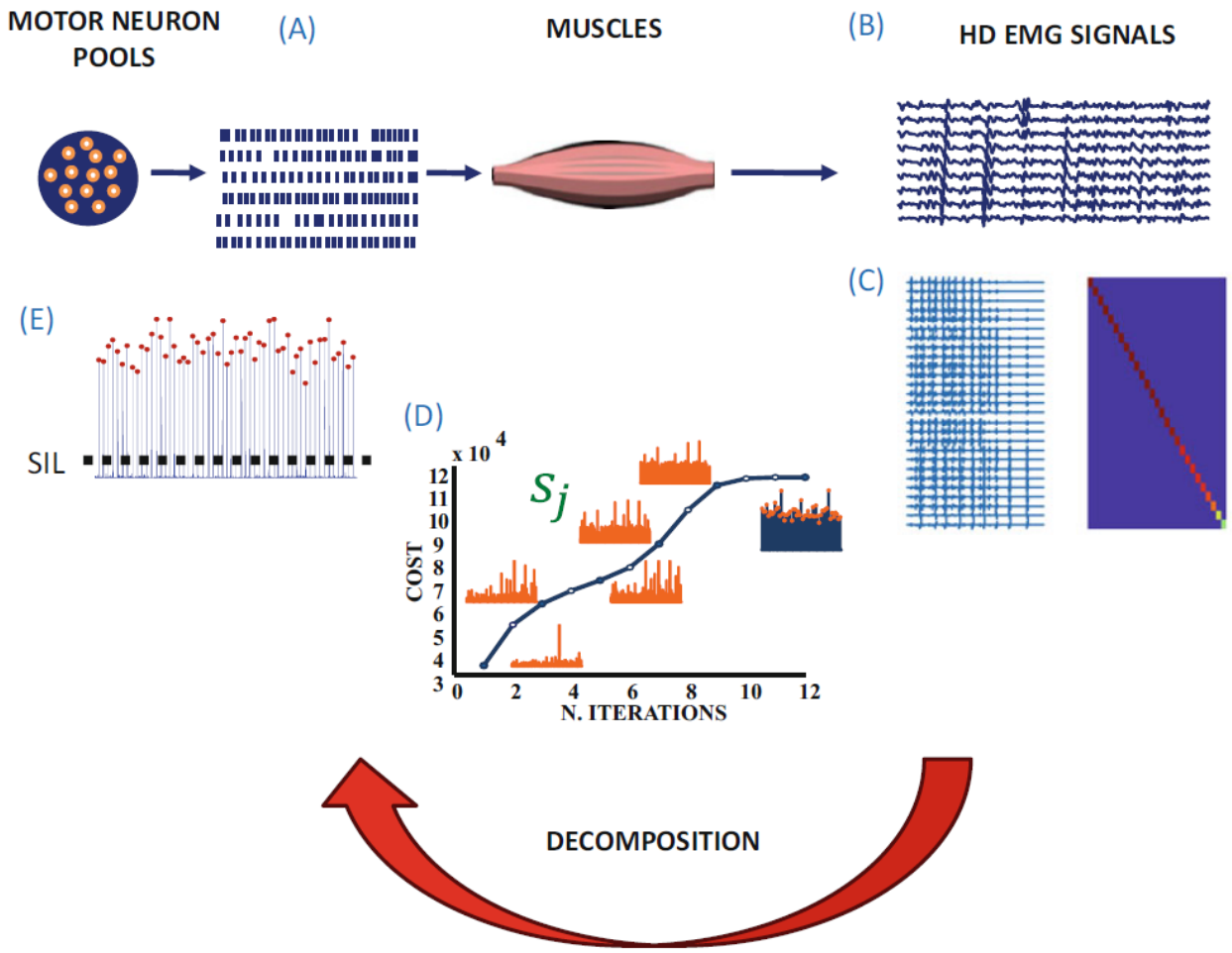


*Figure 2-3: Schematic representation of the convolutive blind source separation approach. Motoneuron pools generate multiple action potentials (a), which can be recorded from the muscle. Motor unit firings of single motor units need to be separated from the interference electromyography signal (b) with blind source separation techniques. The signals are first extended to convert the convolutive model into an instantaneous one. A whitening transformation is then applied to the extended measurements to compensate for the spatial and temporal characteristics of the motor unit potential shape (c). Afterward, the solutions of the inverse problem are extracted by maximizing iteratively a specific cost function selected to identify sparse sources (d). Clustering methods and accuracy measures (i.e., silhouette measure, SIL) are then used to identify the discharge times of the decomposed motor unit (e). SIL, silhouette score.*
*Figure and caption from* (Martinez-Valdes & Negro, 2023).

Upon completing the initial motor unit decomposition, the subsequent phase involves accuracy assessment and manual editing. These are critical steps in refining the extracted motor unit spike trains and ensuring the robustness and reliability of the analysis.

Given that the identification of pulse trains relies on broad statistical characteristics of the sources, there exists a level of uncertainty regarding their attribution to individual motor units or potential combinations of multiple motor units that may not have been accurately separated. To address this challenge, various accuracy metrics have been developed to assess the quality of the decomposition outcome and the accuracy of the identified motor unit spike trains. The most common accuracy measures are the Pulse-to-Noise Ratio (Holobar *et al.*, 2014) and the Silhouette

Measure (Negro *et al.*, 2016). These metrics offer a quantitative evaluation of the decomposition process by analysing the amplitude of the source spikes relative to the underlying baseline noise.

However, it is important to acknowledge that while these metrics provide valuable insights into the overall quality of the motor unit decomposition, they do not assure absolute accuracy. Therefore, manual editing is required to ensure reliable motor unit spike trains (Del Vecchio *et al.*, 2020).

During the manual editing process, an experienced operator examines the decomposed MU pulse trains. This visual assessment aims to identify any anomalies or irregularities, such as missed discharges or erroneous spikes, within the extracted motor unit spike trains. Based on the visual inspection, the operator can add missing firing instants or remove wrong ones to ensure that the extracted spike trains closely align with expected physiological patterns (Hug *et al.*, 2021*a*).

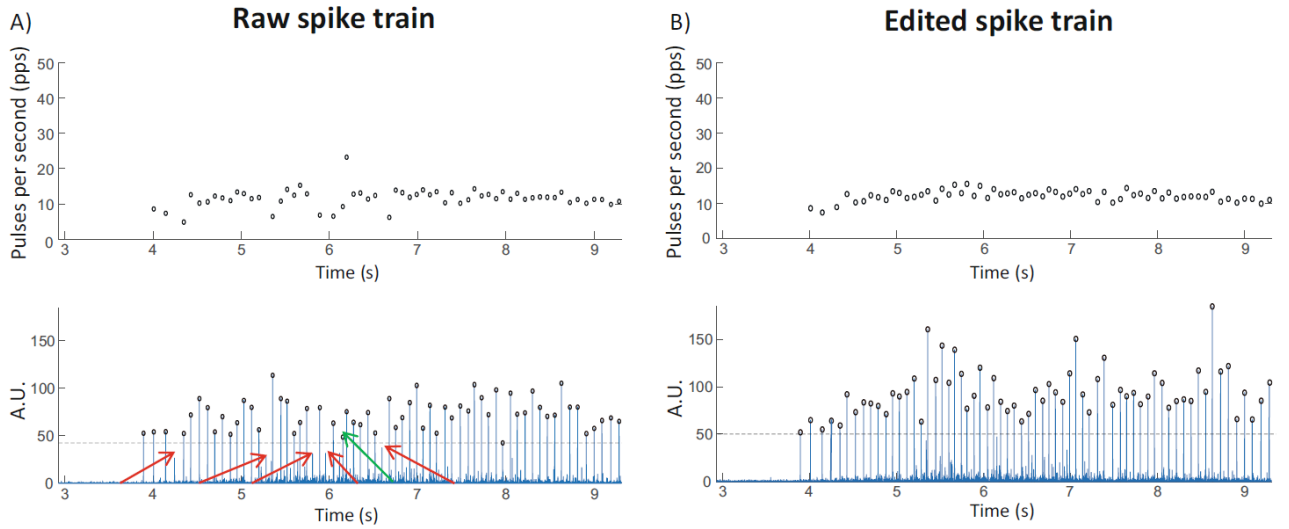


*Figure 2-4: Motor unit spike train editing. Motor unit spike train editing needs to be performed following the automatic decomposition results as missing firings and additional firings can provide unreliable spike train results. (a) Instantaneous firing rate (top of the figure) calculated from the spike train obtained from the automatic decomposition results (bottom of the figure). The red arrows represent missing firings while the green arrow represents an additional firing. These missing and additional discharges increase the variability of motor unit firing (top of the figure). (b) Following the addition of missing firings, removal of the additional firing, and recalculation of spike train results, the variability in instantaneous firing rate is reduced (top of the figure).*
*Figure and caption from* (Martinez-Valdes & Negro, 2023).

## 2.4. Considerations for the Analysis of High-Density Electromyography Recordings

The analysis of HD-EMG recordings can be performed both on the global EMG signal and on the decomposition outcome. In a basic assumption, the two analyses should provide similar results since the global EMG signal generates from the summation of the discharge activity of single MUs. However, this idea does not take into account the filtering effect of the volume conductor and the summation/cancellation of concurrent action potentials, among many other confounding factors (Farina & Enoka, 2023).

Before the development of advanced decomposition algorithms based on blind source separation techniques (Holobar & Zazula, 2007; Negro *et al.*, 2016), the study of the neural drive to the muscle was mainly based on rough estimates from the global EMG signal, as the detection of single MUs activity from the skin surface was particularly challenging (Farina *et al.*, 2016). With time, many simulation (Keenan *et al.*, 2006; Farina *et al.*, 2008) and experimental studies (Del Vecchio *et al.*, 2017) demonstrated that the association between global EMG variables and the underlying behaviour of the active MUs is weak, and suggested that investigating single MUs might provide better estimates of the neural drive to the muscle and its effect (Farina & Enoka, 2023). A clear description of why global EMG cannot be considered a reliable estimator of the neural drive to the muscle was provided by Dario Farina and Roger Enoka (Farina & Enoka, 2023), who stated that "any mathematical descriptor of the EMG signal that does not separate the neural and muscle fibre contributions in the surface EMG cannot be used to infer neural control strategies". A practical explanation of this statement is provided in the next paragraphs.

From global EMG, signal amplitude is often investigated. EMG amplitude is associated to the number and size of active MUs and increases with the number of recruited MUs. This is a valid indicator of the muscle electrical activity and it is closely related to the force produced by the muscle (Milner-Brown & Stein, 1975; Farina *et al.*, 2014*a*). However, since force production depends from both DR modulation and recruitment, global EMG amplitude cannot be used to infer the properties of the single MUs that are recruited and to infer the amount of neural drive. For example, while the amplitude of the global EMG signal increases at increasing intensities of contraction, the amplitude of the action potential of newly recruited MUs is not necessarily larger than that of MUs recruited earlier. Additionally, the rate of change in global EMG amplitude is only weakly correlated with the rate of change in single MU action potential amplitudes (Del Vecchio *et al.*, 2017). When it is impossible to separate the neural and muscular contribution to force production, results can be

misinterpreted and lead to wrong conclusions. For example, it was demonstrated that during leg extension, the global EMG amplitude is different between the *vastus lateralis* and the *vastus medialis* muscle (Martinez-Valdes *et al.*, 2018*b*). If the analysis is limited to the global EMG amplitude, we could conclude that the two muscles receive different amount of neural drive, but if we look also at single MUs properties, and in particular at their DR modulation, we understand that the difference in global EMG amplitude is due to peripheral differences like size of the MUs or amount of volume conductor, but not to the neural drive (Martinez-Valdes *et al.*, 2018*b*; Farina & Enoka, 2023). The same consideration can be misleading also when investigating muscle synergies with global estimates (Hug *et al.*, 2021*b*, 2023).

Apart from a rough estimate of global EMG amplitude, there are cases in which global EMG can provide reliable estimations. Conduction velocity (CV) represents the velocity of propagation of the action potentials along the muscle fibres. If this is investigated from the action potentials pertaining to single MUs, it is possible to estimate the CV of each MU with high precision (Farina *et al.*, 2002). If this is estimated from the global EMG signal, the estimated value will be representative of the CV of the population of active MUs (Farina *et al.*, 2000). Although the estimation of single MUs CV is more informative, the agreement with global CV is high (Del Vecchio *et al.*, 2017). For this reason, global CV is usually considered a reliable estimate. This is probably due to the fact that CV depends on the peripheral properties (e.g., muscle fibre size) and not on the central control (Casolo *et al.*, 2023), therefore not necessarily requiring to separate the central and peripheral contributions.

As a final remark, the global EMG signal from HD-EMG recordings is often used to map the activation level of the muscle. Activity maps can be applied to precisely detect electrical activity across different regions of the muscle and to identify how the muscle activation differs during the execution of specific tasks (Gallina & Botter, 2013) or in conditions such as low-back pain (Murillo *et al.*, 2019). Additionally, activity maps can still provide detailed information in the cases where decomposition of single MUs is not feasible (Lulic-Kuryllo *et al.*, 2022). However, it must be noted that also this technique can be biased by the inhomogeneous distribution of the volume conductor across the muscle area, and this potential limitation should always be considered.

Based on the beforementioned and in agreement with authoritative opinions (Farina & Enoka, 2023), the investigation of the neural strategies of muscle force production should be performed, whenever possible, via analysis of single MU properties. For this reason, the experimental chapters of this thesis will focus on the investigation of populations of single MUs.

## 2.5. Bipolar Surface Electromyography: Use Cases in the High-Density Electromyography Era.

Before the introduction of HD-EMG, non-invasive EMG recordings were commonly performed with pairs of surface electrodes. This simpler setup is often referred to as “bipolar EMG”, a technique that measures the difference in voltage between two electrodes on one muscle (i.e., it allows to observe an EMG signal in differential montage) (Besomi *et al.*, 2019). Although with this approach it is not possible to identify the contribution of single MUs or to investigate spatial features such as conduction velocity, the interference EMG signal is usually processed to extract information concerning the amplitude of the signal and its power spectral density. Amplitude measures such as root mean square and linear envelop are usually associated to the force produced by the muscle, while the frequency content of the signal is often adopted to study muscle fatigue (Merletti & Farina, 2016). In the previous section, we discussed about the major limitations of these global measures performed on the interference EMG when studying human physiology and physiological adaptations. However, there are areas of study that still find the use of this technique helpful and informative.

Although HD-EMG promises to be the new frontier of electromyography recordings (Farina *et al.*, 2016), it is rapidly evolving by increasing the number of utilised electrodes (which could also be considered as the amount of recorded information), and therefore of the complexity of the recorded signal. For this reason, the use of HD-EMG finds noticeable obstacles in fields like biomechanics and sports science. Indeed, these disciplines often involve the study of complex (on multiple planes) and dynamic movements. Additionally, these disciplines frequently demand the collection of EMG signals from multiple muscles (e.g., 10 or more agonist and antagonist muscles) (Mesquita *et al.*, 2023), which is impractical with HD-EMG, and bipolar EMG remains the only solution able to provide an accurate estimate of muscle electrical activity (Luca, 1997). In these scenarios, bipolar EMG proves to be a highly effective tool for studying:

- Onset of muscle activation
- Force produced by the muscle
- Muscle fatigue

In these specific cases, bipolar EMG can provide accurate information with limited complexity in the experimental setup, in addition to simplified analysis and interpretation of the results (Luca, 1997).

Obviously, also bipolar EMG requires accurate selection and implementation of the experimental setup, including the size and spacing of the electrodes, as well as the anatomical location (Vieira *et al.*, 2017). Indeed, bipolar configuration is particularly sensible to muscle cross-talk, as it does not allow to perform double-differential derivation which increases the selectivity of the recording and reduces the contribution of neighbouring muscles to the recorded signal (Luca, 1997).

One of the major challenges to the use of HD-EMG are dynamic tasks, a circumstance under which bipolar EMG can be more effective and accurate. Indeed, plastic HD-EMG grids usually have a certain stiffness, which will cause the grid to detach during repetitive movements or will introduce movement artefacts in the recorded signal. Although some manufacturers began producing textile grids, which adapt better in dynamic movements, these solutions are much more expensive and their use is limited to few (e.g., 2) muscles. Furthermore, the dimension of the HD-EMG recording systems is not compatible with on-field evaluations, especially if the activity of multiple muscles is investigated.

In conclusion, although HD-EMG seems to be the most powerful technique currently available for the study of MUs physiology, it is not by default the best approach, and the complexity of this technique should be weighted based on the necessity of the research question.

## 3. Experimental Chapter 1: Lower Limb Suspension Induces Threshold-Specific Alterations of Motor Units' Properties that are Reversed by Active Recovery

*Authors:*

Giacomo Valli [a]*, Fabio Sarto [a], Andrea Casolo [a], Alessandro Del Vecchio [b], Martino V. Franchi [a], Marco V. Narici [a] and Giuseppe De Vito [a]

* Corresponding author

[a] Department of Biomedical Sciences, University of Padova, Padova, Italy

[b] Department Artificial Intelligence in Biomedical Engineering, Friedrich-Alexander University, Erlangen, Germany

*Author contributions:*

GV, FS, MVF, MVN and GDV conceptualized and designed the study. GV was in charge of the high-density EMG recordings and analysis. GV, FS, AC and ADV were involved in data collection and analysis. GV drafted the manuscript and all the authors revised it.

The article has been published in the *Journal of Sport and Health Science* and can be found at https://doi.org/10.1016/j.jshs.2023.06.004

## 3.1. Background

In healthy people, the motoneuron discharge activity is fundamental for the maintenance of posture and for locomotion (Bączyk *et al.*, 2022). Consequently, any increase or reduction in physical demand will be reflected into different levels of motoneuron discharge activity (Duchateau & Hainaut, 1990; Seki *et al.*, 2001; Del Vecchio *et al.*, 2019*a*; Škarabot *et al.*, 2022).

The adaptation of the neuromuscular system to exercise (i.e., increased physical demand) has been extensively studied both with intramuscular EMG and surface HD-EMG (Del Vecchio *et al.*, 2019*a*; Jones *et al.*, 2022; Škarabot *et al.*, 2022). The majority of these studies have reported an increase in DR after periods of resistance exercise, suggesting that this could be a pivotal adaptation to support enhanced force production (Škarabot *et al.*, 2021).

Surprisingly, limited attention has been given to the adaptation of the neuromuscular system to disuse (i.e., decreased physical demand) and little evidence is available about it. Contrary to what can be expected, disuse periods are common and have significant known consequences on many organs and metabolic functions (Clark, 2009; Reggiani, 2015; Sarto *et al.*, 2023). Indeed, disuse can be experienced at any age and for a variety of reasons, spanning from disease to space flight.

Recently, space agencies like the “European Space Agency” (ESA) and the “Agenzia Spaziale Italiana” (ASI), among others, have funded numerous projects aimed at understanding the consequences of space flight and, in particular, of reduced gravity (Biolo *et al.*, 2017; Monti *et al.*, 2021). These projects drove some of the major advances in our knowledge of the physical adaptations to reduced physical demand. A reduction in gravity translates in a reduced mechanical load on our body, similarly to a reduction of physical activity (Juhl *et al.*, 2021). On earth, this situation is mimicked via models of muscle unloading like bed-rest, cast immobilisation, or limb suspension (Reggiani, 2015; Sarto *et al.*, 2022*b*).

Given our knowledge that increased physical demand drives an increase in motoneuron DR, it is reasonable to hypothesize that the reduced physical demand experienced in low gravity could lead to a reduction in DR. About 30 years ago, two research groups tried to elucidate this, suggesting that a reduced motoneuron DR is one of the factors contributing to force loss following periods of disuse (Duchateau & Hainaut, 1990; Seki *et al.*, 2001, 2007). However, the techniques that they adopted only allowed for a rough estimation of these adaptations and were never applied to muscles involved in locomotion, which is the most affected type of movement in low-gravity environments (Clark, 2009).

## 3.2. Abstract

**Purpose**: To non-invasively test the hypothesis that short-term lower-limb unloading would induce changes in the neural control of force production (based on motor units' properties) in the *vastus lateralis* muscle, and that possible changes are reversed by active recovery.

**Methods**: Ten young males underwent 10 days of unilateral lower limb suspension (ULLS) followed by 21 days of active recovery. During ULLS, participants walked exclusively on crutches with the dominant leg suspended in a slightly flexed position (15-20 degrees) and with the contralateral foot raised by an elevated shoe. The active recovery was based on resistance exercise (leg press and leg extension) and executed at 70% 1RM, 3 times/week. Maximal voluntary contraction (MVC) of knee extensors and motor units' properties of the *vastus lateralis* muscle were measured at baseline, after ULLS and after active recovery. Motor units were identified using High-Density Electromyography during trapezoidal isometric contractions at 10, 25 and 50% of the current MVC and individual motor units were tracked across the three data collection points.

**Results**: 1428 unique motor units were identified and 270 of them (18.9%) were accurately tracked. After ULLS, MVC decreased by -29.77%, motor unit's absolute recruitment/derecruitment thresholds were reduced at all the contraction intensities (with the changes between the two variables strongly correlated) while discharge rate was reduced at 10 and 25% but not at 50% MVC. Impaired MVC and motor units' properties fully recovered to baseline levels after active recovery. Similar changes were observed both in the pool of total and tracked MUs.

**Conclusion**: Our novel results demonstrate, non-invasively, that 10 days of ULLS affected neural control altering predominantly the discharge rate of lower-, but not of higher-threshold motor units, suggesting a preferential impact of disuse on motoneurons with a lower depolarization threshold. However, after 21 days of active recovery, the impaired motor units' properties were fully restored to baseline levels highlighting the plasticity of the components involved in neural control.

## 3.3. Highlights

- Little is known about the consequences of disuse on the neural control of large muscles and how these can be reversed.
- We studied changes in motor units' properties in the vastus lateralis muscle after 10 days of unilateral lower-limb suspension and after 21 days of active recovery.
- A short period of muscle unloading reduces the discharge rate of lower-, but not of higher-threshold motor units, suggesting a preferential impact of disuse on motoneurons with a lower depolarization threshold.
- The restoration of neural control requires about twice the duration of the disuse period.

## 3.4. Abbreviations

In alphabetical order:

| | |
|---|---|
| AR | Active recovery |
| AR10 | Day 10 of AR |
| AR21 | Day 21 of AR |
| COVsteady | Coefficient of variation of the steady-state phase |
| DERT | Derecruitment threshold |
| DR | Discharge rate |
| EMG | Electromyography |
| HD-EMG | High-Density EMG |
| LS0 | Baseline (day 0 of the limb suspension) |
| LS10 | Day 0 of the limb suspension |
| MUs | Motor units |
| MVC | Maximal voluntary contraction |
| PNR | Pulse to noise ratio |
| RT | Recruitment threshold |
| ULLS | Unilateral lower limb suspension |
| XCC | Cross-correlation coefficient |
| $\Delta DR_{R-T}$ | Delta DR from recruitment to target |
| $\Delta Force_{R-T}$ | Delta force from recruitment to target |

## 3.5. Introduction

Skeletal muscle disuse is a condition that can be experienced at any age and for a broad variety of reasons, including injury, hospitalization (e.g., during disease and after surgery), and even during space flight. In order to investigate the effects of disuse on neuromuscular health, and identify potential countermeasures, different experimental models have been proposed (Reggiani, 2015; Sarto *et al.*, 2022*b*) (e.g., limb suspension, limb immobilization and bed-rest). Regardless of the implemented model or the investigated muscle, reduction in muscle force is considered a primary consequence of disuse (Clark, 2009). Currently, several mechanisms underlying disuse-induced muscle force reduction have been proposed, such as muscle atrophy (Clark, 2009) and altered contractile properties of muscle fibres (Monti *et al.*, 2021) (i.e., excitation-contraction coupling) based on what observed after limb suspension and bed-rest. However, these mechanisms are considered insufficient to fully explain the loss of muscle force, suggesting that other key processes might be involved (Clark, 2009; Monti *et al.*, 2021).

Disuse has been also defined as a reduction in the number of action potentials delivered by motoneurons (Reggiani, 2015) and, in light of this, it is surprising that very little attention has been given to the role of neural signalling to the muscle in disuse conditions. Indeed, the available knowledge is limited to the seminal works of Duchateau and Hainaut (Duchateau & Hainaut, 1990) and Seki (Seki *et al.*, 2001, 2007) based on intramuscular electromyographic (EMG) recordings in hand muscles (i.e., *adductor pollicis* and *first dorsal interosseous*). These works consistently reported that hand cast immobilization results in a reduction of motor units' (MUs) discharge rate (DR) across different contraction intensities although discrepant conclusions were reached on whether the alterations in MUs DR were more pronounced for lower- or higher-threshold MUs. Specifically, Duchateau and Hainaut (Duchateau & Hainaut, 1990) directly observed that the gain in MUs DR was predominantly reduced in lower-threshold MUs while, the results of Seki, indirectly suggested that the higher-threshold MUs might be more affected, based on a reduced slope of their force-frequency relationship (Seki *et al.*, 2001). These contrasting results may be attributed to the different interpretation of the data, but also to the pioneering approaches adopted in these investigations that only allowed for the manual identification of a small number of MUs, which could introduce variability into the results. Additionally, it is unknown whether the findings of these studies might be limited to small muscles, since larger muscles use different neural strategies to

control force production (De Luca, 1985) (from now on referred as neural control (Farina *et al.*, 2016)).

Over the last years, the development of EMG technologies and the introduction of multi-channel recording systems, namely High-Density EMG (HD-EMG) (Farina *et al.*, 2016), allowed for the non-invasive detection of a large and representative population of MUs active in different regions of the examined muscle (Del Vecchio *et al.*, 2020). Moreover, these unique features allow for the appropriate investigation of MUs activity in large muscles (Farina *et al.*, 2016) like the knee extensors, which are fundamental for locomotion and independence in daily tasks, and for the identification and tracking of individual MUs over time (Martinez-Valdes *et al.*, 2017). Besides, the concurrent recording of force might provide additional insights on the discharge characteristics of the simultaneously activated MUs and their common synaptic input, especially at lower intensities of contraction (Enoka & Duchateau, 2017).

Therefore, the aim of this study was to take advantage of HD-EMG to investigate how 10 days of unilateral lower-limb suspension (ULLS), a well-established model of disuse induced with limb unloading (Berg *et al.*, 1991), can alter the neural control in a large thigh muscle (i.e., *vastus lateralis*). Furthermore, we also investigated the condition of neural control after 21 days of active recovery (AR) based on moderate to high-intensity resistance exercise. Our hypotheses were that (i) 10 days of ULLS would be sufficient to induce detectable alterations of neural control, particularly via alterations of MUs DR and (ii) that 21 days of AR (about twice the duration of the ULLS) would be sufficient to restore neural control.

## 3.6. Methods

### 3.6.1. Participants and experimental protocol

This study was part of a larger investigation aimed at detecting early biomarkers of neuromuscular degeneration after short-term unloading (Sarto *et al.*, 2022*a*).

The investigation was conducted in accordance with the Declaration of Helsinki, and approved by the Ethics Committee of the Department of Biomedical Sciences of the University of Padova (Italy), reference HEC-DSB/01-18. Volunteers were enrolled in the study after examination of medical history and signing the written consent form.

Twelve recreationally active young adults volunteered to participate in this study. Only male individuals were accepted to reduce the risk of deep venous thrombosis associated with ULLS that is more common in females (Bleeker *et al.*, 2004). Inclusion criteria were 18-35 years of age, body mass index between 20 and 28 kg $m^{-2}$ and involvement in recreational physical activities (1-3 times/week, self-reported). Exclusion criteria were: sedentary lifestyle, smokers, history of deep venous thrombosis and any other condition preventing the safe participation in the study.

Prior to the beginning of the study, participants were familiarized with the study procedures and practiced carrying out daily tasks while performing ULLS (Tesch *et al.*, 2016). Measurements were conducted at baseline (day 0 of the limb suspension, LS0), after 10 days of ULLS (LS10) and following 21 days of AR (AR21) (Fig. 3-1A). At LS10, participants were tested immediately after the interruption of the limb suspension. At AR21, the tests were executed 72 hours after the last exercise session to avoid muscle fatigue.

The duration of the AR phase was based on previous observations that full recovery of muscle function after a two-week lower limb immobilization required an AR period lasting twice as long (4 weeks) as the disuse phase (Suetta *et al.*, 2009). In this study, an intermediate measurement of maximum voluntary isometric contraction (MVC) was also performed after 10 days of AR (AR10) to monitor how much force had been recovered with respect to LS0 (Fig. 3-1A).

Participants were asked to refrain from intense exercise, coffee and alcohol intake during the 24 hours preceding the data collection.

### 3.6.2. Unilateral lower limb suspension

The dominant lower limb (right leg for all the participants) was suspended in a slightly flexed position (15 to 20 degrees of knee flexion) with straps connecting the shoulders and the suspended

foot (Fig. 3-1A) while the opposite foot was fitted with an elevated shoe (50 mm sole) to prevent the suspended lower limb from touching the ground while moving, as originally described by Berg et al. (Berg *et al.*, 1991). Volunteers walked exclusively on crutches during the whole ULLS period and avoided any loading or active contraction of the suspended limb (Berg *et al.*, 1991). The straps were always worn when the participants had the necessity to walk but were removed while sitting or lying in bed. Participants were instructed on how to properly wear the straps during the familiarization session.

Precautionary measures to prevent deep venous thrombosis have been taken as previously described (Sarto *et al.*, 2022*a*). Compliance was evaluated through daily calls and messages.

### 3.6.3. Active recovery

The AR phase started 72 hours after the end of the suspension period and was conducted for the following 21 days. The AR program was based on unilateral resistance exercise performed 3 times/week with at least 24h of recovery between sessions. Every session was composed of 3 sets of 10 repetitions of leg press and leg extension at 70% 1RM after a warm-up period at 30% 1RM. Both exercises were executed from full knee extension (0 degrees) to ∼90 degrees limb flexion. Sets were separated by a 2-min rest. The time under tension was set at ∼2 seconds both in the concentric and eccentric phases.

1RM was estimated from the 4-6RM during the first exercise session (Brzycki, 1993) of each week and the load employed was adjusted accordingly.

The choice of the intensity and the decision to indirectly estimate the 1RM, was based on the participants characteristics, not previously involved in resistance exercise and coming from 10 days of complete unloading of the lower limb.

### 3.6.4. Maximal voluntary isometric contraction

MVC was assessed during maximal voluntary isometric contraction of the knee extensor muscles at 90° knee angle, using a custom-made knee dynamometer fitted with a load cell (RS 206–0290) attached above the ankle through straps as previously described (Monti *et al.*, 2021; Sarto *et al.*, 2022*a*) (Fig. 3-1B).

In order to ensure correct assessment of the MVC (Gandevia, 2001), participants practiced the task during the familiarization session supervised by an experienced operator and were all instructed to "push as hard as possible" by pushing the dominant leg against the load cell, and then to maintain the contraction for 3/4 seconds. After a standardized warm-up executed up to 70% of their perceived maximum, participants practiced the maximal task until they became able to consistently reach their maximum force values. During every contraction, participants were stabilized to the seat with straps at the waist in order to prevent any compensatory movement and loud verbal encouragement was provided to encourage the maximum voluntary effort. At the data collection points, the test was repeated three times with 60 seconds of rest and only the contraction with the maximum value was considered for the MVC calculation.

### 3.6.5. HD-EMG matrix placement

The HD-EMG signal was recorded from the *vastus lateralis* muscle (Fig. 3-1B) using a matrix of 64 equally spaced electrodes (GR08MM1305, OT Bioelettronica, Torino, Italy) filled with conductive cream (Ac cream, OT Bioelettronica, Torino, Italy) and arranged over 5 columns and 13 rows with 8 mm interelectrode distance, which corresponded to 30.72 $cm^2$ of recording area.

The matrix was placed following the muscle fascicle orientation (detected with B-mode ultrasound (Mylab70, Esaote, Genoa, Italy) (Hug *et al.*, 2021*b*) and with the central electrodes of the last two rows of the matrix over the innervation zone (Botter *et al.*, 2011*a*). The ultrasound recordings were used also to detect muscle borders and avoid the placement of the matrix across adjacent muscles.

The innervation zone was detected between 35% and 20% of femur length (Botter *et al.*, 2011*a*) with low-intensity percutaneous electrical stimulation using a pen electrode with an electrical current of 8-16 mA (Digitimer Ltd, Welwyn Garden, Hertfordshire, UK) (Sarto *et al.*, 2022*a*).

Before placing the matrix, the skin was shaved, cleaned with 70% ethanol and then with abrasive-conductive paste (Spes medica, Salerno, Italy). Reference electrodes were placed on the malleolus and patella bones.

After the recordings, the matrix border was marked with a permanent marker and emphasized by the operator at every meeting with the participants to allow the reproducible placement of the matrix in the following data collection points (Casolo *et al.*, 2020).

### 3.6.6. HD-EMG recordings

The HD-EMG signal was recorded during trapezoidal contractions (Fig. 3-1C) at three different submaximal intensities (10, 25 and 50% MVC). All the contractions had a total duration of 30 seconds. The ramp-up and ramp-down phases were performed with a linear force increase/decrease set at 5% MVC per second (Del Vecchio *et al.*, 2019*a*) and the duration of the steady-state phase was adjusted accordingly (Fig. 3-1C) (e.g., at 25% MVC the ramps lasted 5 seconds each and the steady-state 20 seconds, for a total 30 seconds contraction). All the trapezoidal contractions were repeated twice with 60 seconds of rest and the different intensities were proposed in random order. Participants received real-time visual feedback of the force produced and were instructed to match the trapezoidal template as precisely as possible.

EMG and force signals were sampled at 2048 Hz with the EMG-Quattrocento (OT Bioelettronica, Torino, Italy). The EMG signal was recorded in monopolar configuration, amplified (×150) and band-pass filtered (10–500 Hz) at source (Del Vecchio *et al.*, 2019*a*). Force was recorded synchronously with the EMG signal and the offset was removed before starting the recording.

### 3.6.7. Force and HD-EMG signal analyses

The force signal was converted to newton (N) and low-pass filtered (fourth-order, zero-lag, Butterworth, 15 Hz cut-off) (Del Vecchio *et al.*, 2019*a*). Force steadiness was computed as the coefficient of variation of force recorded during the steady-state phase (COVsteady) of the trapezoidal contractions and expressed as percentage (i.e., the ratio of the standard deviation to the mean) (Enoka & Farina, 2021).

The HD-EMG signal was band-pass filtered between 20 and 500 Hz (second-order, Butterworth) and decomposed into discharge times of the MUs with the validated convolutive blind source separation technique (Fig. 3-1D)(OTBioLab+, OT Bioelettronica, Torino, Italy)(Negro *et al.*, 2016). After the decomposition, the pattern of discharge times for each MUs was visually inspected and manually edited (Hug *et al.*, 2021*a*). Only the identified MUs with a pulse to noise ratio (PNR) ≥ 28 decibel (dB) (sensitivity > 85%), were maintained for further analyses (Holobar *et al.*, 2014).

All the MUs decomposed from the two trapezoidal contractions recorded at the same intensity during the same data collection point (for each participant) were pooled and analysed together after the removal of duplicated MUs (as explained in section 2.3.5). This approach allowed to increase the number of unique MUs, to reduce the variability induced by the inability of the

participant to reproduce the trapezoidal path and to avoid results biased by the duplication of values that would occur without removing the duplicated MUs.

For each identified MU, the absolute and relative (as percentage of MVC) recruitment threshold (RT) and derecruitment threshold (DERT), and the average discharge rate (DR) at recruitment, derecruitment and during the steady-state phase were computed.

MUs DR was calculated over the first and last 4 discharges at recruitment and de-recruitment and during the entire steady-state phase (Del Vecchio *et al.*, 2019*a*).

DR modulation was defined as the difference between the DR at recruitment and the DR at the start (first 10 discharges) of the steady-state phase (delta DR from recruitment to target, $\Delta DR_{R-T}$). The difference between the target force (i.e., 10, 25 and 50%) and the force at recruitment ($\Delta Force_{R-T}$) was also computed.

MUs properties were first analysed based on contraction intensity and then by recruitment threshold. In particular, MUs with a RT ≤ 25% MVC were compared to those with a RT ≥ 25% MVC and were defined as lower- and higher-threshold MUs, respectively. The analyses comparing lower- and higher-threshold MUs have been performed both in the pool of total and tracked MUs.

Signal processing and analyses were performed with custom Python scripts (Release 3.9.7, Python Software Foundation, USA).

### 3.6.8. MUs tracking and duplicates removal

MUs action potential waveforms and their spatial distribution (Fig. 3-1E) were used to recognize the same MUs across different recording sessions as previously described (Maathuis *et al.*, 2008; Martinez-Valdes *et al.*, 2017; Del Vecchio *et al.*, 2020). Briefly, the tracking method is based on the normalized two-dimensional cross-correlation value (XCC) between the waveforms of individual MUs generated by spike-triggered average on a 25 ms time-window and accounts both for the shape and the location of the waveforms (Martinez-Valdes *et al.*, 2017; McManus *et al.*, 2021). Different thresholds of similarity were set based on whether MUs tracking was used to remove duplicated MUs within the same recording session or to track them across the different data collection points. Pairs of MUs from the same recording session with XCC ≥ 0.9 were considered duplicates (Maathuis *et al.*, 2008) and, therefore, the MU with the lowest PNR was removed from the following analyses (Holobar *et al.*, 2014). To track the MUs longitudinally, the XCC threshold was

set ≥ 0.8 to account for minor differences in the matrix placement (Maathuis *et al.*, 2008; Martinez-Valdes *et al.*, 2017).

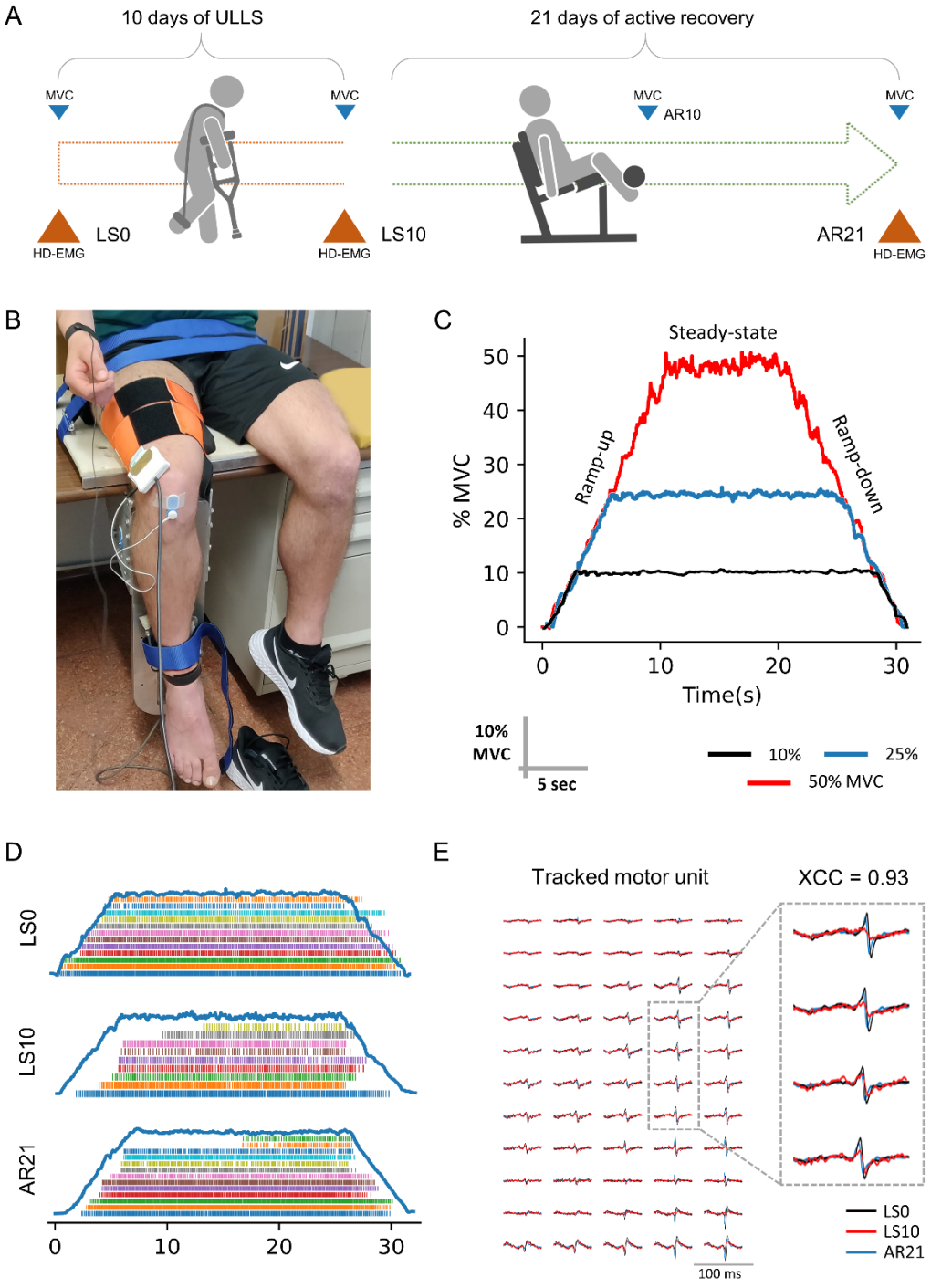


*Figure 3-1: Schematic representation of the study design (A) and procedures of data collection and analysis (B-E). Data were collected at baseline (day 0 of limb suspension), after 10 days of ULLS and after 21 days of active recovery (data collection points were named LS0, LS10 and AR21 respectively) (A). MVC, maximal voluntary contraction was recorded also after 10 days of active recovery (AR10). HD-EMG was recorded from the vastus lateralis muscle (B) during ramp contractions at 10, 25 and 50% MVC. Ramp slope was standardized at 5% MVC per second (C). The recorded electrical activity of the muscle was decomposed to obtain the pattern of discharge times of the MUs (D) and the MUs action potential shape was used to track the MUs longitudinally across the different data collection points (E). XCC, cross-correlation coefficient, is the measure of similarity between the MUs action potential shape.*

### 3.6.9. Statistical analysis

Concerning MVC and force steadiness, variables normality of the distribution was assessed through the Shapiro–Wilk test. Since the normality assumption was satisfied, a one-way repeated measure analysis of variance (ANOVA) was used. Sphericity was tested with Mauchly's test and when the assumption of sphericity was violated, the correction of Greenhouse-Geisser was applied. Post-hoc pairwise T-tests were conducted with Holm's correction when the overall model had a p-value less than 0.05.

All the MUs properties were analysed using linear models (time as fixed effect, random intercept, clustered by participant) as multiple MUs were recorded from each participant (Sarto *et al.*, 2022*a*; Yu *et al.*, 2022). Normality for the residuals of each variable was assessed through visual inspection of the Q-Q plot and histogram. If normality of the residuals was not confirmed, a generalized linear mixed effect models was used instead. Post-hoc comparisons were conducted with Holm's correction when the overall model had a p-value less than 0.05.

Repeated measures correlation was used to determine the common within-individual association for paired measures assessed at the three data collection points (Bakdash & Marusich, 2017). For this analysis, participants average values were used as a representation of the clustered values (i.e., MUs properties) as commonly done in studies with HD-EMG (Del Vecchio *et al.*, 2019*b*; Nuccio *et al.*, 2021). Fixed slopes were employed to estimate a single correlation coefficient for all subjects, which simplifies the model and improves the stability and accuracy of the estimates (Bakdash & Marusich, 2017).

Mixed models were computed with jamovi 2.2.2 (Sydney, Australia – R language) while the other analyses were performed using Python (Release 3.9.7, Python Software Foundation, USA, pingouin package (Vallat, 2018)). Statistical significance was accepted at $p<0.05$. The results are reported and plotted as mean (standard error) for linear models and as mean (standard deviation) for the ANOVAs. Partial eta squared ($\eta^2p$) was also reported for ANOVAs.

## 3.7. Results

### 3.7.1. Participants

Out of 12 participants, one dropped out after baseline measures for personal reasons. All the others successfully completed the study without any adverse event. Participants characteristics were age: 22.1 (2.9) years; height: 178 (3.1) cm; body mass: 72.1 (7.1) kg; BMI 22.9 (2.1) $kg*m^{-2}$. Due to the inability to decompose MUs with a PNR above 28 dB at LS10 and AR21, one participant was excluded from the analyses. Hence, a total of 10 participants were included in the final analyses.

### 3.7.2. Maximal voluntary isometric contraction and force control

Complete statistical summary of MVC and COVsteady is available as Supplementary material (Table Supp 3-1).

For MVC, a main effect of time was observed ($p<0.001$, $\eta^2p=0.842$). Compared to LS0, MVC decreased at LS10 (-29.77%, $p<0.001$), remained lower at AR10 (-15.28%, $p=0.002$) and returned to LS0 values at AR21 (Fig. 3-2A).

COVsteady, showed a main effect of time at all the contraction intensities ($p=0.017$ and $\eta^2p=0.364$ at 10%, $p=0.001$ and $\eta^2p=0.656$ at 25%, $p=0.001$ and $\eta^2p=0.699$ at 50% MVC). Compared to LS0, COVsteady increased at LS10 at 25% MVC (+54.95%, $p=0.008$) and decreased at AR21 for all the contraction intensities (-16.77%, $p=0.020$ at 10%; -22.43%, $p=0.002$ at 25%; -15.36%, $p=0.033$ at 50% MVC)(Fig 3-2B).

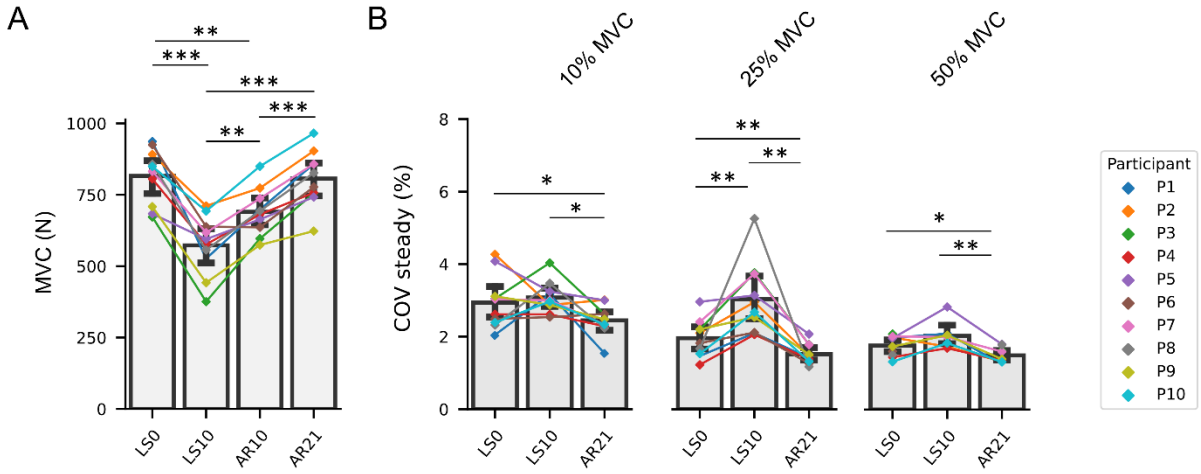


*Figure 3-2: Bar plots representing the maximal voluntary isometric contraction MVC (A) and the COV of the steady state phase (B) at the different data collection points. COV of the steady state phase is also represented at the three different submaximal contraction intensities (i.e., 10, 25 and 50% MVC). Data are displayed as mean ± SD and the changes for every participant are highlighted by a connected point plot. Significance levels are: *p<0.05, **p<0.01, ***p<0.001.*

### 3.7.3. MUs Decomposition and Tracking

A total of 1428 unique MUs (616 at 10%, 541 at 25% and 271 at 50% MVC) were identified, with an average PNR of 35.04 (2.23) dB at 10%, 33.00 (1.87) dB at 25% and 31.80 (1.36) dB at 50% MVC. Of these, 270 MUs (18.90% of the total pool) were tracked (Fig. 3-1E) across the three data collection points with an average XCC of 0.88 (0.04) at 10%, 0.92 (0.03) at 25% and 0.93 (0.03) at 50% MVC. The obtained values are in line with the methodological validation of the technique (Martinez-Valdes *et al.*, 2017).

### 3.7.4. Total pool of MUs

A complete statistical summary of MUs properties is available as Supplementary material (Table Supp 2-4).

MUs absolute RT (Fig. 3-3A) and DERT (Fig. 3-3B) were reduced at LS10 (compared to LS0) for all the contraction intensities (-20.69% at 10%, -15.15 at 25%, -19.56 at 50% MVC; $p<0.001$ for RT. -18.93% at 10%, -25.43% at 25%, -22.34% at 50% MVC; $p<0.001$ for DERT) and completely recovered to the LS0 values at AR21 at 10 and 50% MVC. At 25% MVC, instead, the RT at AR21 exceeded the LS0 level (+10.61%, $p=0.002$).

Compared to LS0, MUs relative RT (Fig. Supp 3-1A) was increased at LS10 at 10 and 25% MVC (+11.10%, p=0.008 at 10%; +19.10%, p<0.001 at 25%). At AR21, relative RT returned to baseline values at 10% but not at 25% MVC (+11.10%, p=0.003). MUs relative DERT (Fig. Supp 3-1B) was increased at LS10 at 10% MVC (+16.10%, p<0.01) and returned to baseline values at AR21.

Compared to LS0, MUs DR at recruitment (Fig. 3-4A) was reduced at LS10 at 10 and 25% (-12.25% at 10%, -12.53% at 25% MVC; p<0.001) while increased at 50% MVC (+10.09%, p=0.039). At AR21, DR at recruitment returned to baseline values at 10 and 50% while exceeded the LS0 values at 25% MVC (+7.05%, p<0.001). At 10% MVC, DR at derecruitment was reduced at LS10 (-5.65%, p=0.002) and returned to baseline values at AR21. At 25 and 50% MVC, DR at derecruitment did not change between LS0 and LS10 (Fig. 3-4B). The DR of the steady-state phase (Fig. 3-4C) decreased at LS10 at 10 and 25% MVC (-12.54% at 10%, -9.80% at 25% MVC; p<0.001) and exceeded the LS0 values at AR21 (+5.51%, p=0.006 at 10% and +7.35%, p<0.001 at 25%). At 50% MVC, the DR of the steady-state phase increased at LS10 (+5.98%, p=0.044) and returned to the LS0 values at AR21.

Changes in the total pool of MUs classified as lower and higher-threshold reflected closely what observed for MUs at 10-25% and those at 50% MVC and are extensively presented in Supplementary material (Fig. Supp 3-3 and Table Supp. 3-3). Briefly, ULLS affected the RT and DERT of both lower- and higher-threshold MUs while DR was affected only for lower-threshold MUs.

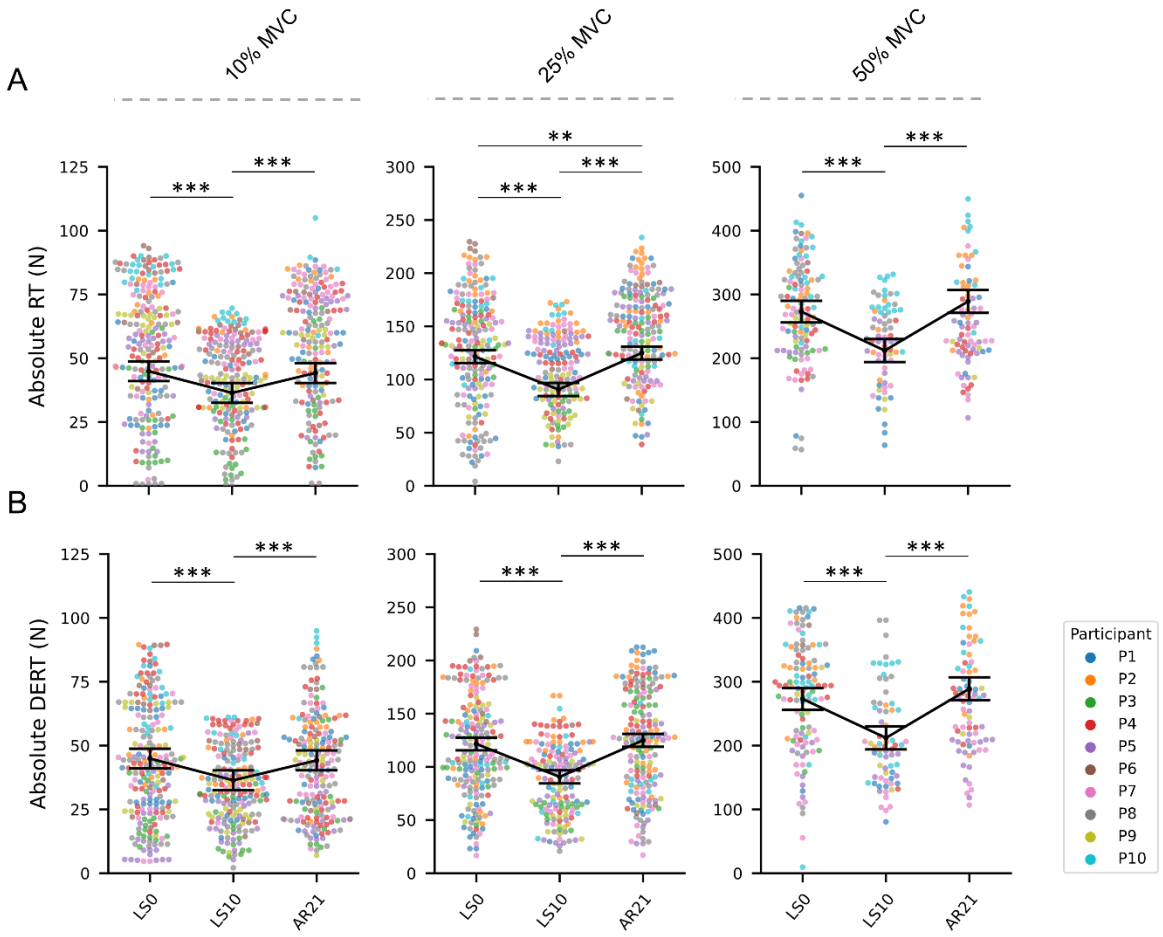


*Figure 3-3: Swarm plots representing the absolute MUs RT (A) and DERT (B) at the three data collection points. From left to right, MUs properties are presented for the three different submaximal contraction intensities (i.e., 10, 25 and 50% MVC). Individual MUs are represented by dots and clustered by subject. Summary data are presented as mean ± SEM and the direction of the changes is highlighted by a connection line. Significance levels are: **p<0.01, ***p<0.001.*

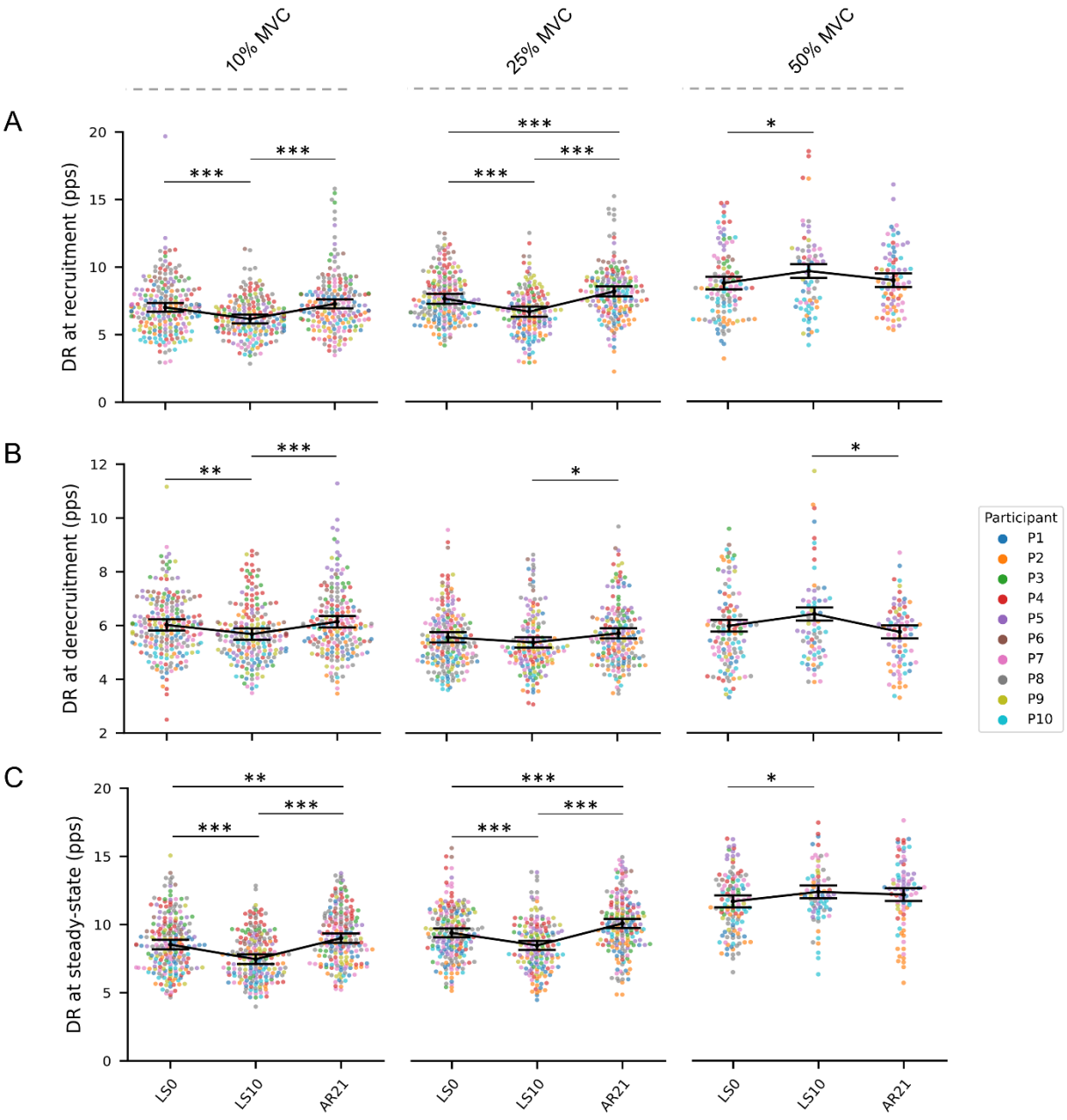


*Figure 3-4: Swarm plots representing the MUs DR at recruitment (A), derecruitment (B) and during the steady-state phase (C) at the three data collection points. From left to right, MUs properties are presented for the three different submaximal contraction intensities (i.e., 10, 25 and 50% MVC). Individual MUs are represented by dots and clustered by subject. Summary data are presented as mean ± SEM and the direction of the changes is highlighted by a connection line. Significance levels are: *p<0.05, **p<0.01, ***p<0.001.*

### 3.7.5. Correlations

Repeated-measures correlations were used to describe the strength of the association between two variables of interest and whether these associations were statistically significant.

A moderate to strong positive correlation was observed between MVC and absolute RT at 10, 25 and 50% MVC (r=0.80, 0.69 and 0.89, respectively)(Fig. 3-5A) as well as between MVC and absolute DERT (r=0.78, 0.73 and 0.96) (Fig. 3-5B) and between absolute RT and DERT (r=0.75, 0.89 and 0.90) (Fig. 3-5C). Significance for all the correlations was p<0.001.

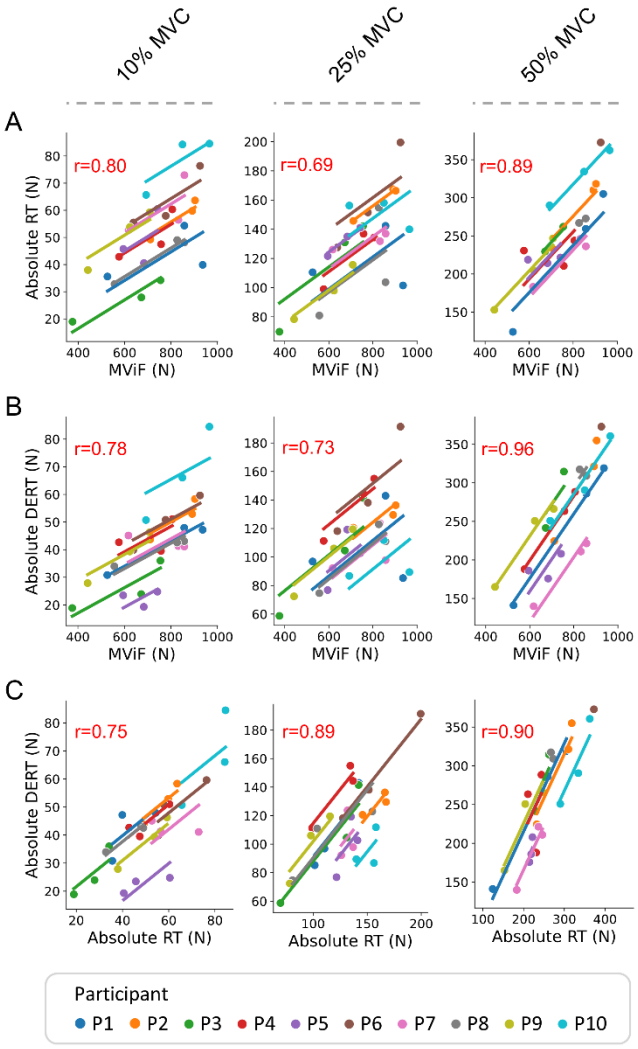


*Figure 3-5: Plots of the repeated-measures correlation describing the common within-individual association between MVC and absolute RT (A), MVC and absolute DERT (B), absolute RT and DERT (C) across the different data collection points. From left to right, correlations are presented at the three different submaximal contraction intensities (i.e., 10, 25 and 50% MVC). r value is reported in the upper-left of each figure. Significance level is p<0.001 for all the correlations.*

### 3.7.6. DR modulation

A reduced $\Delta DR_{R-T}$ between LS0 and LS10 was observed at 10 and 25% (-21.19% at 10%, p=0.035 and -41.6% at 25%, p<0.001) but not at 50% MVC. The $\Delta DR_{R-T}$ returned to LS0 at AR21 at 10 and 25% MVC but exceeded the LS0 values at 50% (+23.73%, p=0.039) (Fig. Supp 3-2A). The relative $\Delta Force_{R-T}$ (Fig. Supp 3-2B) was reduced at LS10 compared to LS0 at 10 and 25% (-23.50% at 10%, p=0.005 and -35.00% at 25%, p<0.001) but not at 50% MVC. The $\Delta Force_{R-T}$ returned to LS0 at AR21 at 10% MVC but not at 25% (-20.10%, p=0.003).

### 3.7.7. Pool of tracked MUs

Absolute RT (Fig. 3-6A) was reduced at LS10 compared to LS0 (-24.95%, p=0.017 for lower- and -21.17%, p=0.003 for higher-threshold MUs) and returned to the LS0 values at AR21. The same trend was observed for DERT (-31.55%, p=0.003 for lower- and -29.48%, p<0.001 for higher-threshold MUs)(Fig. 3-6C). Both the relative RT and DERT of the tracked MUs (Fig. 3-6B and 3-6D) did not differ at any measurement.

DR at recruitment (Fig. 3-6E) and during the steady-state (Fig. 3-6G) phase approached the borderline of a significant reduction for lower (-8.86%, p=0.051 at recruitment and -7.27%, p=0.057 during the steady-state phase for LS0 vs LS10), but not for higher-threshold MUs that did not change. DR at derecruitment was not affected by the interventions (Fig. 3-6F). $\Delta DR_{R-T}$ was not affected by the intervention both for lower- and higher-threshold MUs (Fig. Supp 3-4A). A visual representation of the between and within participants variability of tracked MUs is available in Fig. Supp 3-5.

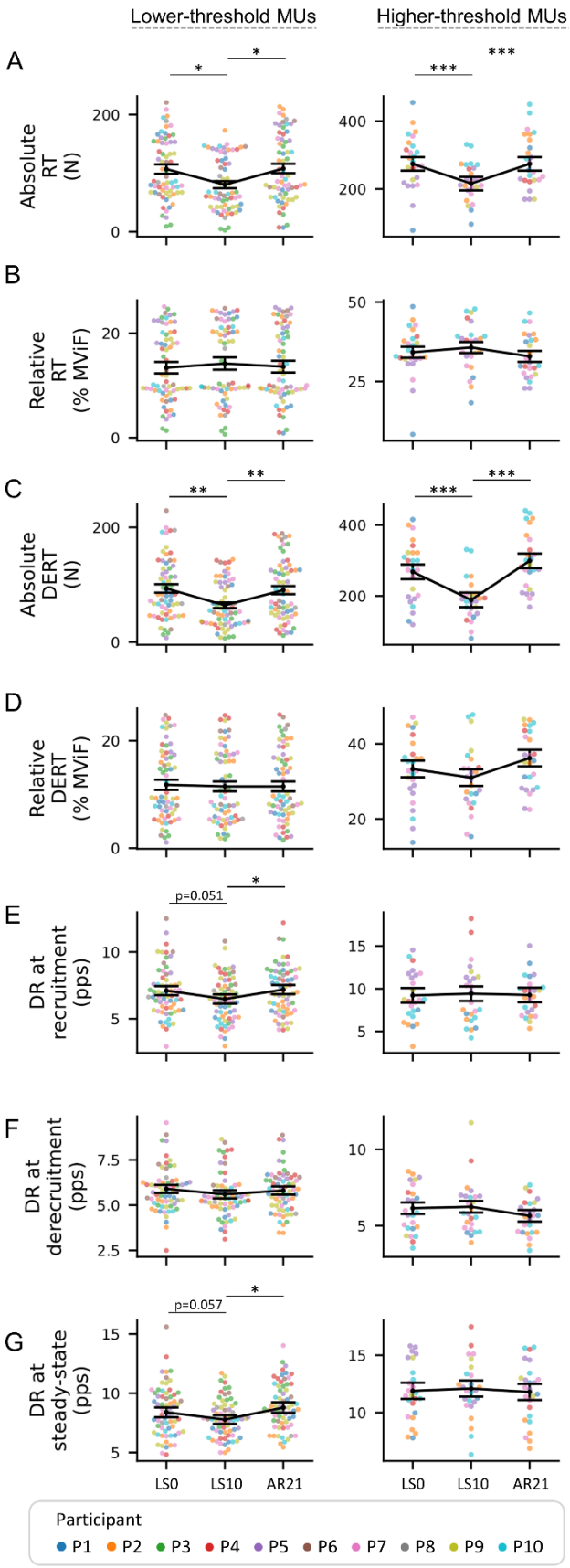


*Figure 3-6: Swarm plots representing the MUs properties obtained from the pool of tracked MUs. MUs RT and DERT are presented in both absolute (A, C) and relative terms (as percent of the MVC)(B, D) and MUs DR is shown at recruitment (E), derecruitment (F) and during the steady-state phase (G), at the three data collection points. From left to right, MUs properties are presented based on the classification of lower- and higher-threshold (i.e., recruited below or above 25% MVC). Individual MUs are represented by dots and clustered by subject. Summary data are presented as mean ± SEM and the direction of the changes is highlighted by a connection line. Significance levels are: *p<0.05, **p<0.01, ***p<0.001.*

### 3.7.8. Summary of MUs properties

In the total pool of MUs, absolute RT and DERT were reduced at LS10 at all the contraction intensities and recovered to baseline levels at AR21. Differently, MUs DR was reduced at LS10 but only at 10 and 25% MVC while, at 50%, DR increased compared to LS0. At AR21, DR returned to baseline levels at 50% MVC while it exceeded the baseline levels at 10 and 25% MVC. The changes in MUs absolute RT, DERT and DR were confirmed in the pool of tracked MUs.

At LS10, relative RT was increased at 10 and 25% but not at 50% MVC. At AR21, it recovered to baseline levels at 10% but not at 25% MVC. Relative RT did not change in the pool of tracked MUs.

The range of DR ($\Delta DR_{R-T}$) and force modulation ($\Delta Force_{R-T}$) was reduced at LS10 compared to LS0 at 10 and 25% but not at 50% MVC. $\Delta DR_{R-T}$ returned to baseline levels at AR21 both at 10 and 25% MVC. $\Delta Force_{R-T}$ returned to baseline levels at AR21at 10% but not at 25% MVC. No changes were identified in the pool of tracked MUs.

## 3.8. Discussion

The main finding of this study was that a short period of unloading of the dominant lower limb (i.e., 10 days of ULLS) in young healthy men is sufficient to induce a detectable alteration of the neural strategies used to control muscle force production (here referred as neural control (Farina *et al.*, 2016; Del Vecchio *et al.*, 2020)) in the *vastus lateralis* muscle predominantly by reducing the DR of lower-, but not of higher-threshold MUs. Moreover, 21 days of AR (about twice the duration of ULLS) based on resistance exercise are sufficient to restore neural control and even to suggest the beginning of an exercise-induced overcompensation, highlighting the remarkable functional plasticity of the neural components.

The threshold-specific alterations of MUs DR demonstrate a different impact of disuse on the motoneurons innervating lower- and higher-threshold MUs in the large *vastus lateralis* muscle. This finding shows a similarity with the seminal work of Duchateau and Hainaut (Duchateau & Hainaut, 1990) on small hand muscles and suggests that that the preferential impact of disuse on the motoneurons innervating lower-threshold MUs is a general phenomenon. In other words, this response appears as a fundamental mechanism independent from the size or the anatomical location and characteristics of the considered muscle (Henneman *et al.*, 1965*a*; De Luca, 1985).

Unveiling the effects of unloading on the neural control of *vastus lateralis*, a large component in the group of knee extensor muscles which are fundamental for daily life motor tasks and with key metabolic roles, may have significant relevance for developing practices aimed at preventing or recovering the disuse-induced neuromuscular impairments. For example, knowing the preferential deterioration of the motoneurons innervating lower-threshold MUs, and the rapid onset of this alteration, might drive the development of rehabilitation protocols specifically designed at targeting these motoneurons (low intensities of exercise) and suitable to be carried out shortly after the cause of disuse (e.g., injury or surgery).

### 3.8.1. MUs DR is affected by ULLS

Our data indicate a difference between the ULLS-induced changes in absolute RT/DERT, observed both in lower- and higher-threshold MUs, and the changes in DR that differed for lower- and higher-threshold MUs. Notably, all these changes were confirmed also in the pool of tracked MUs where there are no confounding effects due to different populations of decomposed MUs

(Martinez-Valdes *et al.*, 2017; Casolo *et al.*, 2020), thereby strengthening the reliability of the results.

The strong correlation between absolute RT and DERT suggests that the order of recruitment and derecruitment was not altered by disuse, in other words, short-term disuse seems to not cause deviations from the Henneman's Size Principle (Mendell, 2005*a*). Additionally, the correlation between MVC and absolute RT/DERT highlights a synergic change of the two parameters and indicates that the reduced RT observed at LS10 at all the contraction intensities should be a consequence of internal muscular impairments affecting equally all the MUs. Indeed, recent evidence suggests that short periods of bed-rest and ULLS are sufficient to impair muscle fibres contractility by altering intracellular calcium handling (Monti *et al.*, 2021) and muscle fibres specific force (Brocca *et al.*, 2015). Interestingly, these changes were identified evenly in slow and fast muscle fibres. In this case, the recruitment of MUs with altered contractile properties will generate lower contractile force and, therefore, all the MUs will be recruited at lower absolute intensities.

Regarding the different effect of ULLS on DR of lower- and higher-threshold MUs, we hypothesized the possibility of alterations specific to the motoneurons with a lower depolarization threshold (that are expected to innervate smaller MUs possibly composed by a prevalence of slow-type muscle fibres (Burke, 1981; Mendell, 2005*a*; Heckman *et al.*, 2009; Casolo *et al.*, 2020)). Indeed, it was demonstrated that 3 weeks of knee immobilization induce a phenotype shift from slow to fast fibres (Hortobágyi *et al.*, 2000; Ciciliot *et al.*, 2013). This phenomenon might be related to, and anticipated by, a different functional preservation of lower- and higher-threshold motoneurons. In this case, although higher-threshold motoneurons might retain largely unaltered DR activity (at least for 10 days), muscle fibres are unable to effectively translate the neural signalling in force production due to impaired contractile properties (Monti *et al.*, 2021).

In addition to the beforementioned, mechanisms such as the recurrent inhibition (Piotrkiewicz *et al.*, 2004) (i.e., motoneuron inhibition mediated by the Renshaw cells) or synaptic noise (Faisal *et al.*, 2008; Dideriksen *et al.*, 2012, 2015) (i.e., random disturbing synaptic activity in neurons that can alter the common input to the motoneurons) could contribute to the modulation of the lower-threshold motoneurons' activity. Indeed, the reduced force steadiness that we observed at LS10 at 25% MVC suggests the presence of synaptic noise induced by ULLS, in light of recent evidence suggesting that altered synaptic noise might be responsible for altered steadiness at lower intensities of contraction (Faisal *et al.*, 2008; Dideriksen *et al.*, 2012, 2015).

Based on what previously mentioned, we hypothesized that as a consequence of peripheral impairment of the muscle fibres mechanical contractile properties after disuse (Monti *et al.*, 2021), MUs are recruited at lower absolute intensities. At the same time, the reduced DR for the lower-threshold MUs introduces an additional neural limitation to force production. Increasing contraction intensity, and recruiting higher-threshold MUs, the higher-threshold motoneurons with preserved functionality may in principle try to compensate for the force-loss caused by impaired lower-threshold motoneurons (already recruited and sustaining force production) but in practice would have little or no effect due to mechanical constraints of muscle fibres (Brocca *et al.*, 2015; Monti *et al.*, 2021). This last hypothesis suggests that DR reduction of lower-threshold MUs, alongside impaired muscle fibres mechanical contractile properties (Monti *et al.*, 2021) (and many other factors), could be responsible for the reduction in muscle force commonly observed after disuse.

### 3.8.2. Reduced DR, but not DR modulation, might be responsible for reduced muscle force

To further investigate the changes in MUs DR, we analysed the DR modulation ($\Delta DR_{R-T}$) of single MUs. In the total pool of MUs, the DR modulation was reduced for lower-, but not for higher-threshold MUs. However, in the same pool, lower-threshold MUs were recruited at a higher intensity in relative terms (i.e., the relative RT of the MUs decomposed at 10 and 25% MVC at LS10 was higher than at LS0). Therefore, we concluded that the DR modulation was only partially affected by ULLS and that the observed difference was mainly a consequence of a differently balanced population of MUs decomposed at LS10 compared to LS0. This was also confirmed in the pool of tracked MUs were no significant difference in DR modulation was observed. It should be noted, however, that tracked MUs showed a trend similar to what observed in the total pool, suggesting that significant alteration of DR modulation might become apparent with longer-term unloading or more severe models of disuse, as previously suggested (Duchateau & Hainaut, 1990). Indeed, the work of Duchateau and Hainaut on hand muscles (Duchateau & Hainaut, 1990) reported a larger reduction in DR modulation for lower- compared to higher-threshold MUs after 6-8 weeks of hand cast immobilization. This finding suggests that the preferential impact of disuse on the motoneurons innervating lower-threshold MUs should be expected for both smaller and larger muscles, despite different utilization of MUs recruitment strategies and DR modulation to sustain force production (i.e., smaller muscles are expected to achieve the full MUs recruitment at lower intensity of contraction, compared to large muscles, and to rely more on DR modulation to achieve the MVC

(Henneman *et al.*, 1965*a*; De Luca, 1985)). Unfortunately, this information is not available in the study of Seki (Seki *et al.*, 2001) which also reported a reduction in DR modulation after 6 weeks of cast immobilization but did not investigate whether this was more pronounced in lower- or higher-threshold MUs.

Altogether, our findings suggest reduced DR, but not DR modulation, as an early determinant of force loss after short periods of unloading and that impaired DR modulation might become a limiting factor at later stages.

### 3.8.3. Neural control is restored by an active recovery period

21 days of AR (about twice the duration of the ULLS intervention) with a resistance-exercise protocol executed at 70% 1RM completely restored the LS0 levels of muscle force and neural control. Our hypothesis is that increased neural drive to the muscle during the AR period, induced by increased demand of motor tasks (Škarabot *et al.*, 2021), stimulated both the recovery of intrinsic properties of the motoneurons and of the contractile muscle tissue. Additionally, some parameters (e.g., force steadiness and MUs DR) also exceeded the LS0 levels suggesting the early onset of some exercise-induced over compensatory adaptations (Škarabot *et al.*, 2021). In particular, the improved force steadiness might suggest an enhanced adaptive response of the superior centres of neuromuscular control (Dideriksen *et al.*, 2015).

The complete recovery observed after 21 days of AR, at least in young and healthy men, highlights the plasticity of the components involved in the regulation of neural control, and the complete reversibility of the changes induced by short periods of unloading. It should be noted, however, that although the full recovery was achieved, a longer time (compared to the duration of unloading) was necessary, likely suggesting a sort of unloading-induced *hysteresis* in the recovery process. Notably, the necessity of a prolonged recovery period for the restoration of the neural control in young and healthy men could have profound implications for fragile populations (e.g., older people), for which the recovery after a period of disuse could be difficult and further delayed (Suetta *et al.*, 2009).

### 3.8.4. Methodological considerations

In line with previous studies (Del Vecchio *et al.*, 2019*a*; Casolo *et al.*, 2021; Nuccio *et al.*, 2021), potential alterations in MUs behaviour could not be assessed during very high contraction intensities or at the MVC due to a progressive increase in the number of superimposed and overlapping MUs action potentials in the recorded EMG signal. Nevertheless, the range of intensity analysed in this study is crucial for most of the daily tasks and has, therefore, clinical and physiological relevance.

The differences in relative RT/DERT between LS0 and LS10 in the total pool of MUs indicate that the populations of MUs decomposed at the two data collection points might slightly differ, suggesting that alterations in the MUs action potential properties (Piasecki *et al.*, 2021; Inns *et al.*, 2022; Sarto *et al.*, 2022*a*) (such as the shape and its complexity (Sarto *et al.*, 2022*b*)) might have affected the results of the decomposition favouring the detection of MUs with a higher RT. This observation carries at least 2 implications; (i) the decomposition algorithm successfully identified active MUs even after an unloading period (ii) while comparing MUs properties before and after severe interventions, close attention has to be paid to the comparability of the decomposed pool of MUs (Power *et al.*, 2022). Therefore, longitudinal tracking of the same MUs provides stronger evidence of changes affecting the single MUs, although it significantly reduces the number of investigated MUs (about 20% of the total pool) and the statistical power. In addition, MUs tracking might preferentially identify MUs with a better-preserved action potential shape and therefore those less affected by the intervention (Power *et al.*, 2022). For this reason, the discussion of the paper focused mainly on the interpretation of the results obtained from the total pool, while the analysis of the tracked pool of MUs was used to validate and support the results.

We acknowledge, as a limitation in the study design, the absence of a control group which could have been useful to experimentally demonstrate the maintenance of the MUs properties across the study period and to verify the performance of decomposition and MUs tracking in absence of intervention.

Finally, even though 10 days of ULLS were sufficient to induce noticeable impairments in neural control, longer duration (de Boer *et al.*, 2007), more severe models of disuse (Widrick *et al.*, 2002) or different populations (e.g., older adults) (Mahmassani *et al.*, 2019) might highlight different adaptations.

## 3.9. Conclusion

Our novel results demonstrate, for the first time in large muscles, that ULLS induces a preferential deterioration of motoneurons innervating lower-threshold MUs and suggest this deterioration as one of the early determinants of force loss after periods of disuse. Furthermore, integrating our findings with the available literature, we propose that the preferential impact of disuse on the motoneurons innervating lower-threshold MUs is a fundamental physiological mechanism independent from the size, location and function of the considered muscle.

Additionally, the possibility to investigate non-invasively the changes in neural control after ULLS and AR with HD-EMG could have significant relevance for the development of perspective countermeasures aimed at delaying or recovering the disuse-induced impairments.

## 3.10. Supplementary Material

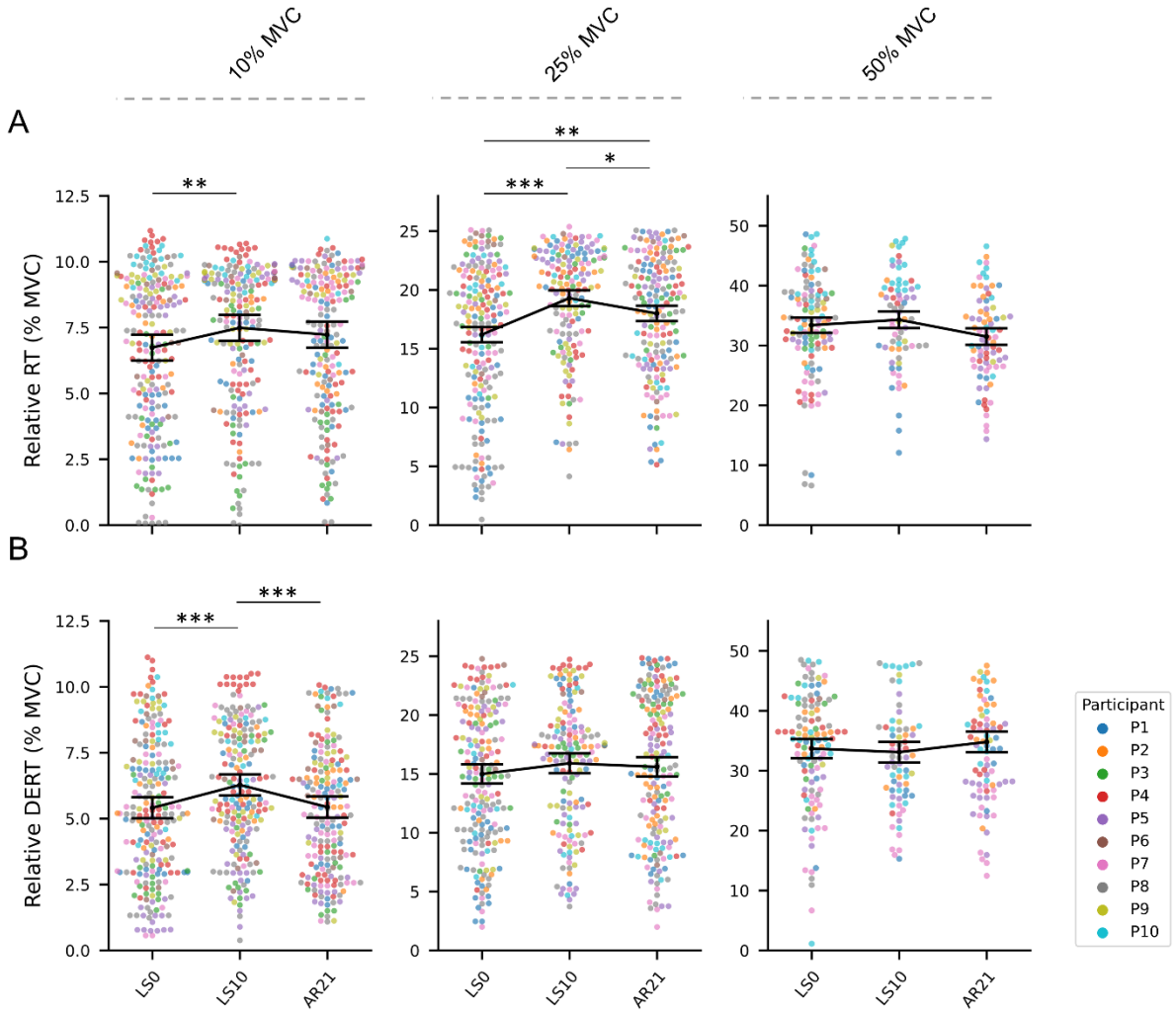


*Figure Supp 3-1: Swarm plots representing the relative (% MVC) MUs RT (A) and DERT (B) at the three data collection points. From left to right, MUs properties are presented for the three different submaximal contraction intensities (i.e., 10, 25 and 50% MVC). Individual MUs are represented by dots and clustered by subject. Summary data are presented as mean ± SEM and the direction of the changes is highlighted by a connection line. Significance levels are: *p<0.05, **p<0.01, ***p<0.001.*

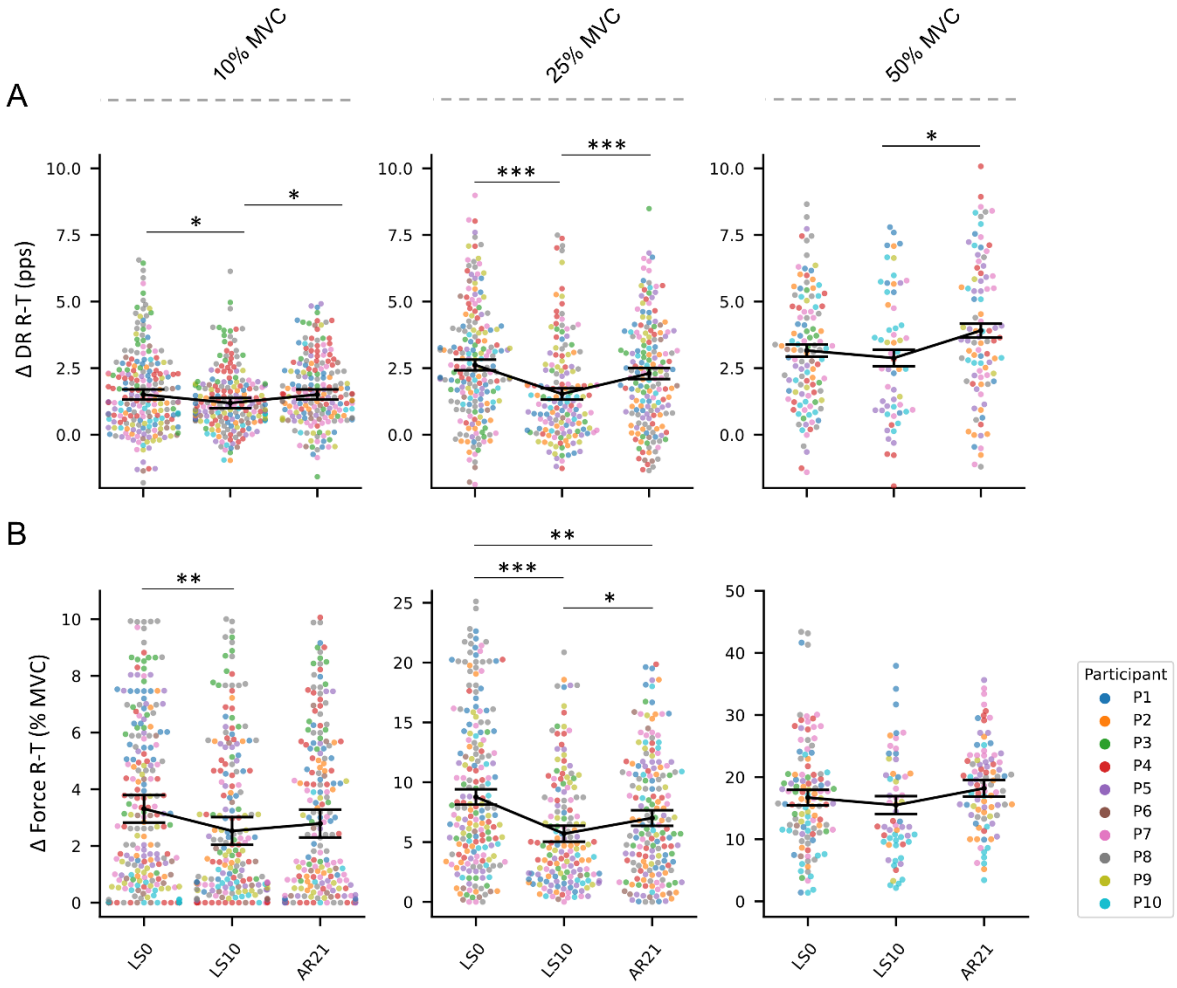


*Figure Supp 3-2: Swarm plots representing the ΔDR from recruitment to target force (A) and the Δ force from recruitment to target (B) at the three data collection points. From left to right, MUs properties are presented for the three different submaximal contraction intensities (i.e., 10, 25 and 50% MVC). Individual MUs are represented by dots and clustered by subject. Summary data are presented as mean ± SEM and the direction of the changes is highlighted by a connection line. Significance levels are: *p<0.05, **p<0.01, ***p<0.001.*

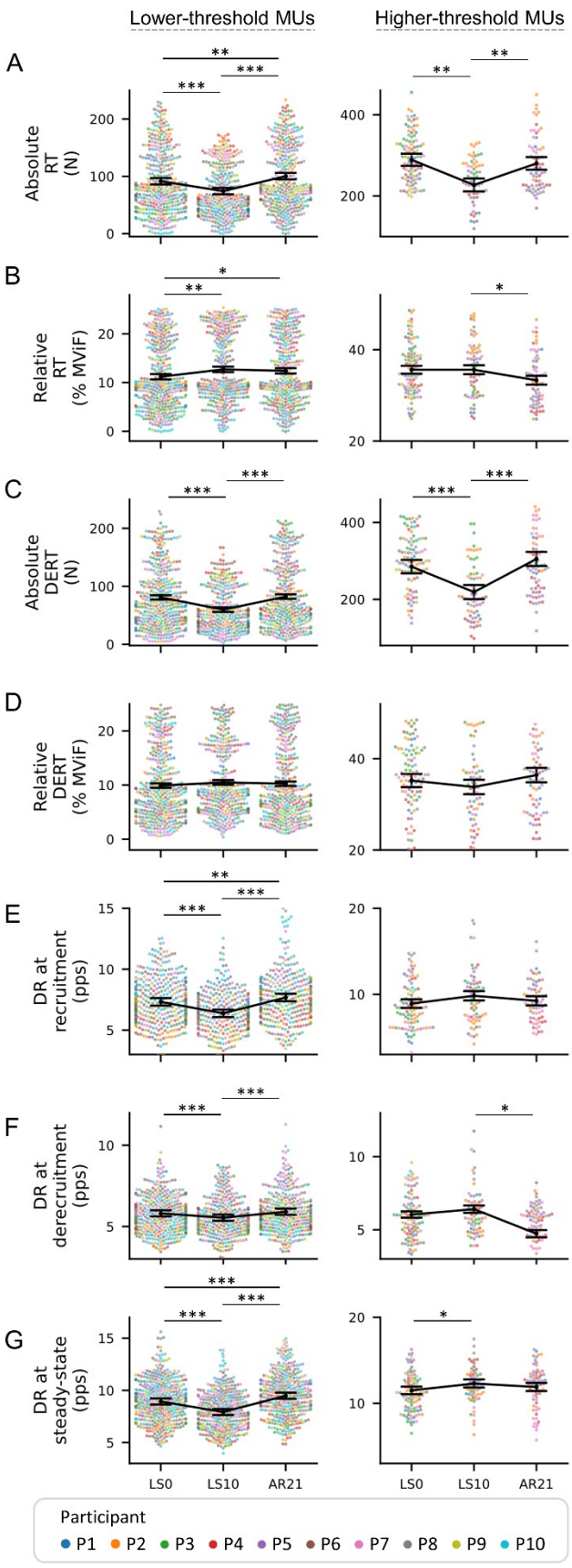


*Figure Supp 3-3: Swarm plots representing the MUs properties obtained from the pool of total MUs classified as lower- and higher-threshold. MUs RT and DERT are presented in both absolute (A, C) and relative terms (as percent of the MVC)(B, D) and MUs DR is shown at recruitment (E), derecruitment (F) and during the steady-state phase (G), at the three data collection points. From left to right, MUs properties are presented based on the classification of lower- and higher-threshold (i.e., recruited below or above 25% MVC). Individual MUs are represented by dots and clustered by subject. Summary data are presented as mean ± SEM and the direction of the changes is highlighted by a connection line. Significance levels are: *p<0.05, **p<0.01, ***p<0.001.*

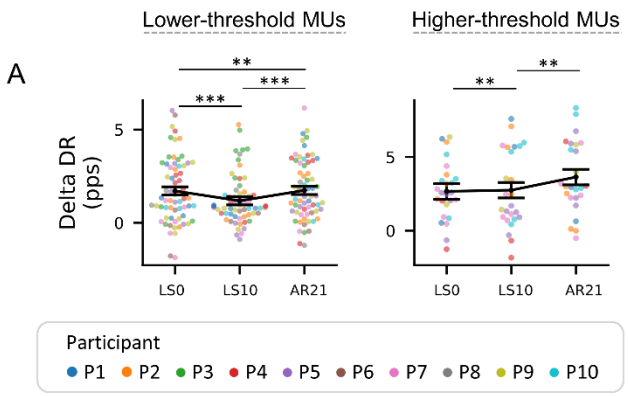


*Figure Supp 3-4: Swarm plots representing the ΔDR from recruitment to target force (A) obtained from the pool of tracked MUs at the three data collection points. From left to right, MUs properties are presented based on the classification of lower- and higher-threshold (i.e., recruited below or above 25% MVC). Individual MUs are represented by dots and clustered by subjects. Summary data are presented as mean ± SEM and the direction of the changes is highlighted by a connection line. No significant change was identified.*

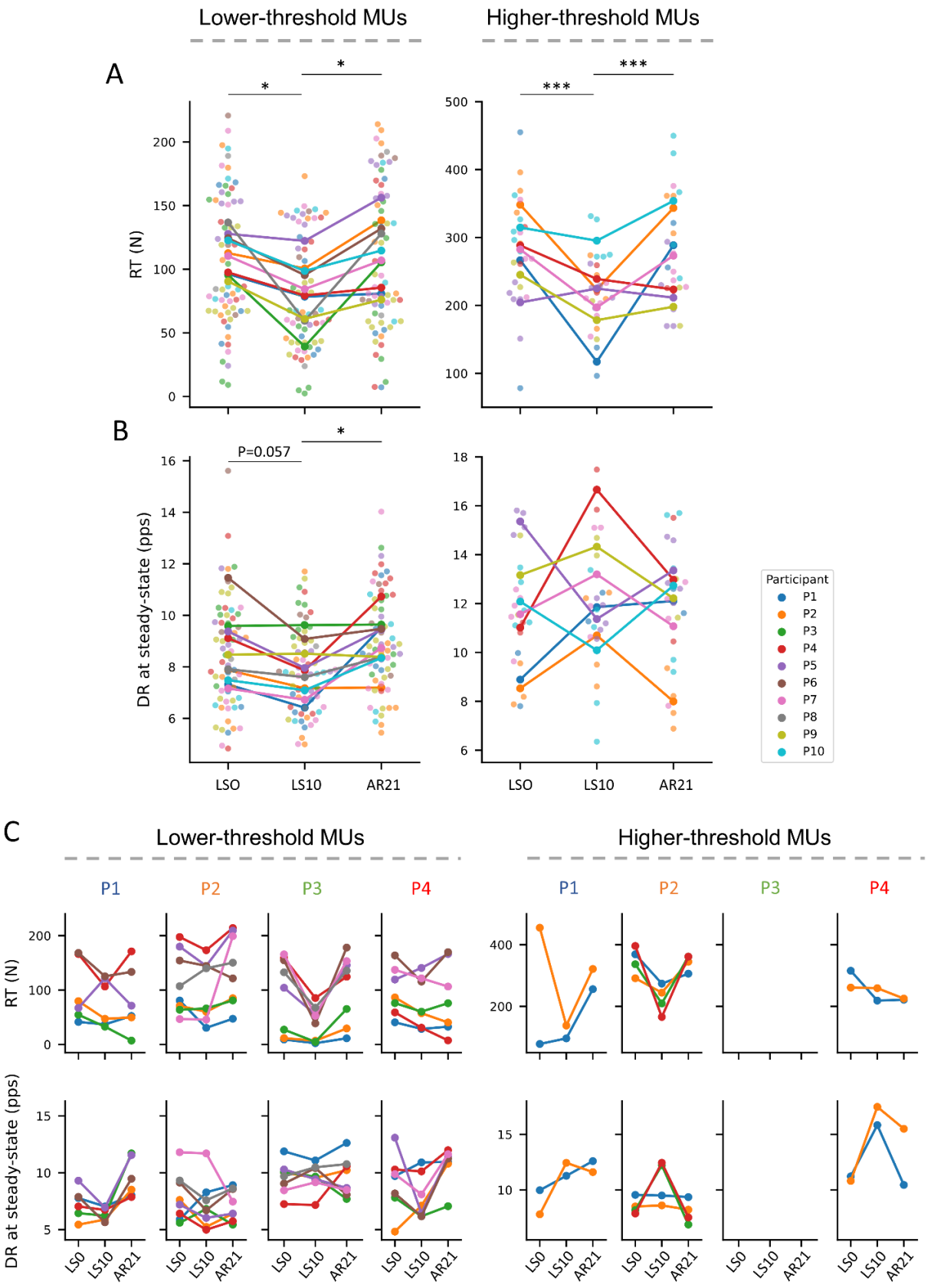


*Figure Supp 3-5: Absolute RT and DR during the steady-state phase of tracked MUs. Swarm plots representing the MUs absolute RT (A) and DR (B) classified as lower- and higher-threshold with the direction of the changes for each participant highlighted by connection lines. Individual MUs are represented by dots and clustered by subject. Significance levels are: *p<0.05, ***p<0.001. Representative pointplot showing the behaviour of the same MUs across the data collection points (C) of participants 1, 2, 3 and 4. No higher-threshold MUs were tracked across the 3 data collection points for participant 3.3.*

**Table Supp. 3-1**. Summary statistics for ANOVAs

| **Parameter** | **LS0** Mean (SD) | **LS10** Mean (SD) | **AR10** Mean (SD) | **AR21** Mean (SD) | **Overall** (p) | **LSO vs LS10** (p) | **LS10 vs AR21** (p) | **LS0 vs AR21** (p) |
|---|---|---|---|---|---|---|---|---|
| MVC (N) | 816.18 (97.22) | 573.20 (104.70) | 690.41 (82.09) | 806.54 (96.68) | < 0.001 | < 0.001 | < 0.001 | 0.769 |

| | **LSO vs AR10** (p) | **LS10 vs AR10** (p) | **AR10 vs AR21** (p) |
|---|---|---|---|
| | 0.001 | < 0.001 | < 0.001 |

| **Parameter** | **LS0** Mean (SD) | **LS10** Mean (SD) | **AR10** Mean (SD) | **AR21** Mean (SD) | **Overall** (p) | **LSO vs LS10** (p) | **LS10 vs AR21** (p) | **LS0 vs AR21** (p) |
|---|---|---|---|---|---|---|---|---|
| COVsteady at 10% (%) | 2.94 (0.73) | 3.07 (0.43) | / | 2.44 (0.42) | 0.017 | 0.619 | 0.020 | 0.020 |
| COVsteady at 25% (%) | 1.95 (0.51) | 3.03 (0.44) | / | 1.52 (0.28) | 0.001 | 0.008 | 0.003 | 0.004 |
| COVsteady at 50% (%) | 1.77 (0.28) | 2.03 (0.38) | / | 1.50 (0.21) | 0.001 | 0.112 | 0.002 | 0.033 |

N, Newton; RT, recruitment threshold; DERT, derecruitment threshold; DR, discharge rate.

**Table Supp. 3-2**. MUs properties in the total pool of MUs divided by contraction intensity

| Parameter | LS0<br>Mean (SE) | LS10<br>Mean (SE) | AR21<br>Mean (SE) | Model results<br>(p) | LSO vs LS10<br>(p) | LS10 vs AR21<br>(p) | LS0 vs AR21<br>(p) |
|---|---|---|---|---|---|---|---|
| **10% MVC** | | | | | | | |
| Absolute RT | 55.1 (4.50) | 43.7 (4.52) | 58.1 (4.53) | < 0.001 | < 0.001 | < 0.001 | 0.116 |
| Relative RT | 6.74 (0.49) | 7.49 (0.49) | 7.23 (0.50) | 0.009 | 0.008 | 0.306 | 0.107 |
| Absolute DERT | 44.9 (3.86) | 36.4 (3.88) | 44.2 (3.89) | < 0.001 | < 0.001 | < 0.001 | 0.667 |
| Relative DERT | 5.41 (0.40) | 6.28 (0.40) | 5.44 (0.40) | < 0.001 | < 0.001 | < 0.001 | 0.920 |
| DR at recruitment | 7.02 (0.33) | 6.16 (0.33) | 7.28 (0.33) | < 0.001 | < 0.001 | < 0.001 | 0.135 |
| DR at derecruitment | 6.02 (0.21) | 5.68 (0.21) | 6.14 (0.21) | < 0.001 | 0.002 | < 0.001 | 0.249 |
| DR at steady-state | 8.52 (0.43) | 7.35 (0.44) | 8.78 (0.44) | < 0.001 | < 0.001 | < 0.001 | 0.247 |
| $\Delta DR_{R-T}$ | 1.51 (0.19) | 1.19 (0.19) | 1.51 (0.19) | 0.017 | 0.035 | 0.035 | 0.998 |
| $\Delta Force_{R-T}$ | 3.31 (0.48) | 2.53 (0.49) | 2.79 (0.49) | 0.006 | 0.005 | 0.302 | 0.078 |
| **25% MVC** | | | | | | | |
| Absolute RT | 132 (6.88) | 112 (7.04) | 146 (6.93) | < 0.001 | < 0.001 | < 0.001 | 0.002 |
| Relative RT | 16.2 (0.64) | 19.3 (0.67) | 18.0 (0.65) | < 0.001 | < 0.001 | 0.025 | 0.003 |
| Absolute DERT | 121.5 (6.0) | 90.6 (6.19) | 124.9 (6.06) | < 0.001 | < 0.001 | < 0.001 | 0.447 |
| Relative DERT | 15.0 (0.81) | 15.9 (0.84) | 15.6 (0.83) | 0.342 | | | |
| DR at recruitment | 7.66 (0.37) | 6.70 (0.37) | 8.2 (0.37) | < 0.001 | < 0.001 | < 0.001 | < 0.001 |
| DR at derecruitment | 5.56 (0.19) | 5.37 (0.19) | 5.71 (0.19) | 0.014 | 0.193 | 0.011 | 0.193 |
| DR at steady-state | 9.39 (0.33) | 8.47 (0.33) | 10.08 (0.33) | < 0.001 | < 0.001 | < 0.001 | < 0.001 |
| $\Delta DR_{R-T}$ | 2.62 (0.20) | 1.53 (0.21) | 2.30 (0.21) | < 0.001 | < 0.001 | < 0.001 | 0.109 |
| $\Delta Force_{R-T}$ | 8.77 (0.64) | 5.70 (0.67) | 7.01 (0.65) | < 0.001 | < 0.001 | 0.025 | 0.003 |
| **50% MVC** | | | | | | | |
| Absolute RT | 271 (15.3) | 218 (16.2) | 264 (16.1) | < 0.001 | < 0.001 | < 0.001 | 0.474 |
| Relative RT | 33.4 (1.26) | 34.3 (1.39) | 31.5 (1.38) | 0.055 | | | |
| Absolute DERT | 273 (17.0) | 212 (18.0) | 289 (17.9) | < 0.001 | < 0.001 | < 0.001 | 0.123 |
| Relative DERT | 33.7 (1.60) | 33.1 (1.73) | 34.8 (1.72) | 0.445 | | | |
| DR at recruitment | 8.82 (0.47) | 9.71 (0.51) | 9.03 (0.50) | 0.04 | 0.039 | 0.159 | 0.558 |
| DR at derecruitment | 5.99 (0.22) | 6.43 (0.24) | 5.76 (0.24) | 0.013 | 0.080 | 0.012 | 0.279 |
| DR at steady-state | 11.7 (0.44) | 12.4 (0.47) | 12.2 (0.47) | 0.038 | 0.044 | 0.499 | 0.178 |
| $\Delta DR_{R-T}$ | 3.16 (0.23) | 2.88 (0.31) | 3.91 (0.26) | 0.022 | 0.484 | 0.039 | 0.062 |
| $\Delta Force_{R-T}$ | 16.7 (1.25) | 15.5 (1.44) | 18.2 (1.33) | 0.070 | | | |

Summary statistics of MUs properties with linear models.
For RT and DERT, absolute values are expressed in newton (N) and relative values are expressed as % MVC. MUs DR is expressed as pulse per second (pps). Normality of residuals was granted for all the variables.
RT, recruitment threshold; DERT, derecruitment threshold; DR, discharge rate; $\Delta DR_{R-T}$, delta DR between recruitment and target force; $\Delta Force_{R-T}$, delta force between recruitment and target; MVC, maximum voluntary isometric force.

**Table Supp. 3-3**. MUs properties in the total pool of MUs divided in lower- and higher-threshold MUs

| Parameter | LS0<br>Mean (SE) | LS10<br>Mean (SE) | AR21<br>Mean (SE) | Model results<br>(p) | LSO vs LS10<br>(p) | LS10 vs AR21<br>(p) | LS0 vs AR21<br>(p) |
|---|---|---|---|---|---|---|---|
| **Lower-threshold** | | | | | | | |
| Absolute RT † | 91.5 (5.58) | 74.2 (5.67) | 100.3 (5.66) | < 0.001 | < 0.001 | < 0.001 | 0.013 |
| Relative RT † | 11.2 (0.54) | 12.7 (0.56) | 12.4 (0.55) | 0.004 | 0.005 | 0.505 | 0.026 |
| Absolute DERT † | 80.9 (3.79) | 59.8 (3.92) | 82.3 (3.89) | < 0.001 | < 0.001 | < 0.001 | 0.677 |
| Relative DERT † | 9.90 (0.41) | 10.48 (0.43) | 10.24 (0.42) | 0.459 | | | |
| DR at recruitment | 7.32 (0.31) | 6.38 (0.31) | 7.68 (0.31) | < 0.001 | < 0.001 | < 0.001 | 0.004 |
| DR at derecruitment | 5.81 (0.19) | 5.54 (0.19) | 5.91 (0.19) | < 0.001 | < 0.001 | < 0.001 | 0.177 |
| DR at steady-state | 8.94 (0.29) | 7.93 (0.29) | 9.49 (2.29) | < 0.001 | < 0.001 | < 0.001 | < 0.001 |
| **Higher-threshold** | | | | | | | |
| Absolute RT | 289 (15.0) | 227 (15.6) | 280 (15.6) | < 0.001 | < 0.001 | < 0.001 | 0.267 |
| Relative RT | 35.6 (0.86) | 35.6 (0.97) | 33.3 (0.97) | 0.020 | 0.990 | 0.035 | 0.035 |
| Absolute DERT | 285 (17.4) | 219 (18.3) | 305 (18.3) | < 0.001 | < 0.001 | < 0.001 | 0.052 |
| Relative DERT | 35.2 (1.45) | 33.8 (1.58) | 36.4 (1.58) | 0.125 | | | |
| DR at recruitment | 8.92 (0.50) | 9.83 (0.54) | 9.24 (0.54) | 0.060 | | | |
| DR at derecruitment | 6.04 (0.22) | 6.41 (0.25) | 4.73 (0.25) | 0.021 | 0.201 | 0.017 | 0.201 |
| DR at steady-state | 11.5 (0.44) | 12.3 (0.47) | 11.9 (0.47) | 0.037 | 0.033 | 0.378 | 0.378 |

Summary statistics of MUs properties with linear models.
For RT and DERT, absolute values are expressed in newton (N) and relative values are expressed as % MVC. MUs DR is expressed as pulse per second (pps). † indicates variables analysed with generalized linear mixed effect models since normality of residuals was not granted.
RT, recruitment threshold; DERT, derecruitment threshold; DR, discharge rate; MVC, maximum voluntary isometric force.

**Table Supp. 3-4**. MUs properties in the tracked pool of MUs divided in lower- and higher-threshold MUs

| Parameter | LS0<br>Mean (SE) | LS10<br>Mean (SE) | AR21<br>Mean (SE) | Model results<br>(p) | LSO vs LS10<br>(p) | LS10 vs AR21<br>(p) | LS0 vs AR21<br>(p) |
|---|---|---|---|---|---|---|---|
| **Lower-threshold** | | | | | | | |
| Absolute RT † | 107.0 (7.99) | 80.3 (5.99) | 108.0 (8.07) | 0.011 | 0.017 | 0.017 | 0.929 |
| Relative RT † | 13.4 (1.11) | 14.2 (1.19) | 13.6 (1.13) | 0.851 | | | |
| Absolute DERT † | 93.5 (7.29) | 64.0 (4.99) | 60.6 (7.06) | 0.002 | 0.003 | 0.004 | 0.774 |
| Relative DERT † | 11.8 (0.942) | 11.5 (0.91) | 11.5 (0.92) | 0.962 | | | |
| DR at recruitment | 7.11 (0.34) | 6.48 (0.34) | 7.19 (0.34) | 0.021 | 0.051 | 0.033 | 0.751 |
| DR at derecruitment | 5.90 (0.22) | 5.60 (0.22) | 5.81 (0.22) | 0.278 | | | |
| DR at steady-state † | 8.39 (0.41) | 7.78 (0.36) | 8.79 (0.45) | 0.002 | 0.057 | 0.001 | 0.157 |
| **Higher-threshold** | | | | | | | |
| Absolute RT | 274 (19.9) | 216 (19.9) | 274 (19.9) | 0.001 | 0.003 | 0.003 | 0.976 |
| Relative RT | 34.2 (1.73) | 35.7 (1.73) | 32.9 (1.73) | 0.399 | | | |
| Absolute DERT | 268 (20.6) | 189 (20.6) | 299 (20.6) | < 0.001 | < 0.001 | < 0.001 | 0.076 |
| Relative DERT | 33.3 (2.21) | 31.0 (2.21) | 36.2 (2.21) | 0.056 | | | |
| DR at recruitment | 9.22 (0.86) | 9.42 (0.86) | 9.27 (0.86) | 0.952 | | | |
| DR at derecruitment | 6.15 (0.38) | 6.24 (0.38) | 5.65 (0.38) | 0.254 | | | |
| DR at steady-state | 11.9 (0.70) | 12.1 (0.70) | 11.8 (0.70) | 0.817 | | | |

Summary statistics of MUs properties with linear models.
For RT and DERT, absolute values are expressed in newton (N) and relative values are expressed as % MVC. MUs DR is expressed as pulse per second (pps). † indicates variables analysed with generalized linear mixed effect models since normality of residuals was not granted.
RT, recruitment threshold; DERT, derecruitment threshold; DR, discharge rate; MVC, maximum voluntary isometric force.

## 4. Experimental Chapter 2: Non-invasive motor unit analysis reveals distinct neural strategies of muscle force production in young people with uncomplicated type 1 diabetes

*Authors:*

Giacomo Valli [a†], Rui Wu [b†], Dean Minnock [b*], Giuseppe Sirago [a], Giosuè Annibalini [c], Andrea Casolo [a], Alessandro Del Vecchio [d], Luana Toniolo [a], Elena Barbieri [c] & Giuseppe De Vito [a]

†Equally contributing authors

*Corresponding author

[a] Department of Biomedical Sciences, University of Padova, Padova, Italy

[b] School of Public Health, Physiotherapy and Sports Science, University College Dublin, Dublin, Ireland

[c] Department of Biomolecular Sciences, University of Urbino Carlo Bo, Urbino, Italy

[d] Department Artificial Intelligence in Biomedical Engineering, Friedrich-Alexander University, Erlangen, Germany

*Author contributions:*

RW, DM and GDV conceptualized and designed the study. RW, DM, ADV and GDV performed data collection. GV and RW analyzed the electromyography data. GV, GS, GA, LT, EB analyzed the biological data. GV and RW performed the statistical analysis. GV drafted the manuscript and all the authors revised it.

The article has been submitted and it is currently under revision.

## 4.1. Background

Type 1 diabetes, is a chronic autoimmune disorder characterized by the destruction of insulin-producing beta cells in the pancreas (Daneman, 2006). The exact trigger for this autoimmune response remains the subject of research, but a combination of genetic predisposition and environmental factors is believed to underpin its onset (Redondo *et al.*, 2001; Devendra *et al.*, 2004). This disease typically develops in children and young adults, although it can occur at any age. The onset is often sudden, with symptoms such as excessive thirst, frequent urination, unexplained weight loss, and fatigue (Devendra *et al.*, 2004).

The destruction of pancreatic beta cells impairs the body's ability to regulate blood glucose levels effectively because, without insulin, glucose accumulates in the bloodstream causing high blood sugar levels (in a condition named hyperglycaemia). Repetitive dysregulation of the physiological glycaemic levels leads to a number of severe complications including heart disease, stroke, kidney disease, neuropathy, and vision problems (Daneman, 2006). Therefore, maintaining blood glucose levels within a target range is essential (ElSayed *et al.*, 2023).

At present, the therapeutic approach remains limited to the exogenous administration of insulin. This indispensable hormone is supplied either through traditional injections or continuous infusion via insulin pumps, constituting the cornerstone of T1D management (von Scholten *et al.*, 2021). Effective management of the type 1 diabetes condition requires careful monitoring of sugars and insulin intake and can delay the onset of long-term complications (Nathan *et al.*, 1993). However, people with type 1 diabetes still face a sevenfold excess in mortality compared to the non-diabetic population (Dorman *et al.*, 1984) and, even when they are controlling diabetes with external insulin administration, still experience a reduction in life expectancy of about 15 years, due to the comorbidities and complications that inevitably arise (Pelletier *et al.*, 2012).

In this framework, a better understanding of the consequences of type 1 diabetes is a driving force behind advancements in treatment and care, as these discoveries lead to new therapies, medications, and technologies, offering hope for improved quality of life and life expectancy (von Scholten *et al.*, 2021). Additionally, the development of new screening techniques allowing for an early detection of these complications, is fundamental to promptly implement optimal interventions, thereby maximizing positive clinical outcomes and alleviating the load on the healthcare system.

## 4.2. Abstract

**Purpose**: to investigate the early consequences of type 1 diabetes on the neural strategies of muscle force production.

**Methods**: motor units (MUs) activity was recorded from the *vastus lateralis* muscle with High-Density surface Electromyography during isometric knee extension at 20 and 40% of maximum voluntary contraction (MVC) in 8 type 1 diabetes (4 males and 4 females, 30.5±3.6 years) and 8 control (4 males and 4 females, 27.3±5.9 years) participants. Muscle biopsies were also collected from *vastus lateralis* and muscle fibre analyses (myosin heavy chain (MyHC) isoforms) were conducted for fibre type distribution (protein content) and mRNA expression.

**Results**: MVC was comparable between groups as well as MUs conduction velocity, action potentials' amplitude and proportions of MyHC protein isoforms. Nonetheless, MUs discharge rate, relative derecruitment thresholds and mRNA expression of MyHC isoform I were lower in type 1 diabetes.

**Conclusion**: young people with uncomplicated type 1 diabetes adopt different neural strategies to control muscle force production compared to control. Furthermore, these differences are detectable non-invasively prior to any functional manifestation (compared to force production and fibre type distribution).

**Significance**: These novel findings suggest that type 1 diabetes has early consequences on the neuromuscular system and highlights the necessity of a more comprehensive characterization of neural control in this population.

## 4.3. Highlights

- Young uncomplicated type 1 diabetes and control participants exhibit different neural strategies of muscle force production
- These differences are detectable non-invasively with High-Density Electromyography before any functional manifestation
- These findings highlight the necessity of an in depth characterization of the neuromuscular functioning in type 1 diabetes

## 4.4. Abbreviations

In alphabetical order:

| | |
|---|---|
| 5-HT | Serotonin, 5-hydroxytryptamine |
| AHP | Afterhyperpolarization |
| AIC | Akaike Information Criterion |
| BMI | Body mass index |
| $Ca^{2+}$ | Calcium |
| COVsteady | Coefficient of variation of the steady-state phase |
| CV | Conduction velocity |
| DERT | Derecruitment threshold |
| DEXA | Dual-energy X-ray absorptiometry |
| DR | Discharge rate |
| HD-EMG | High-Density surface Electromyography |
| MUs | Motor units |
| MVC | Maximum voluntary isometric contraction |
| MyHC | Myosin heavy-chain |
| Nm | Newton-metre |
| PNR | Pulse to noise ratio |
| RMS | Root mean square |
| RT | Recruitment threshold |
| $VO_{2max}$ | Maximum oxygen consumption |

## 4.5. Introduction

Type 1 diabetes is a chronic disease caused by immune-mediated destruction of pancreatic beta-cells that are responsible for insulin production and maintenance of glucose homeostasis. This condition is estimated to affect about 10% of the total diabetic population and its incidence is rapidly increasing worldwide (Daneman, 2006; Mayer-Davis *et al.*, 2017). Although a considerable heterogeneity exists within the clinical phenotype of type 1 diabetes, the progression of the condition leads to the development of comorbidities and complications that could eventually affect quality of life (Alvarado-Martel *et al.*, 2015) and increase the risk of premature mortality (Vergès, 2020). To delay the onset of these complications, early detection of subtle alterations is fundamental and, for this reason, people living with type 1 diabetes undertake regular health screenings. Unexpectedly, during these screenings little attention is being devoted to the neuromuscular system despite its importance not only for maintaining glucose homeostasis, but also for locomotor capacity and independence in carrying out activities of daily living (Periasamy *et al.*, 2017). Additionally, it is now recognised that the degeneration of skeletal muscle health is a direct consequence of type 1 diabetes (Monaco *et al.*, 2019; Minnock *et al.*, 2022).

Muscles of people with uncomplicated type 1 diabetes overexpress pro-inflammatory genes (Minnock *et al.*, 2022), exhibit alterations in mitochondrial ultrastructure and bioenergetics, altered proportions of type 2 (glycolytic) fibres and increased myofiber grouping (Dial *et al.*, 2021), compared to healthy people. Taken together, these molecular alterations cause in people with uncomplicated diabetes, a reduction in muscle force, increased fatigability (Monaco *et al.*, 2019) and reduced adaptations to exercise (Minnock *et al.*, 2022). Interestingly, this cluster of impairments known as "diabetic myopathy" has been defined as a form of accelerated muscle aging, as it manifests also in young adults (Monaco *et al.*, 2019). In this framework, it is important to note that the available literature is focusing on the study of the muscle tissue in people classified as “with” or “without” diagnosed neuropathy, and that this classification has been used to suggest that muscle alterations precede the onset of diabetic neuropathy (Monaco *et al.*, 2017). However, very little is known about the neural condition of this population before the clinical manifestation of neuropathy.

As a matter of fact, muscle health and function do not depend solely on intrinsic properties of the muscle fibres, but rely on the interaction with neural components that determine the neural drive to the muscle (i.e., the sum of the motoneurons spiking activities) (Farina *et al.*, 2014*b*).

Specifically, the transmission of motor stimuli from the motor cortex to the effector muscle is entrusted to specialised cells, the motoneurons, which are concurrently responsible for direct transmission of the activation signal and for the integration of multiple excitatory and inhibitory inputs (Heckman & Enoka, 2004). Therefore, modifications to the motoneuron transmission or dysregulation of its modulatory inputs can significantly impact the neural drive to the muscle.

Relating to the theory of accelerated muscle aging, recent evidence of motoneuron deterioration in the aged-muscle (Hepple & Rice, 2016; Larsson *et al.*, 2019) may indirectly suggest a potentially similar degeneration of the motoneurons and/or alterations of their properties, as a consequence of type 1 diabetes. In addition, it is also plausible to suggest that the chronic inflammation and altered mitochondrial functioning that are evident in people with type 1 diabetes could be associated with neural degeneration (Feldman *et al.*, 2017). Taken together, all these alterations should be likely reflected into a different behaviour and properties of the voluntarily activated motor units (MUs).

In light of this, the main aim of the present study was to investigate the behaviour of single MUs in young people with uncomplicated type 1 diabetes compared to a healthy control group, in order to expand our knowledge on the neural condition of this population and to explore the neuromuscular consequences of the theory of accelerated aging. In line with this theory, our hypothesis was that people with type 1 diabetes should present a different MUs behaviour compared to the control group, possibly reflecting changes in MUs properties commonly observed during aging (e.g., reduced MUs firing frequency). However, we also expected these differences to be mild, in agreement with previous evidence from our group on mild alterations on molecular markers of muscle health (e.g., inflammation) (Minnock *et al.*, 2022).

## 4.6. Methods

### 4.6.1. Participants and experimental protocol

This study was part of a larger investigation aimed at clarifying the neural and muscular condition of those living with type 1 diabetes in comparison to healthy people (Minnock *et al.*, 2022).

This study was approved by the Human Research Ethics Committee of University College Dublin (LS-17-113-Minnock-DeVito) and conformed to the standards set by the Declaration of Helsinki. Details of the study protocol were explained orally and in writing to the participants prior to obtaining their written informed consent to partake in the intervention.

Sixteen participants, 8 living with type 1 diabetes without comorbidities, and 8 healthy controls volunteered for the study. The groups were equally matched for sex (4 males and 4 females per group). Inclusion criteria were age between 18 and 45 years, type 1 diabetes diagnosed for at least 12 months, BMI <30 kg/m2, non-smokers, absence of comorbidities and complications (self-reported) and no ongoing chronic pharmacological treatments. Participants were not habitual exercisers (less than 2h of physical activity per week (Active Australia Survey)) and with mean metabolic equivalent of task expenditure <500 MET weekly (GPAQ scores). The type 1 diabetes group consisted of seven multiple daily injection users and one insulin pump user with an HbA1c of 8.31 ± 2.40% (67.34 ± 26.19 mmol/mol) and diabetes duration of 16.9 ± 7.6 years. All female participants were using oral hormonal contraceptives.

Participants visited the research facility in three different occasions with 7 days between each visit. During the first visit, participants were familiarized with study procedures, anthropometric data and maximum oxygen consumption ($VO_{2max}$) were obtained. In the second visit, the maximum voluntary isometric contraction (MVC) was measured and muscle electrical activity was recorded with HD-EMG. In the third visit, muscle biopsies were collected.

Participants were asked to refrain from intense exercise, coffee and alcohol intake during the 24 hours preceding data collection. All the tests were performed in the morning (Valli *et al.*, 2021).

### 4.6.2. Body composition, maximal oxygen consumption and voluntary isometric torque

Body composition was assessed by dual-energy X-ray absorptiometry (DEXA) (Lunar iDXA, GE Healthcare, London, UK).

$VO_{2max}$ was measured during a one-minute incremental test on a cycle ergometer (Excalibur Sport) to volitional exhaustion using an open circuit metabolimeter (Quarkb2 Cosmed, Rome, Italy).

MVC of the quadriceps muscle was assessed at 90° knee angle, with hip fixed at 90° using a knee dynamometer with a load cell attached above the ankle through straps. The participant's back was supported in an upright position and the hip was stabilised to the table with adjustable straps to limit compensation (Valli *et al.*, 2023). Three attempts were allowed with a 3-min rest between trials. During each trial, participants were instructed to generate force "as strongly and as quickly as possible", and then to maintain the contraction for 3 seconds. Loud verbal encouragement and visual feedback were provided. The highest force (N) was converted to torque (Nm) by multiplying the force value for the lever arm expressed in meters. The maximum torque value attained by each participant was considered for the MVC calculation and used to determine the normalized target torques of the submaximal trapezoidal contractions.

### 4.6.3. High-Density EMG recordings

Myoelectrical activity of the *vastus lateralis* muscle was recorded with HD-EMG during submaximal trapezoidal isometric contractions using an adhesive matrix of 64 equally spaced electrodes (5 columns and 13 rows with 8-mm interelectrode distance (GR08MM1305, OT Bioelettronica, Torino, Italy) filled with conductive cream (Ac cream, OT Bioelettronica, Torino, Italy).

The matrix was positioned and oriented as previously described (Casolo *et al.*, 2020) with a 16-electrode dry array used to identify the innervation zone located in the distal portion of the *vastus lateralis* muscle (Botter *et al.*, 2011*b*). The innervation zone was identified as the point of inversion in the propagation direction of action potentials along the electrode column, and the correct orientation was considered the one providing the clearest visualisation of action potentials propagation (Del Vecchio *et al.*, 2017). Muscle belly was identified by palpation to avoid placing the matrix across adjacent muscles.

Before placing the matrix, the skin was accurately shaved, cleaned with 70% ethanol and then with abrasive-conductive paste (Spes medica, Salerno, Italy).

Trapezoidal contractions were performed at 20 and 40% of the MVC and repeated twice with 1 minute of rest. Each contraction consisted of a ramp-up and a ramp-down phase with a constant increase/decrease speed of 5% MVC per second, with a 10 seconds steady-state phase in between.

The two intensities were proposed in random order to minimise any potential effect of fatigue on MUs activity. Participants received real-time visual feedback of the torque produced and were requested to match it as precisely as possible.

The HD-EMG and torque signals were sampled at 2048 Hz with the EMG-Quattrocento (OT Bioelettronica, Torino, Italy). The HD-EMG signal was recorded in monopolar configuration, amplified (×150) and band-pass filtered (10–500 Hz) at source (Del Vecchio *et al.*, 2019*a*).

### 4.6.4. Torque and High-Density EMG analysis

Torque signal was low-pass filtered (fourth-order, zero-lag, Butterworth) with a cut-off frequency of 15 Hz (Del Vecchio *et al.*, 2019*a*) and converted to Nm. Torque steadiness was computed as the coefficient of variation of the steady-state phase (COVsteady) and expressed as percentage (Wu *et al.*, 2019; Enoka & Farina, 2021).

The HD-EMG signal was band-pass filtered between 20 and 500 Hz (second-order, Butterworth) and decomposed to obtain the discharge pattern of the MUs with a validated technique based on blind source separation (Negro *et al.*, 2016). After the decomposition, the discharge pattern was visually inspected and manually edited (Hug *et al.*, 2021*a*). Identified MUs whose discharge pattern had a pulse to noise ratio (PNR) ≥ 28 dB, which corresponds to a sensitivity above 85%, were maintained for further analyses (Holobar *et al.*, 2014). Signals were processed and analysed using custom-written scripts (MATLAB R2020a, MathWorks, Natick, MA, USA; Python 3.9.7, Python Software Foundation, USA).

All the MUs decomposed from the two trapezoidal contractions recorded at the same intensity (for each participant) were pooled and analysed together after the removal of duplicated MUs, in order to reduce the risk of having too small and non-representative samples of MUs. MUs were considered duplicates if the two-dimensional cross-correlation coefficient between the action potential waveforms of two individual MUs was ≥ 0.9 as previously described (Maathuis *et al.*, 2008; Valli *et al.*, 2023). In case of duplicated MUs, the MU with the lowest PNR was removed from the following analyses. The MUs action potential waveforms were generated by spike-triggered averaging on a 50 ms time-window (Martinez-Valdes *et al.*, 2017).

From the discharge pattern of the individual MUs, the recruitment threshold (RT), derecruitment threshold (DERT), the average discharge rate (DR) at recruitment, derecruitment and

during the steady-state were computed for each identified MU. From the MUs action potential waveforms, MUs conduction velocity (CV) and action potential amplitude were computed.

MUs RT and DERT were defined as the normalised torque level (% MVC) corresponding to the first and last MUs discharge, respectively (McManus *et al.*, 2021).

MUs DR was calculated over the first and last 4 discharges at recruitment and de-recruitment, respectively, and during the entire steady-state phase (Del Vecchio *et al.*, 2019*a*).

MUs CV and MUs action potential amplitude were computed during the steady-state phase on the double differential derivation of MUs action potential waveforms along the electrode columns as previously extensively described (Casolo *et al.*, 2020). Briefly, a minimum of four up to a maximum of eight double differential channels belonging to the same electrode column were selected. Selected channels were those presenting the clearest propagation of action potentials with minimal change in shape and the highest correlation coefficient. Once the channels were selected, a multichannel maximum likelihood algorithm was adopted to calculate MUs CV (Farina *et al.*, 2001).

MUs action potential amplitude was calculated as the root mean square of the waveforms (RMS) on the same channels used for CV calculation.

### 4.6.5. Muscle sampling, myosin heavy-chain isoforms and gene expression analysis

Muscle biopsies were collected using a 14-gauge semi-automatic spring-loaded biopsy system with a compatible coaxial introducer needle (Medax Srl Unipersonale; San Possidonio, Italy). Biopsies were taken at rest from the vastus lateralis muscle, immediately frozen in liquid nitrogen and stored at −80°C (Minnock *et al.*, 2022).

Without thawing, a portion of muscle tissues was weighed (≤30 mg), placed directly into the QIAzol Lysis Buffer (Qiagen, Milan, Italy), and ruptured using a Polytron homogeniser (Kinematica AG, Switzerland). Total RNA was extracted and analysed by real-time PCR as previously described (Minnock *et al.*, 2020).

Sequences of the specific primers are: MyHC1-F 5’-CAG AGA AGC TGC TCA GCT C-3’ and MyHC1-R 5’-GCG TGA TGA TGC GGC TCA-3’; MyHC2A-F 5’-CTG ATT CAC TAT GCT GGT GTT-3’ and MyHC2A-R 5’-TCC TCC AGC TCC CTC TCC TT-3’; MyHC2X-F 5’-ACC TGG TGG ACA AAC TGC AA-3’ and MyHC2X-R 5’-GGT CAC CTT TCA GCA GTT AGA-3’.

Another portion of muscle tissue was used to assess the relative content of Myosin heavy-chain (MyHC) protein isoforms (Monti *et al.*, 2021). Muscle biopsy was mechanically solubilised in Laemmli solution (Laemmli, 1970) in the presence of proteases and phosphatases inhibitors, and subjected to a single cycle of thermal shock at 65°C before being cooled down at −20°C. Protein concentration was determined using the Folin–Lowry method with BSA as a reference (LOWRY *et al.*, 1951). Approximately 25 µg of protein from each sample were separated on 8% SDS-PAGE mini-gels (Mini-PROTEAN Tetra Handcast System, Bio-Rad) for 1 h at 50 V constant and then for ∼40 h at 60 V constant in a cold room. Following the electrophoresis, the gel was stained using a modified Colloidal Coomassie Blue Staining method (Neuhoff *et al.*, 1988; Kang *et al.*, 2002). The protein bands (MyHC-I, MyHC-IIA and MyHC-IIX) were then quantified by densitometric analysis to assess the relative proportion in each subject.

### 4.6.6. Statistical analysis

The normality of the distribution of BMI, Leg Fat (%), leg fat (kg)), $VO_{2max}$, MVC, COVsteady, MyHC protein content of isoform I, IIA, IIX and MyHC mRNA levels of isoform I, IIA, IIX was assessed using the Shapiro-Wilk test. The equality of variance was tested using Levene's test. For variables that met the assumptions of normality and equal variance, independent samples T-tests were performed to examine differences between groups. Leg fat (kg), MVC (Nm), MyHC protein content of isoform IIX and mRNA levels of MyHC-IIA were non-normally distributed and were therefore analysed using the non-parametric Mann-Whitney U test.

All the other variables obtained from the analysis of the decomposed MUs were analysed using linear mixed models as multiple MUs were recorded from each participant (Sarto *et al.*, 2022*a*; Yu *et al.*, 2022; Valli *et al.*, 2023).

To compare MUs behaviours between two groups of both sexes, linear mixed-effects models fit by maximum likelihood were performed using 'lme4' (Bates *et al.*, 2015) and 'lmerTest' (Kuznetsova *et al.*, 2017) from R packages (fixed effect: group, contraction intensity and sex, random effect: subject). The model of each variable was further compared using the Akaike Information Criterion (AIC) to analyse if sex has a significant effect and should be included in the model. The model with a lower AIC was considered as a better fit model.

Mixed models were computed with RStudio (Version 1.4.1103) while T-tests using jamovi 2.2.2 (Sydney, Australia – R language). Statistical significance was accepted at $p<0.05$. The results

are reported and plotted as mean ± standard error for linear models and reported and plotted as mean ± standard deviation for T-tests.

## 4.7. Results

### 4.7.1. Participants characteristics

All the participants successfully completed the study without any adverse event associated with muscle testing, muscle biopsy or glycaemic fluctuations.

Table 4-1 shows data and P-values for differences between groups for body composition, cardiorespiratory fitness, muscle strength and torque steadiness. The two groups were comparable (no significant differences) for all the parameters.

**Table 4-1**. Age, body composition, $VO_{2max}$, muscle strength and contraction steadiness

| | Control (4M/4F) | Type 1 diabetes (4M/4F) | P-value |
|---|---|---|---|
| Age *(years)* | 27.38 ± 5.92 | 30.50 ± 3.66 | 0.225 |
| BMI *($kg/m^2$)* | 23.83 ± 2.89 | 26.25 ± 2.61 | 0.101 |
| Leg fat *(%)* | 28.24 ± 8.06 | 27.85 ± 11.44 | 0.939 |
| Leg fat *(kg)* † | 3.53 ± 0.924 | 4.15 ± 2.20 | 0.798 |
| $VO_{2max}$ *(ml/kg/min)* | 32.86 ± 5.58 | 33.44 ± 9.59 | 0.886 |
| MVC *(Nm)* † | 171.99 ± 101.97 | 182.06 ± 47.65 | 0.279 |
| COVsteady at 20% *(%)* | 2.74 ± 0.61 | 2.30 ± 0.91 | 0.276 |
| COVsteady at 40% *(%)* | 2.57 ± 0.93 | 1.92 ± 0.39 | 0.087 |

Values are presented as mean ± SD. Statistical differences were determined by Independent Samples T-Test or Mann-Whitney U-test based on normality of distributions. Non-normal distribution is reported with a dagger (*†*). Statistical significance was accepted at $p<0.05$.
M, males; F, females; BMI, body mass index; MVC, maximum voluntary contraction; COVsteady, coefficient of variation of the steady-state phase during contractions at 20 and 40% MVC.

### 4.7.2. Motor units' properties

After the removal of duplicated MUs, a total of 306 unique MUs (90 at 20% and 59 at 40% MVC for control, 81 at 20% and 76 at 40% MVC for type 1 diabetes,) were identified. This resulted in an average number of MUs per participant of 11.40 ± 6.83 at 20% and 9 ± 7.29 at 40% MVC. The yield of the decomposition was lower for females with an average number of decomposed MUs of 6.57 ± 3.73 at 20% and 4.00 ± 1.91 at 40% MVC, compared to 15.63 ± 6.14 at 20% and 13.37 ± 7.50 at 40% MVC in males. For one female participant with type 1 diabetes, it was not possible to accurately (PNR > 28 dB) decompose any MUs and, therefore, that participant was excluded from the analysis of MUs properties.

Descriptive statistics for MUs properties are presented in Table 4-2.

MUs RT (expressed as percentage of MVC)(Fig. 4-1A) was comparable between the two groups both at 20 and 40% MVC. MUs DERT (Fig. 4-1B) was lower in the type 1 diabetes group at 40% (p=0.004) but not at 20% MVC.

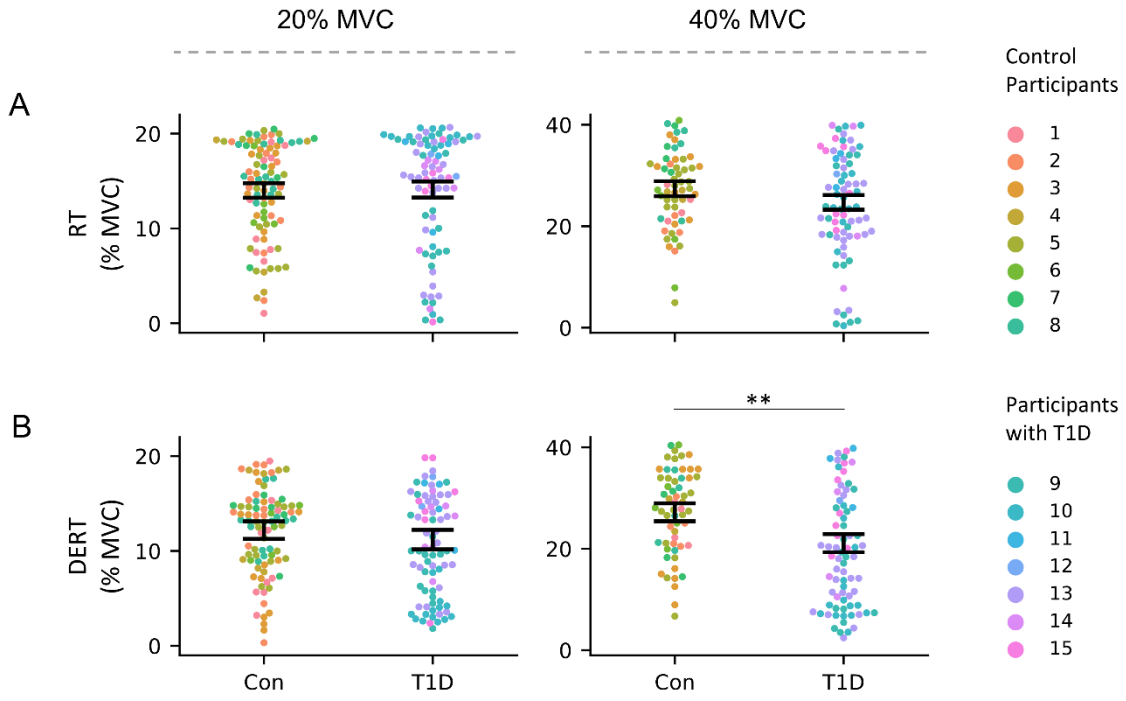


*Figure 4-1: MUs recruitment (RT) and derecruitment (DERT) thresholds. Swarm plots representing the MUs RT (A) and DERT (B) in the two groups. From left to right, MUs properties are presented for the two submaximal contraction intensities (i.e., 20 and 40% MVC). Individual MUs are represented by dots and clustered by subject. Summary data are presented as mean ± SEM. Significance levels are: **p<0.01.*

At 20% MVC, MUs DR at recruitment (Fig. 4-2A) and derecruitment (Fig. 4-2B) was comparable between the two groups while it was lower in the type I diabetes group during the steady-state phase (p=0.026)(Fig. 4-2C). At 40% MVC, MUs DR was lower in the type 1 diabetes group at recruitment (p=0.017) and during the steady-state phase (p=0.027) but not at derecruitment.

Both MUs CV (Fig. 4-3B) and action potential amplitude (Fig. 4-3C) were comparable across the groups. A visual representation of MUs CV estimation can be found in Fig. 4-3A.

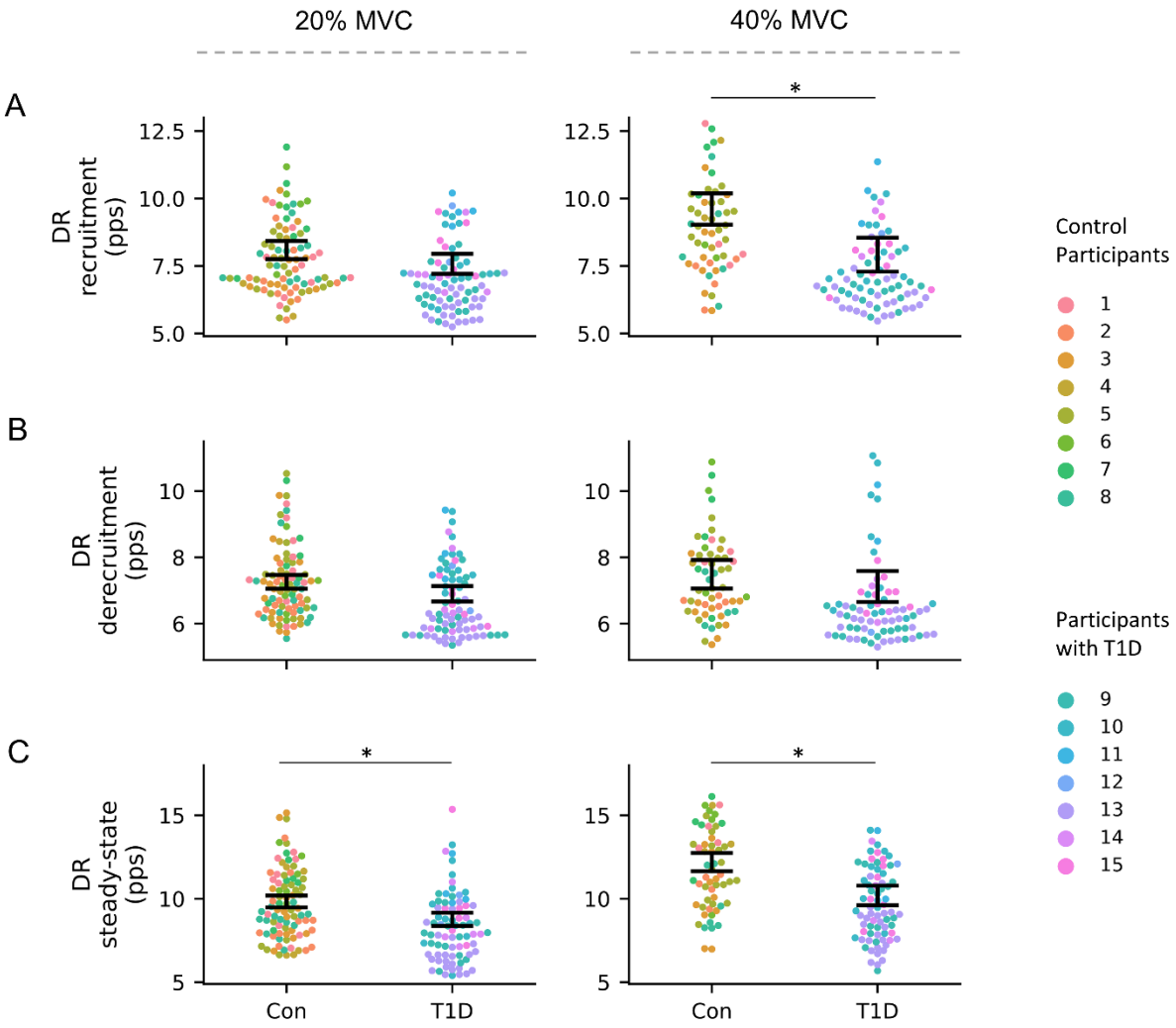


*Figure 4-2: Discharge rate (DR). Swarm plots representing the MUs DR at recruitment (A), derecruitment (B) and during the steady-state phase (C) in the two groups in pulses per second (pps). From left to right, MUs properties are presented for the two submaximal contraction intensities (i.e., 20 and 40% MVC). Individual MUs are represented by dots and clustered by subject. Summary data are presented as mean ± SEM. Significance levels are: *p<0.05.*

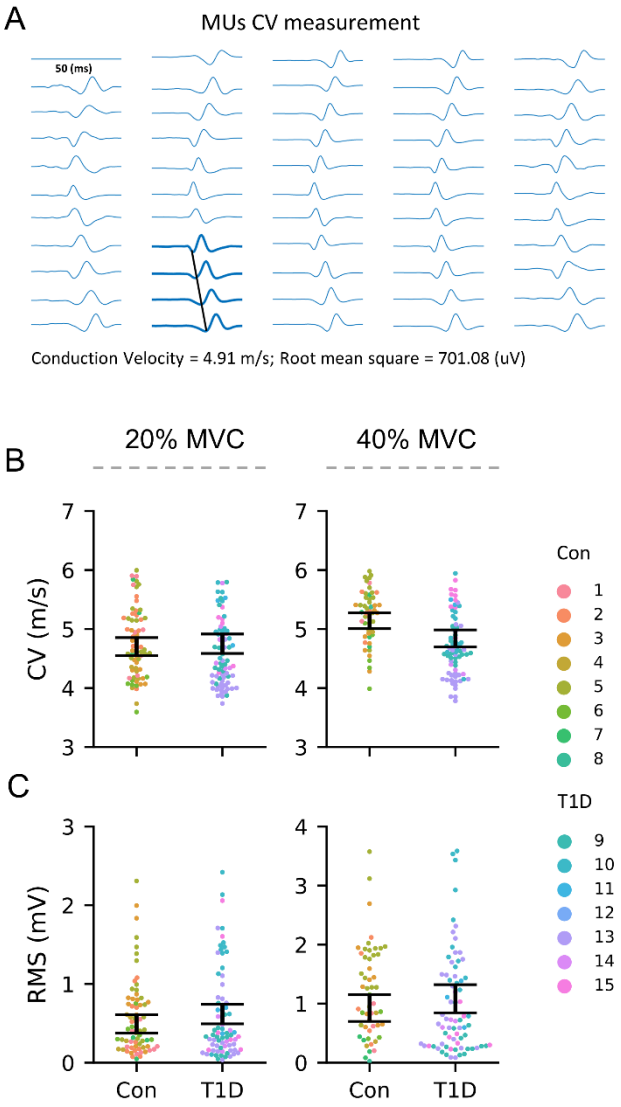


*Figure 4-3: MUs Conduction velocity (CV) and root mean square (RMS). Visual example of conduction velocity calculation based on the MUs action potential shape across the grid of recording electrodes (A). Swarm plots representing the MUs CV (B) and RMS (C) calculated during the steady-state phase in the two groups. From left to right, MUs properties are presented for the two different submaximal contraction intensities (i.e., 20 and 40% MVC). Individual MUs are represented by dots and clustered by subject. Summary data are presented as mean ± SEM. No significant differences were identified.*

### 4.7.3. MyHC proteins and mRNAs

Both the relative proportions of MyHC protein isoforms (I, IIA and IIX)(Fig. 4-4A) and the mRNA levels of MyHC-IIA and MyHC-IIX (Fig. 4-4B) were comparable between the two groups. Nevertheless, a reduced mRNA expression of MyHC-I was observed in the type 1 diabetes group compared to control (p=0.038). Descriptive statistics for MyHC isoforms is presented in Table 4-2.

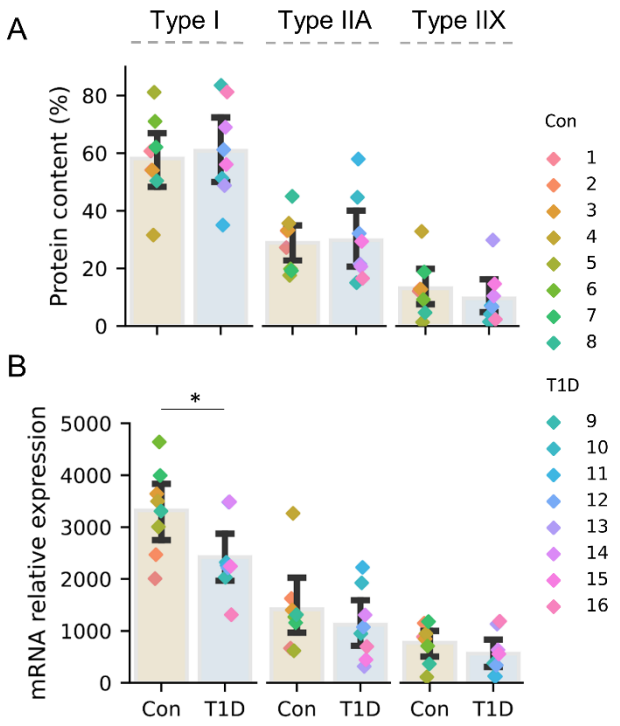


*Figure 4-4: Myosin heavy-chain (MyHC). Bar plots representing the percent protein content (A) and mRNAs expression relative to the housekeeping gene (B) of MyHC isoforms (i.e., I, IIA and IIX) in the two groups. Individual values for every participant are represented by diamonds of different colours. Summary data are presented as mean ± SD. Significance levels are: *p<0.05.*

**Table 4-2**. Descriptive statistics for MUs properties and myosin heavy-chain isoforms.

| | Control (4M/4F) | Type 1 diabetes (4M/3F) | P-value |
|---|---|---|---|
| **MUs properties at 20% MVC** | | | |
| RT *(%)* | 14.00 ± 0.77 | 14.10 ± 0.85 | 0.866 |
| DERT *(%)* | 12.10 ± 0.90 | 11.20 ± 1.20 | 0.444 |
| DR at recruitment *(pps)* | 8.00 ± 0.30 | 7.30 ± 0.30 | 0.171 |
| DR at derecruitment *(pps)* | 7.30 ± 0.20 | 6.90 ± 0.20 | 0.147 |
| DR at steady-state *(pps)* | 9.80 ± 0.33 | 8.60 ± 0.37 | 0.026 * |
| CV *(m/s)* | 4.70 ± 0.15 | 4.80 ± 0.17 | 0.990 |
| RMS *(mV)* | 0.48 ± 0.11 | 0.62 ± 0.12 | 0.769 |
| **MUs properties at 40% MVC** | | | |
| RT *(%)* | 26.90 ± 1.20 | 24.40 ± 1.10 | 0.213 |
| DERT *(%)* | 26.70 ± 1.30 | 19.90 ± 1.20 | 0.004 ** |
| DR at recruitment *(pps)* | 9.20 ± 0.46 | 7.40 ± 0.49 | 0.017 * |
| DR at derecruitment *(pps)* | 7.50 ± 0.43 | 7.10 ± 0.47 | 0.330 |
| DR at steady-state *(pps)* | 12.20 ± 0.55 | 10.20 ± 0.59 | 0.027 * |
| CV *(m/s)* | 5.10 ± 0.13 | 4.80 ± 0.15 | 0.340 |
| RMS *(mV)* | 0.93 ± 0.23 | 1.08 ± 0.24 | 0.994 |
| | Control (4M/4F) | Type 1 diabetes (4M/4F) | P-value |
| **MyHC isoforms - Proteins** | | | |
| MyHC-I *(%)* | 58.10 ± 14.7 | 60.70 ± 16.60 | 0.742 |
| MyHC-IIA *(%)* | 28.80 ± 9.63 | 29.70 ± 15.00 | 0.892 |
| MyHC-IIX *(%)* † | 13.00 ± 9.62 | 9.54 ± 9.25 | 0.382 |
| **MyHC isoforms - mRNAs** | | | |
| MyHC-I *(relative expression)* | 3321.00 ± 835.00 | 2419.00 ± 732.00 | 0.038 * |
| MyHC-IIA *(relative expression)* † | 1414.00 ± 825.00 | 1117.00 ± 678.00 | 0.442 |
| MyHC-IIX *(relative expression)* | 774.00 ± 371.00 | 559.00 ± 412.00 | 0.292 |

Values are presented as mean ± SE for MUs properties and as mean ± SD for MyHC.
Statistical differences were determined by linear mixed models for MUs properties and by Independent Samples T-Test or Mann-Whitney U-test based on normality of distributions for MyHC. Non-normal distribution is reported with a dagger (*†)*. Statistical significance was accepted at $p<0.05$. Significance levels are reported as * $p<0.05$ and ** $p<0.01$.
M, males; F, females; RT, recruitment threshold; DERT, derecruitment threshold; DR, discharge rate; pps, pulses per second; CV, conduction velocity; RMS, root mean square; MyHC myosin heavy-chain.

## 4.8. Discussion

The main findings of this study were that young people with uncomplicated type 1 diabetes and control peers utilize different neural strategies (based on MUs activity) to control muscle force production, and that HD-EMG is able to detect these differences before any functional manifestation.

These findings unveil unknown consequences of type 1 diabetes on the neuromuscular system and challenge the conventional notion that muscle degeneration precedes neural degeneration (Monaco *et al.*, 2017). Instead, they suggest an interconnection between these processes.

Our novel findings emphasize the need for a deeper understanding of how type 1 diabetes affects both neural and muscular aspects of the neuromuscular system, potentially reshaping our perspective on this condition.

For easy of reading, the concept of "neural strategies used to control muscle force production" will be referred as "neural control" (Farina *et al.*, 2016) through the manuscript.

### 4.8.1. Neural control of force production

In the present study, the two groups were matched for age and sex and, after the functional assessment, they resulted also comparable for anthropometrics, aerobic capacity and muscle strength (i.e., MVC). Considering the similar MVC between the two groups, a similar MUs behaviour was expected since MUs properties are directly associated to force production and control (Mendell, 2005*a*). Nevertheless, differences in MUs derecruitment thresholds and DR have been detected between the two groups.

During contractions at 40% MVC, it was observed that the threshold at which MUs are derecruited was lower in individuals with type 1 diabetes whilst no differences were detected in the recruitment threshold. This suggests that in individuals with type 1 diabetes, at least during moderate intensity contractions (i.e. up to 40% MVC), MUs remain active for a longer period of time. Moreover, since no differences were detectable at 20% MVC, it is possible that initial signs of altered recruitment/derecruitment strategies are unveiled only at higher intensities of contraction, when more and faster MUs are required to sustain force production. Moreover, in order to increase force production, the already recruited MUs are expected to increase their DR proportionally to the contraction intensity (Mendell, 2005*a*; Dideriksen & Del Vecchio, 2023). Interestingly, DR was lower

in those with type 1 diabetes and, also for this parameter, the differences were more evident at 40% than at 20% MVC. Taken together, the beforementioned differences in derecruitment thresholds and DR suggest that the neural strategies used to control force production differ between those with and without type 1 diabetes, especially at higher contraction intensities, where larger and faster MUs have to be recruited.

Although differences in neural control have been identified in this study, more complex is to search for the underlying mechanisms responsible for them. Since motoneurons are the structure integrating and converting the neural inputs into an output signal appropriate to control force production in the innervated muscle fibres, alterations in the motoneuron firing will necessarily reflect in altered MUs properties (Heckman & Enoka, 2004). Action potentials of the motoneuron originate in the soma through different channels and, among these, calcium ion ($Ca^{2+}$) channels are considered fundamental for the initiation and modulation of action potentials (Rekling *et al.*, 2000). Although there is no direct evidence of altered motoneuron functioning in those living with uncomplicated type 1 diabetes, a number of factors point toward this possibility. Specifically, mitochondrial impairments and increased ROS production are detectable in the skeletal muscle of people living with type 1 diabetes (Monaco *et al.*, 2018; Minnock *et al.*, 2022) and a compromised interplay between mitochondria and the endoplasmic reticulum (and therefore $Ca^{2+}$ handling) has been widely demonstrated in this population (Guerrero-Hernandez & Verkhratsky, 2014). These two alterations can induce dysregulation of $Ca^{2+}$ homoeostasis and aberrant $Ca^{2+}$ signalling and recent evidence shows that this is happening in neurons and glia at later stages of the diabetic condition, when diabetic neuropathy is clinically evident (Verkhratsky & Fernyhough, 2014). Therefore, motoneurons suffering of impaired mitochondrial functioning would consequently present altered $Ca^{2+}$ flux and $Ca^{2+}$ handling which would eventually affect the generation and modulation of action potentials. Regarding action potentials modulation, $Ca^{2+}$-activated potassium channels are responsible for the long-lasting afterhyperpolarization (AHP) happening after each action potential. Increased duration of the AHP would delay the consequent depolarisation of the motoneuron and reduce the MUs DR (Heckman & Enoka, 2004; Power *et al.*, 2022) and, therefore, impaired mitochondria and $Ca^{2+}$ flux/handling in the motoneuron might be responsible for the lower DR observed in type 1 diabetes.

Obviously, other mechanisms could be involved in the reduction of MUs DR such as the numerous ionotropic inputs that control motoneuron gain and DR. For instance, there is evidence highlighting the key role of serotonin (5-hydroxytryptamine, 5-HT) in regulating the discharge rate

of motoneurons via excitatory 5-HT receptors on the soma and dendrites by modulating persistent inward currents, $Ca^{2+}$ currents and AHP (Heckman *et al.*, 2005; Kavanagh *et al.*, 2022). Since alterations of serotonergic neurotransmission have been demonstrated in type 1 diabetes (Manjarrez *et al.*, 2006; Martin *et al.*, 2021), it is plausible to suggest that altered levels of 5-HT could contribute to the manifestation of neural impairments by reducing MUs DR (Heckman & Enoka, 2004).

In summary, our hypotheses regarding potential motoneuron function alterations and monoaminergic system changes support the association between type 1 diabetes and the aging process. Specifically, it is widely accepted that motoneurons deteriorate during aging (Hepple & Rice, 2016; Larsson *et al.*, 2019) and recent evidence shows reduced intrinsic motoneuron excitability as a consequence of aging, likely mediated by decreases in the amplitude of persistent inward currents (Hassan *et al.*, 2021*a*; Orssatto *et al.*, 2021).

Aging often results in a decline in motoneuron DR (Hepple & Rice, 2016), a trend we observed in individuals with type 1 diabetes. However, as aging progresses, motoneuron degeneration leads to muscle fibre denervation, followed by reinnervation through collateral sprouting (Tam & Gordon, 2003). While sprouting is crucial to prevent severe muscle atrophy and fibre loss, it often causes a shift in fibre phenotype to match that of the innervating motoneuron (Udina *et al.*, 2011). Slower motoneurons tend to be better preserved during aging and are more likely to support reinnervation. Consequently, faster (type 2) muscle fibres, typically innervated by slow motoneurons, are prone to degeneration, transitioning towards slower type 1 fibres due to insufficient stimulation from overly branched motoneurons, leading to muscle fibre atrophy (Tam & Gordon, 2009).

Given that our participants with type 1 diabetes were young, it is plausible that initial motoneuron alterations affecting DR were present. However, the innervation pattern and fibre size/function remained relatively intact. Therefore, only the observed reduction in DR of some MUs in the type 1 diabetes group may not be sufficient to induce a noticeable reduction in muscle force.

Furthermore, if the process of sprouting and MU enlargement had commenced in our type 1 diabetes group, it might still be in its early stages, and the newly innervated fibres could have retained their contractile properties (Gordon *et al.*, 2004). In this larger MUs, each motoneuron discharge would activate more muscle fibres, possibly resulting in a similar force output achieved with lower DR (Enoka & Fuglevand, 2001).

The interpretation of the findings of this study suggests possible molecular mechanisms that may be altered in individuals with uncomplicated type 1 diabetes, which could contribute to the different neural control in this population.

However, further research is needed to confirm these hypotheses and to understand the underlying causes of these differences. This necessity is particularly relevant in light of our finding of delayed DERT that might be contradictory with the hypothesis of altered serotoninergic neurotransmission, as delayed DERT is often associated to an increase in persistent inward currents (Heckman *et al.*, 2005).

### 4.8.2. Differences in neural control are detectable before functional manifestation

Since participants with type 1 diabetes presented different MUs properties while levels of force production were comparable to the healthy controls, we investigated whether peripheral adaptations might have compensated for these differences.

Muscle fibres are the physical effector of the motoneuron signalling and, therefore, we examined whether the two groups would exhibit a different distribution of fibre types (Miller *et al.*, 2015). However, the protein distribution of MyHC isoforms (i.e., I, IIA and IIX) were comparable between the groups and although the mRNA levels of MyHC-I were lower in people with type 1 diabetes, this was not reflected in a different slow/fast phenotype, suggesting that a transcriptional reprogramming may be occurring but muscle fibres are still resilient to metabolic changes. Indeed, our findings of lower expression of MyHC-I mRNAs in type 1 diabetes align with the literature suggesting that muscle fibres may undergo a shift towards a glycolytic phenotype at later stages in the diabetic condition (Fritzsche *et al.*, 2008; Andreassen *et al.*, 2014), at least in males (Dial *et al.*, 2021).

In addition, MUs amplitude and velocity of propagation of the action potentials across the muscle fibres (i.e., MUs CV) were comparable between the two groups. Similar CV suggests that the mechanisms responsible for transmitting the depolarisation through the membrane of muscle fibres are preserved (i.e., ion channels) (Jurkat-Rott & Lehmann-Horn, 2004) and, given the relationship between MUs CV and diameter of muscle fibres (Blijham *et al.*, 2006; Methenitis *et al.*, 2016; Casolo *et al.*, 2023) we could also expect similar muscle fibres size between the two groups. Additionally, comparable amplitude of action potentials suggest that MUs size could also be similar between the two groups (Pope *et al.*, 2016).

Altogether, these findings indicate that people with type 1 diabetes present different neural strategies of muscle force production even without any evident deterioration of muscle fibres composition and functioning.

### 4.8.3. Methodological considerations

As a constraint of the decomposition of HD-EMG recordings, it is currently difficult to accurately discriminate active MUs at high intensities of contraction. This is due to a progressive increase in the number of superimposed and overlapping MUs action potentials in the recorded EMG signal (Valli *et al.*, 2023). Therefore, potential alterations in MUs behaviour could not be assessed during MVC or very high intensities of contractions, de facto preventing us from observing the behaviour of higher-threshold MUs and of motoneurons with a higher depolarisation threshold.

In addition, decomposition of HD-EMG recordings from female participants usually yields a relatively low number of identified MUs compared to males, mainly as a consequence of the thickness of the volume conductor, which, acting as a filter on the recorded signal, negatively influences the separation of the contributions of the different MUs (Oliveira *et al.*, 2022).

Nevertheless, we believe that the range of intensity analysed in this study is crucial for most of the daily tasks and the inclusion of female participants (Lulic-Kuryllo & Inglis, 2022) allows for a broader generalizability of the findings providing, despite some technical limitations, noticeable clinical and physiological relevance.

In this study, we used the amplitude of the MUs action potential as an indicator of MUs size. However, it is widely recognized that estimation of MUs action potential amplitude from surface EMG is not sensitive to small changes and that it can be biased by a number of factors, including the volume conductor (Del Vecchio *et al.*, 2017). Therefore, future studies adopting more sensitive techniques (e.g., intramuscular recordings) are necessary to clarify this aspect.

As a major limitation of this study, we acknowledge that the limited sample size did not allow for the identification of differences between sex, especially regarding the adaptations of lower/higher threshold MUs and of slower/faster muscle fibres that have been demonstrated to differ between males and females with type 1 diabetes (Dial *et al.*, 2021).

### 4.8.4. Final considerations and future perspectives

This study provides unique evidence of detectable differences in the neural control of force production between people with uncomplicated type 1 diabetes and control peers, before any functional manifestation.

Notably, the available literature suggests that the muscle degeneration observed in type 1 diabetes is independent from the neurological condition, and that it anticipates the development of diabetic neuropathy (Monaco *et al.*, 2017). However, the findings from our study challenge this notion by suggesting that variations in neural function exist even before the manifestation of diabetic neuropathy. Consequently, our results hint at the possibility that neural and muscular degeneration may not be as distinct as previously believed, implying that these two systems may undergo changes concurrently or with less clear delineation than previously proposed.

Expanding our knowledge on the neural consequences of type 1 diabetes might guide the development of screening procedures aimed at the early detection of neural alterations in type 1 diabetes with non-invasive techniques, as well as for the design of interventions to delay the onset of diabetic myopathy and accelerated muscle aging.

It would be valuable for future research to examine the impact of factors such as sex, age, glycaemic control, and presence of diabetic complications on neural control, or how the diabetic population responds to exercise or disuse interventions compared to healthy controls. This would provide a more comprehensive understanding on how this condition can affect neural control.

## 5. Experimental Chapter 3: Tutorial: a step-by-step guide to the analysis of central and peripheral motor unit properties from High-Density Electromyography with *openhdemg*

*Authors:*

Giacomo Valli [a]*, Paul Ritsche [b], Andrea Casolo [a], Francesco Negro [c] & Giuseppe De Vito [a]

*Corresponding author

[a] Department of Biomedical Sciences, University of Padova, Padova, Italy

[b] Department of Sport, Exercise and Health, University of Basel, Basel, Switzerland

[c] Department of Clinical and Experimental Sciences, University of Brescia, Brescia, Italy

*Author contributions:*

GV conceptualised and designed *openhdemg* and the tutorial. GV implemented the functions for electromyography data handling, visualisation, editing and analysis. PR implemented the graphical user interface. FN provided technical support and supervision for the development of the analysis algorithms. AC tested the functions and the graphical user interface and provided guidance for the implementation of missing functionalities. GDV provided overall direction and organisation of the project. GV drafted the manuscript with the support of AC, and all the authors revised it. GV maintains the GitHub and PyPI repositories and supervises the future development of *openhdemg*.

The article has been submitted and it is currently under revision.

## 5.1. Background

The final experimental chapter of the thesis is a tutorial article presenting the fundamental steps for a complete investigation of MUs properties from HD-EMG recordings. This tutorial article represents the culmination of my research experience with the HD-EMG technique during the PhD and, for the first time, it clearly explains step-by-step all the notions necessary to analyse HD-EMG recordings, filling a significant gap in the existing literature by offering detailed insights into this process.

Additionally, in this tutorial article I introduce *openhdemg*, an innovative open-source framework specifically designed for the analysis of central and peripheral MUs properties from HD-EMG recordings. Unlike proprietary software, openhdemg is freely accessible, enhancing accessibility and efficiency for researchers in the field of EMG. This framework plays a pivotal role in democratizing the analysis of HD-EMG data, empowering researchers with its user-friendly interface and advanced capabilities.

The key functionalities of the *openhdemg* library are presented in the tutorial article and extensively explained at (https://www.giacomovalli.com/openhdemg/).

*openhdemg* has been developed in Python 3. Users might wonder why Python was chosen over the more traditional MATLAB, especially given MATLAB's prevalence in the scientific community working with HD-EMG. The choice of Python aligns with the principles of open-source software, promoting transparency, collaboration, and knowledge sharing. Python's flexibility, vast ecosystem of libraries, and a thriving community make of it an ideal platform for *openhdemg* development. By adopting Python, we foster an environment where researchers can easily extend and customize *openhdemg* to suit their specific needs, ensuring the framework's longevity and adaptability.

The *openhdemg* framework has been publicly released on July 4, 2023, and it stands as the only available free and open-source solution for the analysis of MUs properties. The commitment to open-source principles reflects a dedication to fostering collaboration and knowledge sharing among HD-EMG researchers worldwide.

## 5.2. Abstract

High-Density surface Electromyography (HD-sEMG) is the most established technique for the non-invasive analysis of single motor unit (MU) activity in humans. It provides the possibility to study the central properties (e.g., discharge rate) of large populations of MUs by analysis of their firing pattern. Additionally, by spike-triggered averaging, peripheral properties such as MUs conduction velocity can be estimated over different regions of the muscles and single MUs can be tracked across different recording sessions. In this tutorial, we guide the reader through a step-by-step investigation of MUs properties and provide both the theoretical knowledge and practical tools necessary to lower the barriers in the implementation of the HD-sEMG technique. The practical application of this tutorial will be based on *openhdemg*, a free and open-source framework for the automated analysis of MUs properties built on Python 3 and composed of different modules for HD-sEMG data handling, visualisation, editing, and analysis. *openhdemg* is interfaceable with most of the available recording software and equipment, and all the built-in functions are easily adaptable to different experimental needs. The framework also includes a graphical user interface which enables users with limited coding skills to perform a robust and reliable analysis of MUs properties without coding.

## 5.3. Highlights

- There is an urgent need for clear guidelines, instructions and open-source software to analyse motor units' activity from High-Density Electromyography recordings.
- This tutorial guides the reader through all the steps necessary to perform a complete investigation of MUs properties providing both theoretical knowledge and practical tools.
- In this context, we introduce *openhdemg*, an innovative, free, and open-source framework for the automated analysis of motor units' properties from High-Density Electromyography.

## 5.4. Abbreviations

In alphabetical order:

| | |
|---|---|
| CNS | Central Nervous System |
| COVisi | Coefficient of variation of Interspike interval |
| DR | Discharge Rate |
| EMG | Electromyography |
| HD-EMG | High-Density Electromyography |
| HD-sEMG | High-Density surface Electromyography |
| iEMG | Intramuscular Electromyography |
| ISI | Interspike interval |
| MUAP | Motor Units Action Potential |
| MU | Motor Unit |
| MUCV | Motor Unit Conduction Velocity |
| MVC | Maximum Voluntary Contraction |
| PNR | Pulse to Noise Ratio |
| PPS | Pulse Per Second |
| RMS | Root Mean Square |
| SIL | Silhouette Score |
| XCC | Cross-Correlation Coefficient |

## 5.5. Introduction

The motor unit (MU) is the basic functional component of the neuromuscular system that consists of an alpha motoneuron, its axon, and the muscle fibres it innervates (Sherrington, 1925; Heckman & Enoka, 2012). The central nervous system (CNS) responds to the locomotor functional demands by sending trains of axonal discharges (i.e. neural information or activation signal), which in turn elicit action potentials in the innervated muscle fibres (i.e. MUs action potentials (MUAPs)) (Heckman & Enoka, 2004, 2012). In simple terms, MUs act as a transducer that converts the neural activation signal into muscular forces. Indeed, because of a large physiological safety factor in synaptic transmission at the neuromuscular junction (Wood & R. Slater, 2001; Sarto *et al.*, 2022*a*), there is a one-to-one relation between the discharges of a motoneuron and the MUAPs evoked in the muscle (Wood & R. Slater, 2001; Duchateau & Enoka, 2011).

During voluntary muscle contractions, the MUAPs can be detected at the muscle level via electromyographic (EMG) recordings, therefore making the motoneurons the only cells of the CNS that can be recorded in humans with non-invasive or minimally-invasive techniques (Farina *et al.*, 2004; Merletti & Farina, 2009). Recent advancements in EMG techniques have led to the development of High-Density surface EMG (HD-sEMG), where densely populated grids of closely spaced small-diameter recording electrodes are applied directly to the skin overlying the muscles (Gallina *et al.*, 2022). The elevated spatial sampling of these grids allowed the researchers to record MUAPs from different regions of the muscle, thus increasing the possibility to discriminate spatially non-overlapping MUAPs and the number of single MUs that could be accurately decomposed (Farina *et al.*, 2016). These advancements have allowed, for the first time, the simultaneous discrimination of large and representative populations of concurrently active MUs without invasive procedures (Farina *et al.*, 2016).

These peculiar features established HD-sEMG as the preferred tool for the investigation of how the CNS controls voluntary movements in physiological conditions, and opened a new era in the study of MUs physiology and activity in response to different stimuli (Martinez-Valdes *et al.*, 2018*a*; Casolo *et al.*, 2021; Škarabot *et al.*, 2022; Valli *et al.*, 2023), in health and pathology (Drost *et al.*, 2001; Gallego *et al.*, 2015*b*), to injury (Nuccio *et al.*, 2021) and for man-machine interface applications (Farina *et al.*, 2017).

In this tutorial, we provide the reader with the theoretical knowledge necessary to perform a complete investigation of central and peripheral MUs properties from decomposed HD-sEMG

recordings. Additionally, in this context we introduce *openhdemg*, an innovative, freely available, and open-source framework specifically designed for the automated analysis of MU properties in HD-EMG recordings (Fig. 5-1).

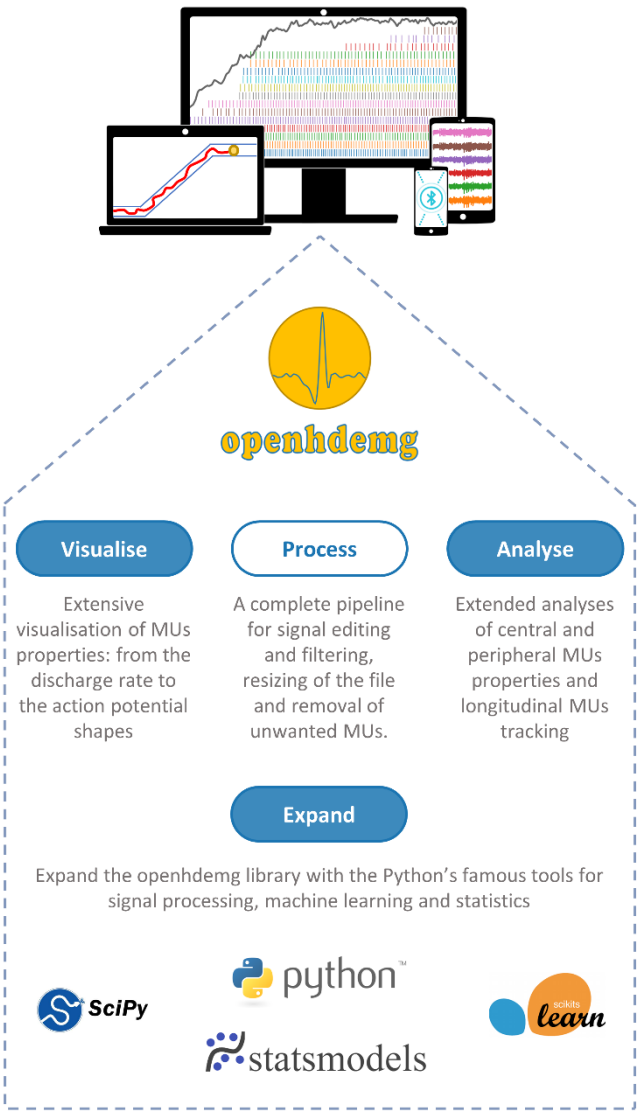


*Figure 5-1:* The *openhdemg* framework. *openhdemg* is a free, versatile and open-source framework for the analysis of single motor unit (MU) properties from High-Density Electromyography (HD-EMG) recordings. It can be virtually interfaced with any custom or commercial system for HD-EMG data acquisition and decomposition. Starting from the discharge pattern of the identified MUs, *openhdemg* automates the steps of visualisation, processing and analysis of the decomposed HD-EMG file. Developed using Python 3, a widely recognized programming language for data analysis, *openhdemg* provides a rich set of built-in functions that can be further expanded using popular tools for signal processing, machine learning, and statistics available in the Python ecosystem.

## 5.6. Lowering the barriers to the use of HD-sEMG with *openhdemg*

Although some general consensus and standardisation on HD-sEMG data acquisition and analysis has been recently proposed (Gallina *et al.*, 2022; Martinez-Valdes *et al.*, 2023), the implementation of this technique still faces notable challenges. One such challenge is the limited availability of practical guidelines, instructions and user-friendly open-source software for the analysis of MUs activity (Felici & Del Vecchio, 2020). Indeed, proper analysis of HD-sEMG recordings requires specialized knowledge and expertise in signal processing and computational methods, alongside advanced coding skills, which may preclude some laboratories from such type of research.

The aim of this tutorial article is to lower the barriers to the implementation of the HD-sEMG technique by providing the reader with the theoretical knowledge and practical tools necessary to investigate MUs properties from HD-sEMG recordings.

Specifically, this tutorial has been structured as a step-by-step guide to the analysis of central and peripheral MUs properties and combines simple and clear guidelines with an easy-to-read code implementation of all the showed concepts.

The tutorial will briefly cover basic concepts of signal acquisition and decomposition (as these phases generate the information to be analysed) and will then cover, in detail, the following steps:

- Load the decomposed HD-sEMG file in a working environment;
- Visualise, inspect and process the decomposition outcome;
- Discard unwanted MUs based on objective criteria;
- Track MUs within and between recording sessions;
- Analyse central and peripheral MUs properties;

For organisational purposes, the main text of the manuscript will focus on the theoretical aspects necessary to correctly investigate MUs activity. Alongside the text, figures and figures' captions will illustrate the application of all the discussed notions. Furthermore, a clear and in-depth documentation of the code implementation will allow the users to interactively follow all the steps of this tutorial and to implement their own analyses.

The practical application of the tutorial can be easily followed by readers with any scientific background and no advanced or strong knowledge of signal processing and coding will be required.

In order to achieve or purpose, we developed *openhdemg*, a free and open-source framework specifically designed for the analysis of MUs properties from HD-EMG recordings. *openhdemg* is written in Python 3 (Python Software Foundation, USA) and, at the time of writing, it is composed of 8 modules and 60 functions for HD-EMG data handling, visualisation, editing and analysis easily adaptable to different experimental needs (Fig. 5-1). All the functions are designed for the maximum simplicity and convenience of the user and are extensively documented at https://www.giacomovalli.com/openhdemg/. Of note, the use of the *openhdemg* framework can be extended also to intramuscular HD-EMG recordings, although this tutorial article will only focus on HD-sEMG recordings.

Noticeably, *openhdemg* is designed to be interfaced with any available system for data acquisition and decomposition, starting from the commercially available software up to any personal implementation of these phases, with little or no customisation required by the user.

For didactic purpose, the user is encouraged to follow the tutorial article with the provided code implementation of all the showed concepts. This approach enables users to directly utilise the individual functions within the *openhdemg* framework. These functions are designed to offer maximum customization and flexibility, allowing for further extension with well-known Python libraries dedicated to signal processing and data analysis (as depicted in Fig. 5-1). By doing so, users can leverage their ability to perform advanced investigations.

However, the reader can also decide to use the built-in graphical user interface (presented in Fig. 5-2), which enables users to perform analysis tasks with ease and efficiency without writing a single line of code. The graphical interface contains all the tools needed to follow this tutorial article and to analyse MUs properties in real-life scenarios. For the interested readers, the use of the graphical interface is well documented at (https://www.giacomovalli.com/openhdemg/gui_intro/).

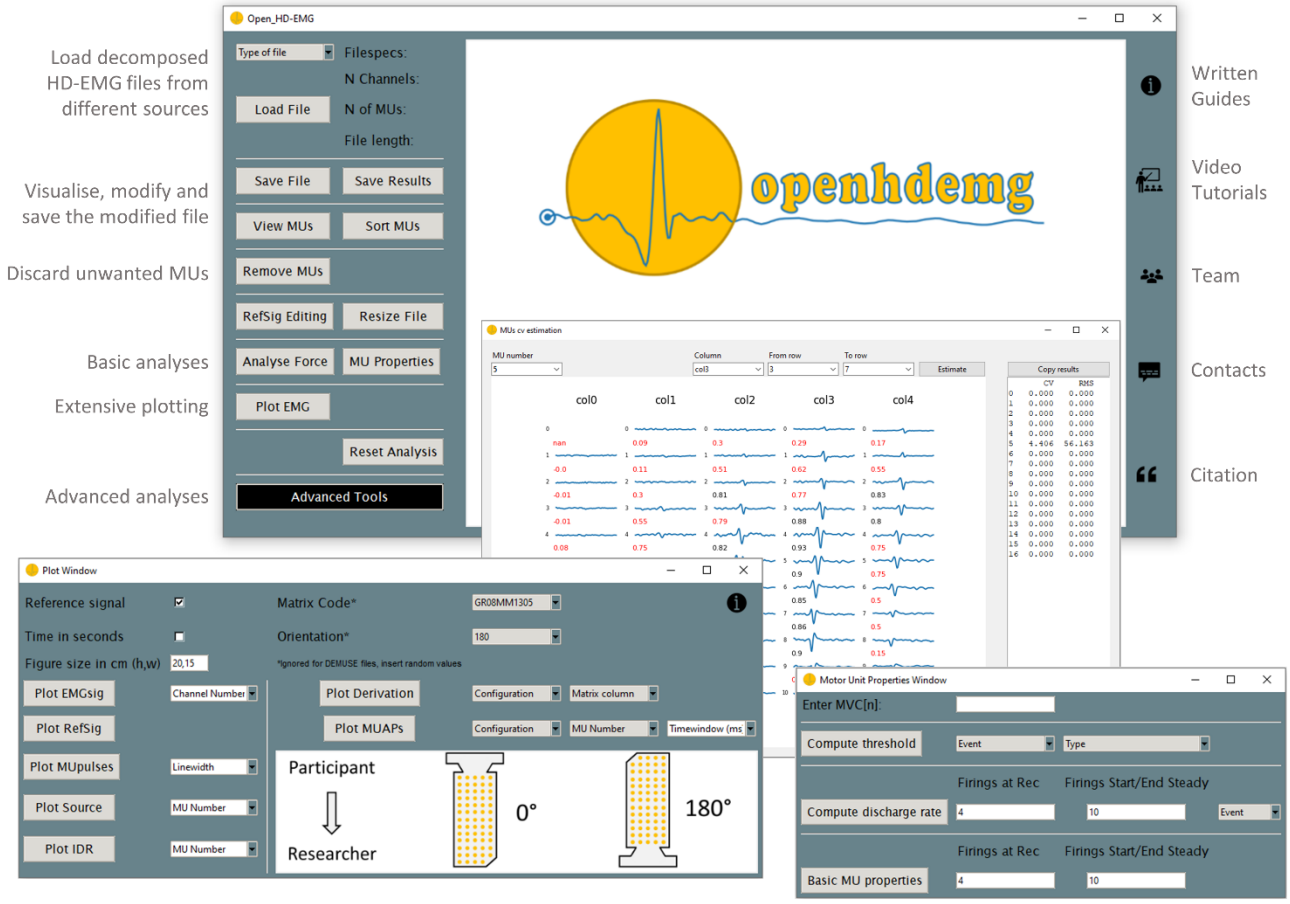


*Figure 5-2:* The Graphical user interface. The *openhdemg* framework is equipped with a practical and functional graphical interface that integrates the most relevant high-level functions of the *openhdemg* library and that allows users to perform a broad range of visualisation, processing and analysis tasks in a time-efficient manner and without coding. High-Density Electromyography, HD-EMG; Motor units, MUs.

## 5.7. Fundamentals of HD-sEMG signal acquisition and decomposition

Although the explanation of procedures for HD-sEMG signal acquisition and decomposition into MUs discharge patterns goes beyond the scope of this article, these are the prerequisites for generating the output that is subsequently analysed, and are determinant for the quality of the analysis. Therefore, the following two sections are intended to provide a brief overview of the fundamental concepts for HD-sEMG data acquisition and decomposition in light of the subsequent analyses. For the readers that need further explanations, we redirect to more specialised articles covering these topics (Besomi *et al.*, 2019; Merletti & Muceli, 2019; Del Vecchio *et al.*, 2020; Merletti & Cerone, 2020; McManus *et al.*, 2020). Additionally, Fig. 5-3 provides a visual representation of the key steps in HD-sEMG signal acquisition and decomposition in light of the subsequent analyses.

### 5.7.1. Signal acquisition

Being the primary step of all the studies involving HD-sEMG recordings, the signal acquisition phase will determine the type of analysis that can be performed, the number of accurately identified MUs and the reliability of the obtained results.

According to recent consensus (Gallina *et al.*, 2022), if the scope is to investigate both central and peripheral properties of single MUs, the HD-sEMG signal should be recorded during isometric contractions (Fig 5-3A-C) with densely populated grids of closely spaced (2.5 – 10 mm) electrodes of small diameter (0.5 – 3 mm). Additionally, the number and distribution of the recording electrodes should be adequate to accurately represent the propagation of MUAPs through the muscle fibres. Nowadays, it is common practice to use 32 or more recording electrodes, especially on large muscles (Del Vecchio *et al.*, 2017; Cohen *et al.*, 2023; Okudaira *et al.*, 2023).

Given that HD-sEMG signals have a bandwidth of approximately 10–500 Hz, the signal should be preferentially recorded with a sampling rate of at least 2000 Hz (McManus *et al.*, 2020). Additionally, the signal should be recorded in monopolar configuration (montage), in order to maximise the information that can be collected and to allow for different off-line spatial filtering (e.g., single or double differential) (Fig. 5-3G) (Gallina *et al.*, 2022).

For the investigation of peripheral MUs properties such as MUs conduction velocity (MUCV) or amplitude of the MUAPs, it is absolutely necessary to standardise the location in which the grid is attached and its orientation (Merletti & Muceli, 2019). Indeed, the estimation of peripheral MUs properties is affected by the dimension and direction of muscle fibres, which vary across the muscle

area (Casolo *et al.*, 2023). For these analysis, the grid should be placed following the muscle fibres anatomical orientation and its position should be standardised with respect to an easily-identifiable superficial innervation zone (Martinez-Valdes *et al.*, 2023). Both the direction of the fibres and the innervation zones can be accurately identified with different methods, including the use of linear electrode arrays (Del Vecchio *et al.*, 2017; Casolo *et al.*, 2020) or with low-intensity percutaneous electrical stimulations (Botter *et al.*, 2011*a*) coupled with ultrasound imaging (Hug *et al.*, 2021*b*; Valli *et al.*, 2023).

### 5.7.2. Signal decomposition

MUs decomposition is a semi-automated process aimed at extracting the discharge pattern of single MUs from interference EMG signals. Over the last 20 years, different decomposition techniques have been specifically implemented for HD-EMG recordings (Holobar & Zazula, 2007; Ning *et al.*, 2015; Negro *et al.*, 2016; Chen & Zhou, 2016). Among these, the ones based on convolutive blind source separation have gained widespread adoption because of their ability to efficiently resolve superimposition of action potentials and their robustness in the presence of signal artefacts (Holobar & Zazula, 2007; Negro *et al.*, 2016). These techniques are considered "semi-automated" since an automated phase aimed at identifying and refining the mathematical vectors representing the contribution of single MUs is usually followed by a manual refinement of the decomposition outcome (as briefly showed in Fig. 5-3D-F) (Enoka, 2019; Del Vecchio *et al.*, 2020).

While technicalities of MUs decomposition are beyond the scope of this tutorial, it is essential to comprehend the output it generates, which contains the foundational variables for all subsequent analyses on single MUs.

The basic and most important output variable is the time at which each MU is active (Fig. 5-3F). The times of discharge of each MU are usually represented as a one-dimensional array containing the instants of discharges or, alternatively, as a binary representation of the MUs behaviour over time (i.e., each sample is assigned 0 if the MU is not discharging or 1 if the MU is discharging) (Fig. 5-3H). This very basic information is fundamental to perform the majority of the analysis, including MUs recruitment and derecruitment threshold (RT and DERT), discharge rate (DR) and MUCV.

In order to estimate the RT and DERT, the information about the times of discharge has to be associated with an auxiliary input signal. Similarly, for the estimation of MUCV or other peripheral

properties, the times of discharge have to be associated with the raw multichannel EMG signal. Therefore, these variables have to be included in the decomposed EMG file when the researcher wants to investigate both central and peripheral MUs properties.

Finally, the decomposed file must contain information about the sampling rate, which is fundamental to express all the estimated parameters in time units.

The beforementioned variables in the decomposed HD-sEMG file are sufficient to perform a complete investigation of central and peripheral MUs properties. However, it must be noted that the times of discharge provide very limited information on the reliability of the identified MUs and do not allow to apply any signal-based metrics of accuracy, therefore preventing the discrimination of a properly identified MU from decomposition errors. To overcome this limitation, the files decomposed via blind-source separation contain also the decomposed source, which is the result of the decomposition from which the times of discharge are detected, and which allows to estimate the relative magnitude of the spikes in respect to the baseline noise (Holobar *et al.*, 2014; Negro *et al.*, 2016).

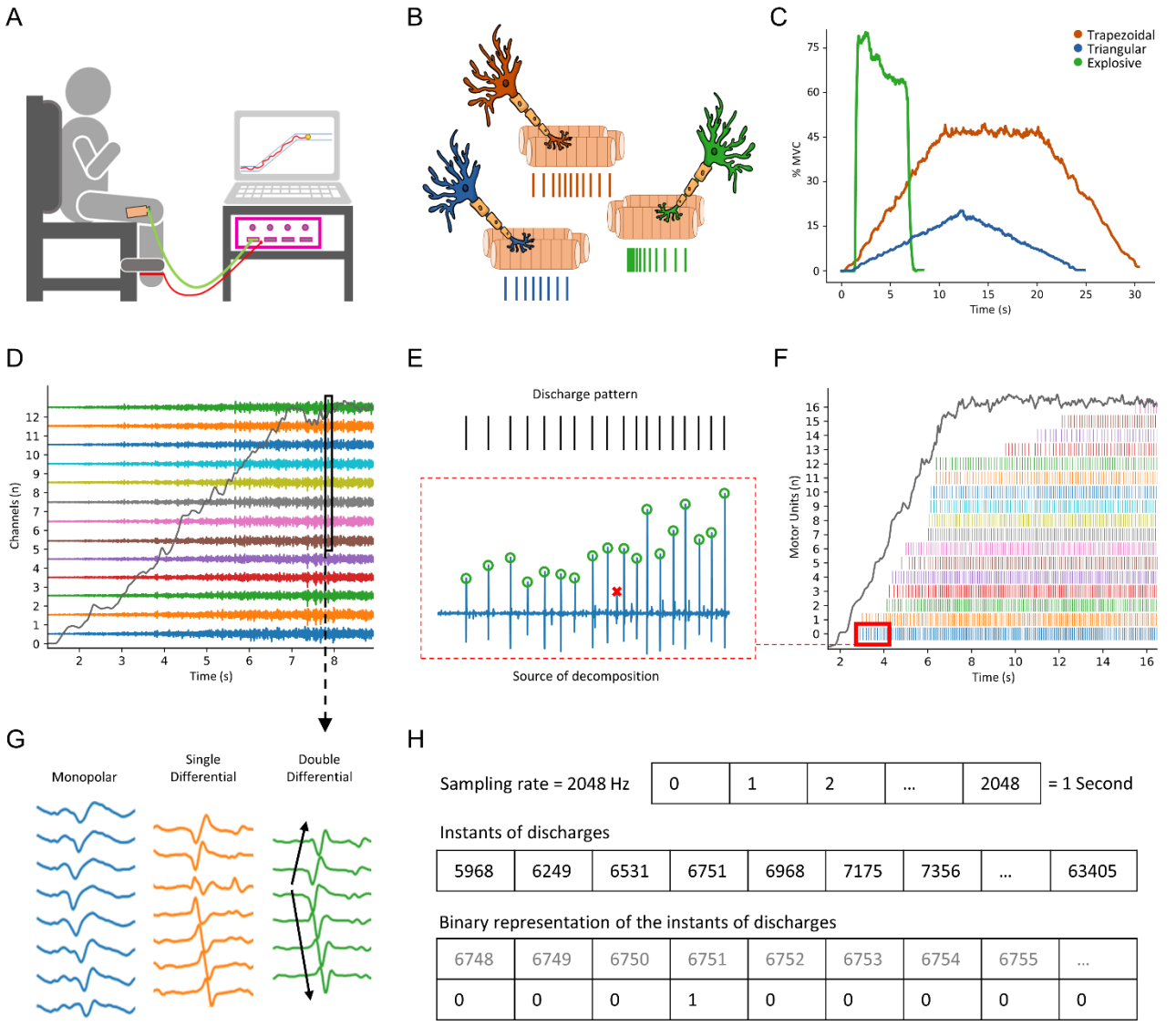


*Figure 5-3:* High-Density surface Electromyography (HD-sEMG) signal acquisition and decomposition. Representative example of HD-sEMG recordings performed during isometric and standardised contractions (A). Specific pools of motoneurons are recruited depending on the target task, resulting in a series of precisely modulated action potentials (B) that cause the depolarisation of the sarcolemma and the generation of the desired muscle force. (C). The summation of all the action potentials generated by different motoneurons generates the interference EMG signal (D) which, if acquired during isometric tasks, can be decomposed in the discharge pattern of individual motor units (MUs) (E, F). For flexibility in the off-line analysis, the interference EMG signal is usually recorded in monopolar montage, although other spatial filtering techniques can be adopted (G). Regardless of the contraction type and setup for EMG signal acquisition, the decomposed HD-sEMG file should contain all the variables necessary for the subsequent analysis of central and peripheral MUs properties, including at least the times of discharge of each MU (H), the raw EMG signal, the auxiliary input signal, the sampling rate, and ideally the decomposed source (E). Maximum voluntary contraction, MVC; number, N; Hertz, Hz.

## 5.8. Load the decomposed HD-sEMG file in a working environment

The analysis of the decomposed HD-sEMG files requires specific algorithms or software, which are typically implemented in programming languages such as Python and MATLAB. Therefore, the decomposed HD-sEMG file needs to be imported into a suitable working environment. Since this tutorial is based on *openhdemg*, the only user-friendly solution currently available for the analysis of single MUs activity, the proposed working environment has been specifically designed to enhance the user experience with this framework.

A working environment generally refers to the set of resources necessary to carry out a particular task or job. In the context of this tutorial, we refer to the combination of a computer, a programming language, an integrated development environment and a set of algorithms.

The programming language required by *openhdemg* is Python (v3.11), which can be downloaded and installed from (https://www.python.org/). The integrated development environment is a software that facilitates to write, test, and debug code. The suggested integrated development environment to follow this tutorial is Visual Studio Code (can be downloaded and installed from https://code.visualstudio.com/). Once Python and Visual Studio Code are installed, the user needs to download the set of pre-built algorithms (usually named "library" in Python, which indicates a collection of reusable code modules and functions). As previously mentioned, *openhdemg* is the library used in this tutorial. *openhdemg* is hosted at PyPI (https://pypi.org/project/openhdemg/) and can be installed as "pip install openhdemg" from the Python terminal. The user is encouraged to install *openhdemg* and other libraries in a specific "virtual environment", which is a self-contained directory that contains a specific version of Python and its dependencies. The users without previous experience using Python are strongly encouraged to follow the detailed guide through the beforementioned steps at (https://www.giacomovalli.com/openhdemg/tutorials/setup_working_env/).

Once the working environment is set, the user is ready to perform the analyses presented in this tutorial exploiting the functionalities of *openhdemg*. As previously introduced, the code necessary to analyse the decomposed HD-sEMG file will not be presented in the main text of the manuscript, which will instead prioritise the theoretical and visual aspects. However, from the supplementary material section of this article, the user can download different Python files (.py extension) that contain all the code necessary to replicate the analyses presented in this tutorial

alongside an extensive step-by-step explanation of the code provided. These files can be opened and executed directly in Visual Studio Code.

The user that immediately wants to test the example code can download 4 decomposed example files (named Pre_25_a, Pre_25_b, Post_25_a and Post_25_b) from Mendeley Data (link to include upon acceptance of the article). The recordings have been performed 4 weeks apart (i.e., “Pre” and “Post”) in a young subject performing moderate physical activity and in duplicates (i.e., “a” and “b” indicate the same contraction repeated twice at each timepoint). These sample files contain all the variables necessary to investigate both central and peripheral MUs properties.

## 5.9. Visualization, inspection and processing of decomposition outcome

As shown in Fig. 5-4A, the sample decomposed HD-sEMG file contains a trapezoidal contraction ranging from 0 to 25% MVC for a total duration of about 30 seconds. In this example file, the auxiliary input signal represents the participant's generated force and is expressed as % MVC. This type of contraction is very common in HD-sEMG studies and it has been preferred for the scope of the tutorial as it allows to detect the progressive and ordered recruitment and derecruitment of different MUs and their DR modulation during voluntary isometric contractions (Nuccio *et al.*, 2021; Valli *et al.*, 2023).

As research in HD-sEMG advances, however, different types of contraction such as triangular and explosive contractions, are also becoming of common use to address specific research questions (Del Vecchio *et al.*, 2019*b*; Hassan *et al.*, 2021*b*; Mesquita *et al.*, 2022). Obviously, the flexibility and customisability of the *openhdemg* framework makes it suitable also to work with these (and other) novel contraction types.

In Fig. 5-4B, the same MUs have been sorted based on their order of recruitment. This visualisation is useful to detect the distribution of the decomposed MUs and whether the decomposition procedure identified MUs through the whole or the majority of the volitional recruitment range of the tested muscle, or only at specific force levels. The latter phenomenon can be typically observed in contractions executed at higher force levels (e.g., 50 or 70% MVC) where the superimposition of larger MUAPs generated by MUs with higher RT might prevent the observation of the smaller MUAPs generated by lower-threshold MUs (Fig 5-4C-D) (Del Vecchio *et al.*, 2019*a*; Casolo *et al.*, 2021; Valli *et al.*, 2023).

From the visualisation of the discharge times, however, it is difficult to have a complete understanding of the MUs discharge activity. Therefore, it is usually more informative to visualise each MUs discharge pattern both as a function of time (X axis, in seconds) and as a function of DR (left Y axis, in pulses per second) as shown in Fig. 5-4E. Indeed, from this representation of the MUs discharge activity, it is possible to observe some typical physiological characteristics of the MUs discharge such as the motoneuron's linear response to the depolarizing current it receives (Fig. 5-4E) (Mendell, 2005*b*) and the common drive to the muscle (Fig 5-4B) (De Luca & Erim, 1994).

Regarding muscle force, Fig. 5-4B highlights two common problems in HD-sEMG recordings: (i) the auxiliary input signal shows the presence of a signal offset and (ii) of a noisy component that might affect some analyses like the MUs RT and DERT.

The beforementioned examples and observations, although do not provide any objective measurement, present a clear overview of the quality of the HD-sEMG recording and decomposition output, and grant enough guidance for editing the HD-sEMG file before estimating the MUs properties.

In this regard, the *openhdemg* library offers a complete pipeline for the processing of the decomposition outcome before MUs analysis, including the removal of auxiliary input signal offset and different filtering techniques to reduce electric noise, both in the auxiliary input and in the raw EMG signal when needed (as exhaustively shown in the code implementation and in Fig. 5-4F-H).

In the context of this tutorial article, we recognize the need to explicitly state that signal filtering is a complex topic and that the appropriate filter type should be selected based on the user's specific needs. We therefore redirect the reader to more specific articles covering this topic (Clancy *et al.*, 2002; McManus *et al.*, 2020).

A final adjustment, often necessary while preparing the HD-sEMG file for analyses, is to remove areas of the recording with unwanted neuromuscular activation before and after the actual contraction phase (e.g., movement artefacts). This editing can be efficiently performed by resizing the HD-sEMG file in a narrower time-window that only includes the active contraction phase. During this process, the user should be careful to resize the EMG and auxiliary input signal in the same time window but, at the same time, all the other variables in the time domain, or depending from the time-window of interest, should be adjusted accordingly. For example, If the EMG signal is resized, all the instants of discharge will take a different value, which can be simplified as the original value minus the number of samples removed from the initial part of the HD-sEMG file.

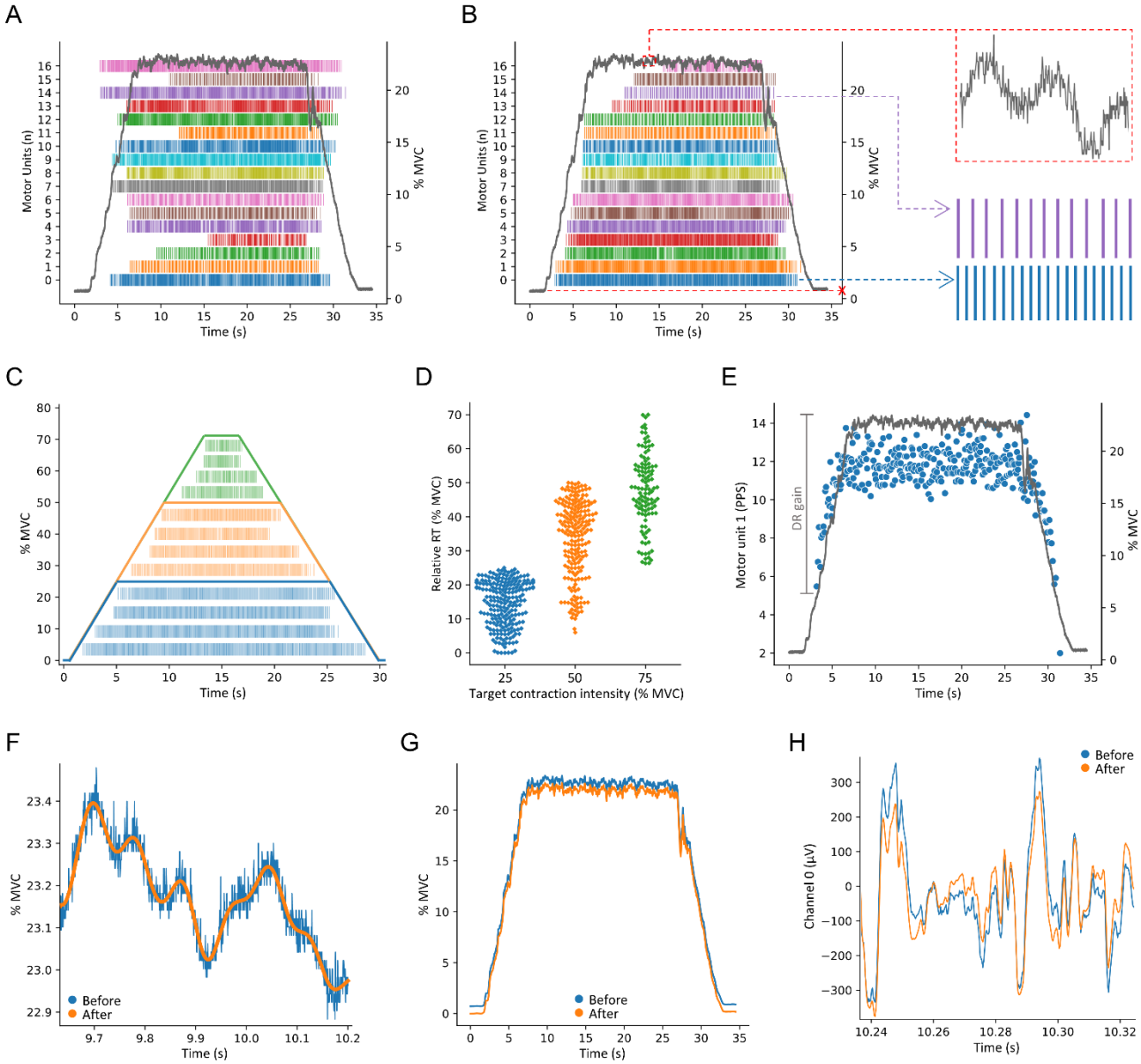


*Figure 5-4:* Visualization, inspection and processing of decomposition outcome. The content of the decomposed High-Density surface Electromyography (HD-sEMG) file can be practically inspected by visualising the binary representation of motor units (MUs) discharge times eventually coupled with the auxiliary input signal (A). To better detect the distribution of the decomposed MUs, these can be visualised based on their order of recruitment (B). In this visualisation, the recruitment thresholds provide information on whether the decomposition procedure identified MUs through the majority of the volitional recruitment range of the tested muscle, or only at specific force levels, as typically observed in contractions executed at higher force levels (C, D). The discharge behaviour of single MUs can be better visualised by the instantaneous discharge rate which, in the showed example, reflects the motoneuron's linear response to the depolarizing current it receives (E). The auxiliary input signal can be adjusted before the analysis via filtering of the noisy components (F) (in this example figure, a 4th order, zero-lag low-pass Butterworth filter with 15 Hz cut-off frequency was used) and via removal of signal offset (G). Similarly, also the EMG signal can be filtered if the decomposed HD-sEMG file only contains its unprocessed version (H) (in this example figure, a 2nd order, zero-lag band-pass Butterworth filter with a frequency range of 20-500 Hz was used). Maximum voluntary contraction, MVC; number, N; recruitment threshold, RT; pulses per second, PPS.

## 5.10. Discard unwanted MUs based on objective criteria

The term “unwanted MUs” is used to indicate those MUs that do not respect some qualitative criteria of accuracy or with irrelevant features for the intended analysis. In the context of HD-sEMG and MUs detection, the term” accuracy” refers to the accurate identification of the MUs discharge behaviour with respect to their physiological discharge pattern, which can be either known a priori in simulation studies or assumed from intramuscular recordings (Mambrito & De Luca, 1984; Holobar *et al.*, 2009).

One of the reasons why MUs activity is usually investigated during standardised tasks is that the discharge behaviour of the MUs is highly predictable from the performed task. Consequently, unexpected and unregular discharge profiles might indicate errors in the identification of the specific MU discharge times, at least in healthy individuals.

For example, during trapezoidal contractions, the frequency of the discharge pattern of each MUs is expected to progressively increase from the moment of recruitment through all the ascending phase of the contraction. Similarly, the steady-state phase should show a maintenance of the frequency (or a slow and constant decrease) that is then progressively reduced during the descending phase (Fig. 5-5A) (Pascoe *et al.*, 2014*b*; Del Vecchio *et al.*, 2017).

In light of this, a common parameter used to estimate the physiological behaviour of the identified MUs (and to indirectly infer on their accuracy) is the variability of the MUs discharge pattern during the steady-state phase of the contraction (Hu *et al.*, 2014). This variability can be estimated as the coefficient of variation of the interspike interval (COVisi), which is the ratio between the standard deviation of the interspike interval (ISI) array and its average value, usually expressed in percent. The ISI array represents the time-difference between consecutive discharge instants of each MU.

High values of the COVisi indicate high variability in the MUs discharge pattern and, according to recent consensus and research articles, the COVisi during the steady-state phase of the contraction could serve as a criterion for identifying inaccurate MUs and excluding them from subsequent analyses (Martinez-Valdes *et al.*, 2017; Gallina *et al.*, 2022).

However, there are limitations in the use of the COVisi as a criterion to determine the reliability of the decomposition. Indeed, the type of contraction heavily influences the MUs ISI and its variability, which might be elevated also in accurately identified MUs whenever the steady-state phase is either very short (2-5 seconds) or completely absent (as showed in Fig. 5-5B-C). Additionally,

MUs behaviour in non-physiological conditions such as neuromuscular diseases and extreme muscle fatigue might not respect the assumption of regular discharge activity of the MUs, therefore preventing the use of COVisi as a metric to evaluate the accuracy of the decomposition (Holobar *et al.*, 2012; Taylor *et al.*, 2016).

Another approach for the discrimination of accurately identified MUs consists in the use of signal-based metrics of accuracy such as the pulse to noise ratio (PNR) (Holobar *et al.*, 2014) or the silhouette score (SIL) (Negro *et al.*, 2016), which are estimated from the decomposed source.

The PNR is a ratio between the signal and the noise (i.e., the time moments in which the MU is estimated to have or not to have discharged) expressed in decibels (dB). Specifically, the distinction between signal and noise is determined by a threshold estimated via a heuristic penalty function that accounts for the variability of the ISI and for the MUs DR (Holobar *et al.*, 2012). Therefore, also the PNR value is influenced by the MUs discharge behaviour (Holobar *et al.*, 2014). Common PNR thresholds used to determine a sufficient level of accuracy are PNR ≥ 30 dB, although also PNR ≥ 28 dB could be accepted if supported by a careful visual inspection of the MUs discharges by experienced investigators (Holobar *et al.*, 2014; Valli *et al.*, 2023).

The SIL provides an estimation of reliability similar to the PNR although with a different approach. Indeed, the SIL is defined as the normalized measure of the distance between the clusters of the detected discharge points and the cluster of the noise values (Fig. 5-5D and 5-5E). Compared to the PNR, the SIL has two main advantages in the estimation of accuracy as (i) it does not depend on the discharge behaviour of the MUs and (ii) being a normalised measure ranging from 0 to 1, it is of easy interpretation and directly associated to metrics like the rate of agreement that are commonly used in the validation of the decomposition algorithms (Negro *et al.*, 2016).

Common SIL thresholds used to determine a sufficient level of accuracy are SIL ≥ 0.9. However, as for the PNR, lower values of about 0.88 can be accepted if supported by careful visual inspection of the MUs discharges by experienced investigators (Negro *et al.*, 2016).

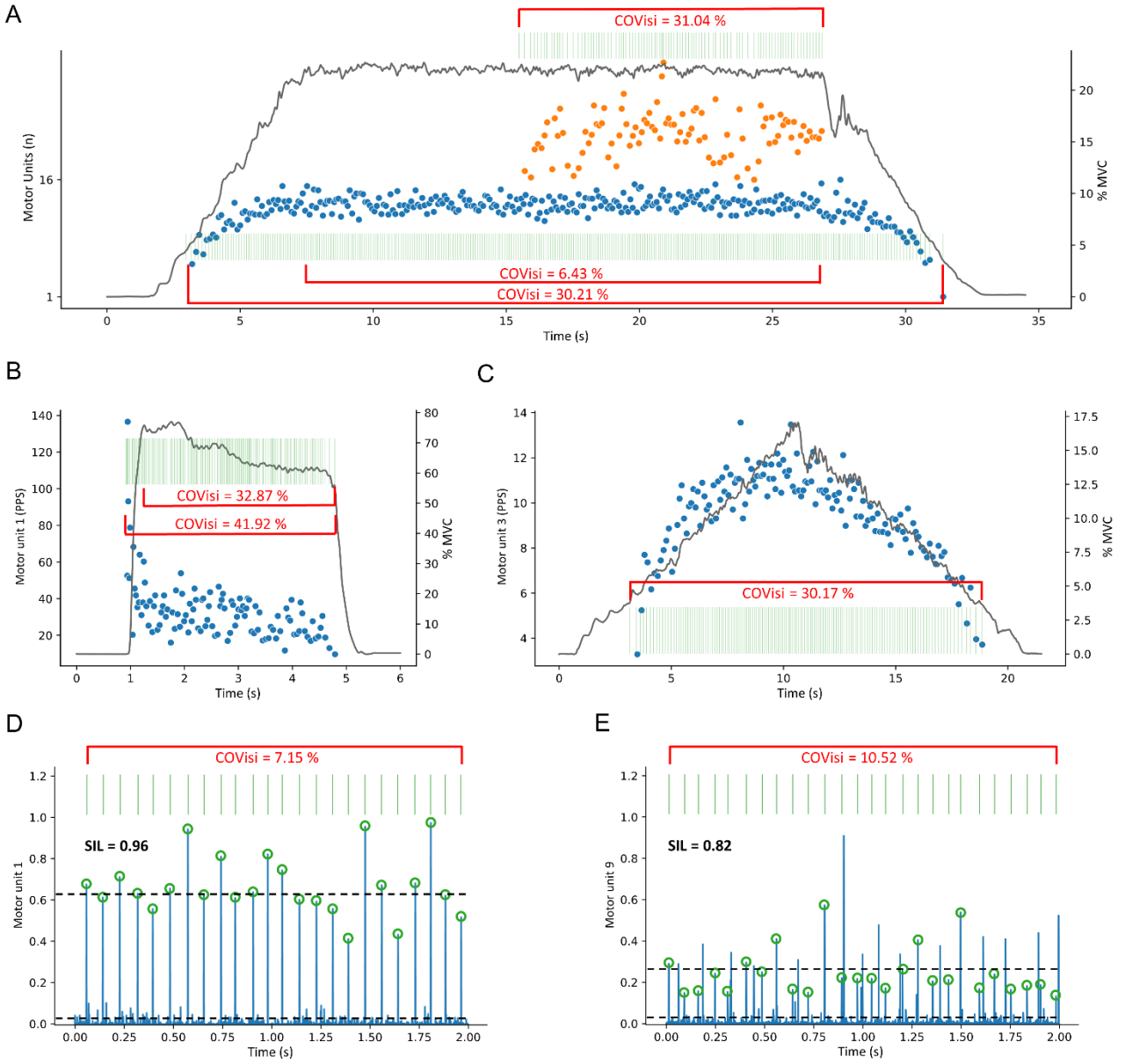


*Figure 5-5:* Accuracy of the identified motor units. The coefficient of variation of interspike interval (COVisi) estimates the regularity of the motor units (MUs) discharge events. When applied to the steady-state phase of trapezoidal contractions, it can be used to estimate the accuracy of the identified MU (e.g., MU 1 vs MU 16 in panel A). However, the COVisi is greatly affected by the discharge rate (DR) modulation necessary to increase or decrease muscle force production. Indeed, the COVisi is not an appropriate metric for contractions with a very short (B) or completely absent (C) steady-state phase. The silhouette score (SIL) is a signal-based metrics of accuracy estimating the separation between the signal (the source signal at the time of firing of the identified MU) and the noise. The SIL is therefore estimated on the decomposed source and is not affected by the discharge behaviour of the MU. Additionally, being a normalised value, it provides a clear indication of correctly (D) and incorrectly (E) identified MUs. Maximum voluntary contraction, MVC; pulses per second, PPS.

## 5.11. Track MUs within and between recording sessions

The possibility to recognise and track the same MU across different recordings and recording sessions opened new possibilities in the understanding of how MUs adjust to various types of interventions, including muscle disuse and pharmacological treatments (Goodlich *et al.*, 2023; Valli *et al.*, 2023). Indeed, comparing the same population of MUs over time provides a more robust estimation of their changes and filters the contribution of different MUs that can be detected at different data collection points (Maathuis *et al.*, 2008; Martinez-Valdes *et al.*, 2017).

The recognition of the same MU is based on the comparison of their MUAPs representation across the channels of the recording grid, thus accounting both for the shape of the MUAPs and their spatial distribution. The estimation of the MUAPs is accomplished via spike-triggered averaging of the EMG signal (Stein *et al.*, 1972; Taylor *et al.*, 2002). Spike-triggered averaging involves identifying a specific time window (e.g., 50 ms) in the EMG signal centred on each firing event of a MU, and then averaging all the signals within that window. This procedure, that has to be performed in each grid channel, enhances the definition of the MUAP by reducing the contribution of action potentials generated by neighbouring MUs. A visual representation of the spike-triggered averaging technique is provided in Fig. 5-6A.

For MUs tracking, the spike-triggered averaging is often performed on the single differential derivation of the EMG signal, because the comparison of the MUAPs in monopolar configuration tends to overestimate similarities (Martinez-Valdes *et al.*, 2017). The single differential signal is calculated by subtracting the EMG signal in two adjacent channels of the grid along the direction of the muscle fibres.

The estimation of similarity between the MUAPs representation of two MUs is usually achieved via two-dimensional cross-correlation analysis (Martinez-Valdes *et al.*, 2017). This analysis returns a two-dimensional array of values representing a subset of the discrete linear cross-correlation between the input that is then normalised for the different energy levels of the two MUs. The cross-correlation coefficient (XCC) is computed as the maximum value of the normalised cross-correlation array. XCC represents the degree of correlation between the two arrays, with values closer to 1 indicating a stronger correlation. In cases where a MU exhibits high correlation with multiple MUs in the other contraction, only the MU with the highest XCC is considered for the pair matching (Martinez-Valdes *et al.*, 2017).

The tracking technique maximises the likelihood of observing the same MU in different recordings and proved to be effective also after weeks of various interventions (Martinez-Valdes *et al.*, 2018*a*; Del Vecchio *et al.*, 2019*a*; Casolo *et al.*, 2020; Valli *et al.*, 2023). It should be noted, however, that a number of factors can undermine the successful tracking. When the tracking is performed in different recording sessions, the grid of electrodes has to be re-applied at each data collection point and changes in the grid position will alter the MUAPs representation over the different electrodes. Therefore, it is fundamental to re-apply the grid in the same exact position at each recording session. To date, the most precise way to ensure correct placement consists in marking the skin with a permanent marker. Apart from technical aspects, muscle morphology and MUAPs can also be affected by particular interventions (Inns *et al.*, 2022; Sarto *et al.*, 2022*b*), thus requiring extra attention in the validation of the tracking results.

Due to the possible confounding factors in the longitudinal MUs tracking, it becomes of extreme importance to check the reliability of the cross-correlation measure by visualising the overlying MUAPs from the pair of MUs across each channel, and to determine the inclusion/exclusion by verifying the effective overlapping of the MUAPs shape and their spatial distribution (Fig. 5-6B-D).

In order to account for the minor differences in grid placement or changes in the MUAPs profile, the XCC threshold is commonly set ≥ 0.8 (Lulic-Kuryllo *et al.*, 2021; Oliveira & Negro, 2021; Cudicio *et al.*, 2022), although some authors adopted also XCC ≥ 0.7 (Del Vecchio *et al.*, 2019*a*; Casolo *et al.*, 2020).

After identifying pairs of MUs, the user can decide to perform the subsequent statistical analyses considering both the populations of total and tracked MUs. In this case, the tracked population can be used as a validation of the results observed in the total population (Valli *et al.*, 2023). Alternatively, if the tracked population of MUs is sufficiently large and representative, the analysis can be exclusively performed on the tracked MUs. This elegant approach allows for the precise detection of single MU changes over time, offering valuable insights into the dynamics and adaptations of the neuromuscular system (Casolo *et al.*, 2020).

Recently, MUs tracking has also been employed for the identification of the same MUs within the same recording session (Valli *et al.*, 2023) with an XCC threshold ≥ 0.9 because this condition doesn’t need to account for a different placement of the recording grid or for changes in MUAPs due to interventions, as previously proposed (Maathuis *et al.*, 2008).

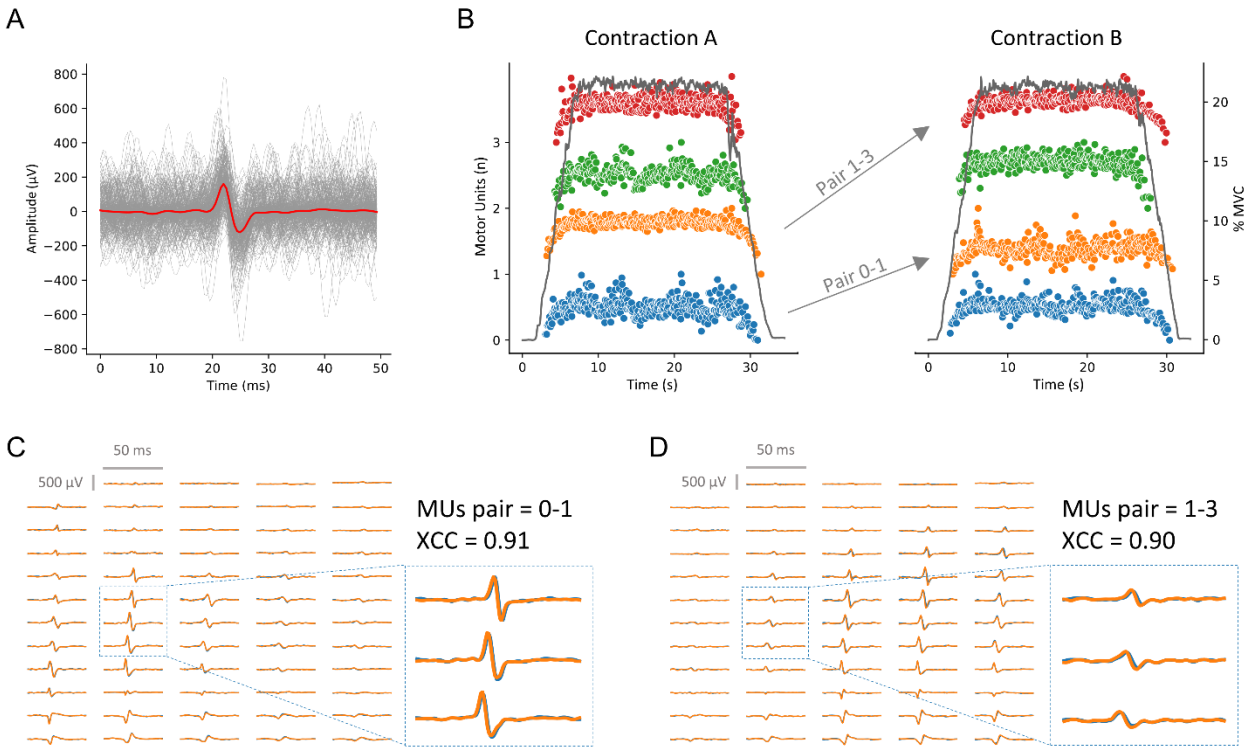


*Figure 5-6:* Motor units tracking. The shape and spatial representation of motor units (MUs) action potentials (MUAPs) shape allows for the recognition of the same MU within and between recording sessions. The estimation of smooth MUAPs is performed via averaging of all the MUAPs representations at each discharge event of the investigated MU (A). The tracking procedure is performed via two-dimensional cross-correlation analysis of the MUAPs representation (B, C, D). In these example figures, the MUAPs have been estimated from the single differential spatial filtering. The visualisation of the overlapping MUAPs of tracked pairs is fundamental for the validation of the cross-correlation analysis and must be always performed, regardless of the cross-correlation coefficient (XCC) valueb (C, D). Number, N; maximum voluntary contraction, MVC.

## 5.12. Analyse central MUs properties.

Sections 8 and 9 will introduce a number of fundamental parameters for the analysis of MUs properties that are often tuned based on empirical observations, personal experience and experimental needs. Therefore, the proposed values should only be considered as representative examples that do not constitute standards. Indeed, this necessity of flexibility is embraced by the *openhdemg* framework, which allows the user to fully customise any implemented function based on specific needs (as demonstrated in the code implementation).

The definitions of the various properties presented in section 8 and 9 are based on recent consensus statements. For more comprehensive explanations, readers are directed to (McManus *et al.*, 2021; Gallina *et al.*, 2022; Martinez-Valdes *et al.*, 2023).

MUs RT/DERT and DR are often referred as "central" properties due to their close relation with the discharge behaviour of the innervating motoneurons (Heckman & Enoka, 2004). Indeed, these variables reflect the intrinsic properties of each motoneuron and the integrated modulatory stimuli it receives, making them of primary interest in the study and characterisation of the neural control of voluntary muscle force production (Heckman & Enoka, 2012).

MU RT and DERT are simply defined as the force level at which a motor unit begins and ends to discharge action potentials repetitively. Therefore, for the analysis of MUs RT and DERT, the presence of an auxiliary input signal representing the participant's muscle force is fundamental. The auxiliary input signal can be expressed in different units of measurement (e.g., V, mV, Kg, N, Nm) and it is often reported in both absolute and normalised terms (i.e., as % MVC).

In practical terms, the estimation of these two parameters can be simply performed by identifying the first and last element in the array containing the times of discharge of each MU, and then extracting the value for the auxiliary input signal at the corresponding instants (Fig. 5-7A).

MUs DR represents the neural drive to the muscle and is defined as the number of action potentials discharged per second by a single MU. However, given its variability during contractile tasks, it is common practice to visualise the instantaneous DR, which is obtained dividing the sampling rate by the ISI between two consecutive discharges (Fig. 5-7A). Of note, MUs DR is expressed as pulses per second (PPS), unlike typical frequency units.

In order to reduce this variability and to obtain a more robust estimation, MUs DR is usually analysed and reported as the average instantaneous DR over a number of consecutive discharges. MUs DR can be estimated within different phases of a voluntary contraction, such as in the

recruitment phase, derecruitment phase and the steady-state phase. For recruitment and derecruitment, it is necessary to find a compromise between robustness and sensitivity (Del Vecchio *et al.*, 2020). This is often achieved by averaging the intervals generated by few (e.g., 3-5) consecutive discharges at the beginning and at the end of the contraction (Fig 5-7A) (Del Vecchio *et al.*, 2019*a*; Valli *et al.*, 2023). During the steady-state phase, all firings can be averaged (Škarabot *et al.*, 2022). However, if the steady-state phase is long (e.g., > 20-25s), the estimation of MUs DR is affected by the physiological decline in DR, especially for MUs with lower recruitment thresholds (Pascoe *et al.*, 2014*b*). In such cases, it is possible to limit the estimation of MUs DR to a fixed number of discharges (e.g., 20-50) at the beginning of the steady-state phase.

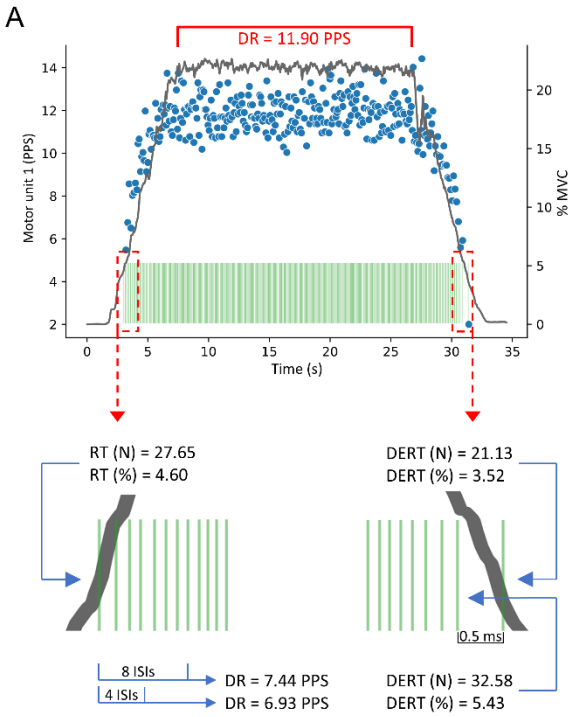


*Figure 5-7:* Analysis of central motor units properties. Motor units (MUs) recruitment threshold (RT) and derecruitment threshold (DERT) are estimated as the force value (which can be expressed both in absolute and relative terms) at which the MU begins or stops to discharge action potentials repetitively. In this example, MUs discharge rate (DR) is estimated as the average value of a number of consecutive discharges at recruitment, derecruitment and during the entire steady-state phase. Based on the criteria used to manually determine the inclusion and exclusion of firings, the results of these analyses can vary significantly. Therefore, it is necessary to consistently adopt the same criteria for the manual editing of MUs discharges in order to have consistent and reliable results from the analysis of central MUs properties. Pulses per second, PPS; maximum voluntary contraction, MVC; interspike intervals, ISIs.

## 5.13. Analyse peripheral MUs properties

MUCV and amplitude of the action potentials are often referred to as “peripheral” properties, as they primarily depend on the morphology and biology of the innerved muscle fibres (Casolo *et al.*, 2023). Therefore, these two parameters have significant physiological relevance in the investigation of aspects concerning the generation and propagation of the MUAPs in response to the motoneuron discharges (Blijham *et al.*, 2006; Campanini *et al.*, 2009).

MUCV represents the speed at which the MUAPs propagate along the sarcolemma of the muscle fibres belonging to single MUs and it is considered a “size principle parameter” due to its linear association with MUs RT and with muscle fibre diameter (Andreassen & Arendt-Nielsen, 1987; Del Vecchio *et al.*, 2017; Casolo *et al.*, 2023).

MUAP amplitude is considered an important parameter for inferring the size of single MUs, but it must be noticed that estimation from surface HD-sEMG recordings presents high variability. Indeed, MUAP amplitude is considerably influenced by muscle architecture, subcutaneous tissue thickness and proximity of the MU among other factors. Although this value can be informative, the direct estimation of MUs size from measures of MUAP amplitude is not generally recommended (Martinez-Valdes *et al.*, 2023). MUAP amplitude can be quantified using various measures, including peak-to-peak distance or root-mean-square of the MUAPs. When reported alongside MUCV, MUAP amplitude can be calculate on the same MUAPs and channels used for MUCV estimation (Del Vecchio *et al.*, 2017).

The estimation of the MUAPs for the analysis of peripheral MUs properties is usually performed via spike-triggered averaging of the EMG signal as previously described. For the estimation of MUCV, the spike-triggered averaging is usually computed on the double differential derivation of the EMG signal along the direction of the muscle fibres. This spatial filtering decreases the presence of non-propagating components and attenuates the end-of-fibre effect, thus enhancing the representation of MUAPs propagation (Fig. 5-8A-C) (Gallina *et al.*, 2022). The double differential signal is calculated over three adjacent channels of the grid by subtracting the EMG signal in the first channel from twice the EMG signal in the second channel, and then subtracting the EMG signal in the third channel.

Given the definition of MUCV as a size principle parameter, the spike triggered average for this analysis is usually calculated over a number of discharges that provide a balance between the smoothing in the MUAPs (improved by a higher number of averaged samples) and the

representation of the MUCV value at the recruitment phase. Although there is no reference value, the actual literature seems to favour the computation of the spike-triggered average over the first 20-50 discharges at recruitment (Martinez-Valdes *et al.*, 2018*a*; Casolo *et al.*, 2023).

On the generated MUAPs, the estimation of MUCV is performed via maximum likelihood estimation of the time delay over a number of channels with specific characteristics. Given its complexity, the technical implementation of the maximum likelihood estimation cannot be explained adequately in this tutorial and the reader is encouraged to read specific articles on the topic (Farina *et al.*, 2000, 2002).

The identification of channels for estimating MUCV involves a manual selection process. It requires the visual examination of adjacent channels within a column of the grid to identify those that show the clearest propagation of the action potential and exclude the innervation zone (identified as the inversion of the action potential shapes and of their direction of propagation). The choice of the channels is supported by the cross-correlation value between adjacent pairs. This cross-correlation analysis helps in identifying pairs with strong similarities in their MUAP patterns, indicating consistent propagation characteristics. Additionally, a minimum cross correlation threshold is often employed to ensure the acceptability of pairs. Similarly to MUs tracking, a threshold ≥ 0.8 is expected to yield most reliable estimations, although a cross-correlation threshold ≥ 0.7 is also often adopted (Škarabot *et al.*, 2022). A minimum of 2 channels are technically sufficient for MUCV estimation via maximum likelihood. However, it is strongly recommended to include 3 or more channels to increase the accuracy of the estimates.

It is important to note that the physiological range of MUCV during voluntary contractions typically falls between 2 and 8 m/s (Farina *et al.*, 2002; Beretta-piccoli *et al.*, 2019). Any values outside of this range are likely to be the result of errors in data collection (e.g. electrodes misalignment) or analysis (e.g., wrong selection of the channels) and should be disregarded.

Given the complexity of the selection of appropriate channels, and the necessity of visual inspection, the user is encouraged to refer to Fig. 5-8D-F for a clear presentation of this procedure.

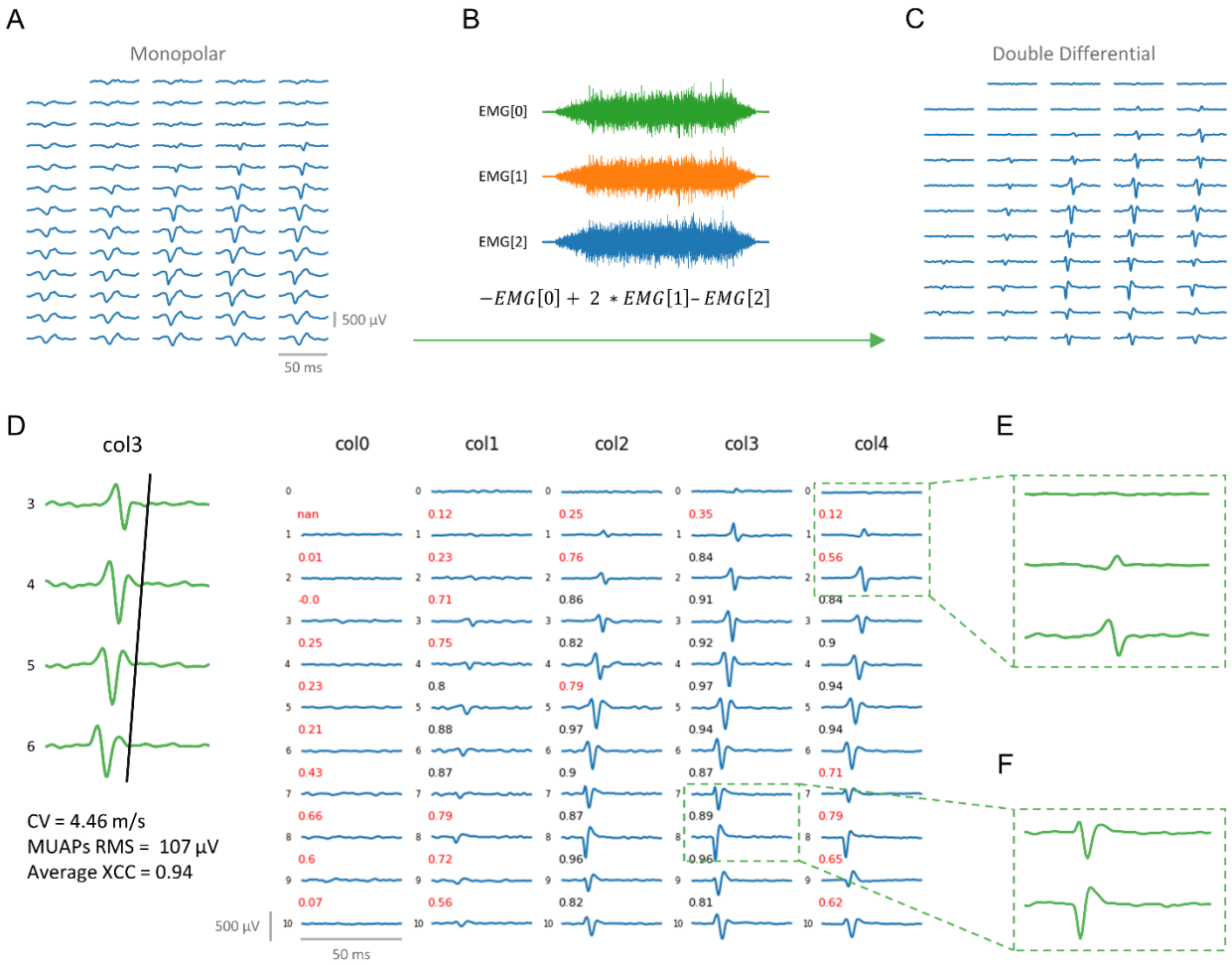


*Figure 5-8:* Analysis of peripheral motor units properties. The estimation of motor units (MUs) conduction velocity (MUCV) is usually performed on the MUs action potentials (MUAPs) representation estimated from the double differential spatial filtering of the raw EMG signal (A, B, C). MUCV represents the speed at which the MUAPS propagate along the sarcolemma of the muscle fibres (D). For the reliable estimation of MUCV, it is fundamental to select the largest number of adjacent channels (in the direction of muscle fibres, represented in columns in the *openhdemg* interface) showing a clear propagation of action potentials and high cross-correlation coefficients (XCC). In the selection of the channels, it is necessary to avoid the MUAPs presenting the end-of-fibres effect (extinction of action potentials) (E) and the innervation zone (inversion in the propagation direction) (F), as these will significantly alter the estimation of the MUCV value.

## 5.14. Final remarks and conclusions

This tutorial provides a detailed explanation of crucial steps for the analysis of MUs properties from HD-sEMG recordings. Furthermore, it introduces the possibility to perform MUs analyses with *openhdemg*, an efficient tool that can lower the barriers to the implementation of the HD-EMG technique thanks to its user-friendly structure, extensive documentation, and flexible architecture easily accessible to researchers with varying levels of programming experience.

*openhdemg* is an opensource framework in continuous expansion and will continue to evolve based on user feedback and emerging research needs, fostering collaboration and knowledge sharing within the HD-EMG community.

# 6. General discussion

This thesis is constituted by two experimental chapters in which the HD-EMG technique has been used to investigate the consequences of muscle disuse and type 1 diabetes on the neural control of muscle force production. In addition to these investigations, the last chapter is dedicated to the development of an open-source framework designed to facilitate the analysis of HD-EMG recordings.

HD-EMG is a relatively modern evolution of surface EMG that allows for the investigation of neural control by monitoring directly and non-invasively the behaviour of active MUs (Gallina *et al.*, 2022). It provides insights into the properties of muscle membrane and of the innervating motoneurons, which are particularly valuable when studying conditions that affect the neuromuscular system (Gallego *et al.*, 2015*b*).

Due to the only recent introduction and evolution of the HD-EMG technique, our previous understanding of the adaptation and degeneration of neural control to different conditions was often limited by the absence of suitable techniques. For example, the classic bipolar surface EMG does not allow to detect individual MUs and can only provide a rough and indirect estimate of MUs behaviour (Farina & Enoka, 2023). Before the introduction and evolution of HD-EMG, intramuscular EMG was the most common method to identify single MUs. Indeed, intramuscular EMG has been widely adopted in the study of MUs behaviour in humans, it allowed for major advances in the field and is widely adopted in clinical settings (Piasecki *et al.*, 2021). However, this technique presents several limitations, such as the invasiveness, the small sampling area, and the capacity to identify only a small number of MUs, therefore limiting the range of possible analysis (Farina *et al.*, 2016). Given these technical limitations, the neuromuscular consequences of muscle disuse and other chronic conditions, including type 1 diabetes, have been under-researched.

For example, the few available studies on muscle disuse predominantly focused on small muscles, where intramuscular EMG can provide the best results (Duchateau & Hainaut, 1990; Seki *et al.*, 2001, 2007). However, small muscles may substantially differ in properties and adaptations from larger muscles, which adopt different strategies of muscle force production (De Luca, 1985). Given the significance of large muscles for locomotion and daily activities, this limitation significantly impacts the existing knowledge base.

In the context of type 1 diabetes, it is well-established that this condition leads to various long-term complications, including neuropathy (Daneman, 2006). Yet, there is a considerable lack

of knowledge concerning the neuromuscular status of individuals with type 1 diabetes prior to the clinical diagnosis of neuropathy, and how this degeneration evolves over time, before becoming manifest (Monaco *et al.*, 2017).

In both type 1 diabetes and muscle disuse, the limited understanding of their effects on the neuromuscular system prevents the development of effective countermeasures and the design of early detection screenings, therefore demanding additional investigation with appropriate techniques.

Finally, while HD-EMG holds great potential for investigating neural control and neuromuscular degeneration, its widespread adoption has been limited by the technical complexities associated with data collection and analysis (Felici & Del Vecchio, 2020). Indeed, sophisticated algorithms are necessary to analyse the acquired data, requiring expertise in signal processing and coding. This barrier prevented many researchers from adopting this technique and slowed down the progress in the study of neuromuscular degeneration. Consequently, this work also addressed the development of a tool aimed at enabling researchers to overcome these challenges and leverage HD-EMG for further advancements in this field.

## 6.1. Altered neuromuscular function: a common outcome of Muscle disuse and type 1 diabetes

Muscle disuse (as investigated in Experimental Chapter 1) and type 1 diabetes are distinct conditions, differing primarily in their aetiology, duration, and progression.

Aetiology: Muscle disuse can arise from various factors that reduce limb loading, including diseases requiring hospitalization, injuries preventing movement, and conditions like space flights that reduce gravitational load. In these scenarios, reduced muscle activation leads to decreased neural drive to the muscle, driving adaptations within the neural components and resulting in a significant decline in force production (Reggiani, 2015). Conversely, type 1 diabetes is an autoimmune disease primarily affecting pancreatic beta cells (Devendra *et al.*, 2004). Consequently, the associated comorbidities and complications mainly result from disrupted glycaemic control. For instance, type 1 diabetes adverse effects on skeletal muscle likely arise from extreme glucose fluctuations in both muscle and motoneurons, potentially leading to increased production of reactive oxygen species and higher inflammation, thereby damaging the affected structures (Monaco *et al.*, 2017).

Duration: Muscle disuse typically lasts for relatively short periods, ranging from days to months (excluding chronic forms of reduced physical activity that are not the focus of this thesis). In contrast, type 1 diabetes persists throughout all the lifespan from the initial onset. This disparity in duration corresponds to differences in the intensity and pace of the conditions' consequences.

Progression: Due to the different magnitude of the physiological alterations induced by the two conditions, neural degeneration progresses more rapidly during muscle disuse than in type 1 diabetes. However, the chronic nature of diabetes fundamentally alters its management and long-term outcomes. Muscle disuse can often be counteracted by exercise interventions after a period of reduced mobility, potentially allowing complete recovery, especially in young individuals (Valli *et al.*, 2023). Conversely, for type 1 diabetes, while interventions can slow progression and maintain the condition, manifest neuromuscular alterations are likely to develop over time, making a complete prevention of the progression improbable (Monaco *et al.*, 2019).

Despite these differences, both conditions inevitably lead to a decline or change in neuromuscular function, as elucidated in the experimental chapters of this thesis. The effective management of these conditions necessitates of a comprehensive understanding of the ongoing changes, alongside with sophisticated techniques capable of precisely detecting even subtle alterations in the neural condition. Such capabilities facilitate the early detection of neuromuscular degeneration and guide the implementation of timely and individual-tailored interventions.

In this context, the experimental chapters presented in this thesis not only contribute to our understanding of muscle disuse and type 1 diabetes but also underscore the critical importance of cutting-edge techniques like HD-EMG in advancing our ability to detect and manage neuromuscular conditions effectively.

## 6.2. Discharge rate as an indicator of the neural condition

HD-EMG can provide different estimates of the neural and muscular condition, yet, MUs DR emerges as one of the primary indicators of the consequences associated with the underlying neuromuscular conditions. This observation finds support in the existing literature (Nuccio *et al.*, 2021; Škarabot *et al.*, 2022; Nishikawa *et al.*, 2022) and is also corroborated by the experimental chapters presented in this thesis. Additionally, MUs DR exhibits a remarkable capacity to reflect changes in response to both positive interventions (e.g., exercise) (Škarabot *et al.*, 2021) and

negative stressors (e.g. disuse) (Duchateau & Hainaut, 1990), with a particular sensitivity to even minor modifications (Dideriksen & Del Vecchio, 2023).

in the present thesis, the two experimental chapters involving negative stressors such as disuse and type 1 diabetes, both induced a reduction in DR, which might be caused by changes in the intrinsic properties of the motoneuron, diminished descending neural inputs to the motoneuron, altered excitatory/inhibitory feedback mechanisms, or perturbations in neuromodulatory processes at the spinal level (Heckman & Enoka, 2012).

In this regard, although the understanding of the precise causes of reduced DR is challenging and should be further investigated in the context of the specific disease (i.e., type 1 diabetes in our case), DR might still represent a biomarker for assessing neural condition. Indeed, the potential utility of such a parameter as a robust biomarker for assessing neural condition hides in its simplicity, making it an interesting tool for both clinical and research applications. Furthermore, its sensitivity to both subtle and pronounced changes might allow for early detection of neural adaptations or abnormalities.

In clinical settings, early detection is crucial for timely interventions, especially in conditions where neural alterations can progress insidiously. From a research perspective, researchers can utilize MUs DR to investigate the effects of different interventions, and use this information to guide further investigations aimed at understanding the processes that drive these adaptations.

It is necessary to mention, however, that although MUs DR can be informative, in research settings it is often not sufficient to obtain a complete picture of the underlying changes or of the mechanisms responsible for them. For example, in our study of type 1 diabetes, it has been necessary to combine this information with additional analyses uncovering the muscular condition, which allowed for a more comprehensive understanding of the disease (Minnock *et al.*, 2022). Indeed, we combined the analysis of MUs DR with the estimation of peripheral MUs properties such as MUs CV and amplitude of the action potentials. Given the strong relationship between peripheral MUs properties and the size of muscle fibres (Casolo *et al.*, 2023), we could exclude structural alterations in the muscle, hypothesis that also found support in the analysis of muscle biopsies.

It must be noted, however, that analyses such as MUs CV are more time-consuming and technically more complicated than the straightforward estimation of MUs DR, especially until 2022, when no software was available to perform these analyses.

## 6.3. Challenges and solutions for the widespread adoption of HD-EMG

As evidenced in this thesis and in the existing literature, HD-EMG can be successfully adopted to investigate the neuromuscular condition. Furthermore, its potential applications in screening and monitoring are promising. However, despite its clear benefits, the widespread adoption of HD-EMG for both research and non-research purposes remains a challenge (Felici & Del Vecchio, 2020).

There are a number of factors limiting the use of HD-EMG, including:

- Data Collection Complexity: HD-EMG requires precise electrode placement, both in position and orientation, in addition to requiring a good skin-electrode contact. This is time-consuming and requires specialised training.
- Signal Processing Complexity: The raw data generated by HD-EMG is of complex interpretation and sophisticated algorithms are necessary to extract the discharge activity of single MUs.
- Equipment Cost and Availability: Acquiring the necessary hardware for HD-EMG can be expensive (20.000 to 50.000 €), limiting access for many researchers.
- Interpretation Complexity: Interpreting HD-EMG data requires expertise in neuromuscular physiology and understanding of the underlying signal processing techniques.
- Knowledge Dissemination: Resources for training and education, both for data collection and analysis are rarely available, impeding the approach of new users.

To overcome these barriers, a collaborative approach across multiple disciplines is necessary, and it should encompass engineers to design user-friendly and cheaper machines for data collection, those developing the algorithms for the analysis, and those knowing the physiological principles required to interpret the results.

In the third experimental chapter of this thesis, we aimed at lowering some of the barriers by developing the first (and currently unique) available tool for HD-EMG data analysis. This open source framework, named *openhdemg,* is oriented to a broad range of users, as previously described, and aims to address the limitations in signal processing complexity, interpretation complexity and knowledge dissemination.

Indeed, *openhdemg* is not simply a software or tool to perform analysis tasks, as it represents a community-driven project. It provides a platform where individuals from various backgrounds can collaborate, share their expertise, and collectively advance the field. Additionally, the project's

website will be enriched with authoritative tutorials aimed at providing guidance to those approaching the technique.

This collaborative and inclusive approach is expected to contribute significantly to the wider adoption of HD-EMG, making it more accessible to researchers and professionals across different disciplines.

# 7. Future perspectives

The studies presented in the experimental chapters provide novel insights on the neural condition in disuse and type 1 diabetes, expanding on the available literature. However, they also open to more research questions and highlight the necessity of a better characterisation of the studied conditions. In this final section, I will present some hypothetical or planned extensions to the presented projects and the associated research hypothesis.

Furthermore, an open-source community project is, by definition, a long-term activity with expected future developments. As the project grows and collaborations increase, we expect evolutions and advancements. Some of these anticipated developments are also discussed in this final section.

## 7.1. Muscle disuse

We demonstrated that 10 days of unilateral lower limb suspension induce a noticeable reduction in muscle force production and MUs DR in young adult males during isometric submaximal contractions. At the same time, we also demonstrated that the neural consequences were specific for lower-threshold motoneurons. Furthermore, we also demonstrated that an active recovery period, lasting twice as much as the disuse period, is necessary to recover from the disuse-induced impairments.

In light of this, many questions and considerations arise:

- What happens with longer duration of disuse?
- What happens if more or less severe models of disuse are adopted?
- What would be the manifestation of the neural impairment in different types of contractions?
- Could we observe differences between males and females?
- How would older individuals respond compared to younger ones?
- How would all these variables and the type of exercise affect the recovery period?

Although we observed a preferential impairment of 10 days of disuse on lower-threshold motoneurons, it is unknown whether this response will be preserved during longer disuse periods or with more severe models, such as complete limb immobilisation. Therefore, this aspect will benefit from a direct assessment. Looking at literature, we will be facing with very limited evidence

on neural adaptations to disuse (Duchateau & Hainaut, 1990; Seki *et al.*, 2001, 2007), although one study suggests that the preferential degeneration of lower-threshold MUs is present also after 3 weeks of cast immobilisation on hand muscles (Duchateau & Hainaut, 1990). Additionally, if we look at the more extensive literature on molecular and structural changes after disuse, we could expect this finding to remain valid, considering the studies suggesting a preferential degeneration of slower muscle fibres in response to different disuse models and duration (Appell, 1990; Ohira *et al.*, 2002; Widrick *et al.*, 2002) and even to complete muscle denervation (e.g., after spinal cord injury) (Ciciliot *et al.*, 2013).

For what concerns the different types of contraction that can be performed during the neuromuscular assessment, we could expect contrasting findings when applied to different disuse models or duration. For example, it has been demonstrated that the changes in rate of force development after disuse do not closely match those in muscle force, whit the changes in rate of force development that might manifest at later stages, or even not manifest at all (Campbell *et al.*, 2019). Additionally, biological studies demonstrated that bed rest induces a greater reduction in fibres' maximum shortening velocity compared to limb suspension (Reggiani, 2015). Overall, the available literature suggests that faster or slower types of contraction, such as trapezoidal or explosive, might detect different adaptations to disuse.

Regarding sex differences, we have no evidence of how males and females respond to disuse for what concerns neural control, and we also know very little about the physiological differences in neuromuscular recruitment strategies that seem to be present between males and females (Guo *et al.*, 2022; Lulic-Kuryllo & Inglis, 2022). Therefore, studies aimed at investigating the different neuromuscular response to disuse between males and females are needed. Additionally, in line with our approach to other parameters, it could be helpful to consider the existing literature on sex differences in molecular adaptations to disuse (Rosa-Caldwell & Greene, 2019), which suggests that a noticeable difference on the impact of disuse in males and females should be expected, with females that appear to be more susceptible to disuse.

Aging has been associated with increased susceptibility to disuse-related effects (Mahmassani *et al.*, 2019), as well as with a reduced capacity to activate the muscle (i.e., reduced activation capacity) (Suetta *et al.*, 2009). Consequently, we could expect that neural degeneration may be more pronounced in older individuals, although possibly following a similar trajectory to that observed in younger individuals.

Lastly, the time required for recovery from disuse consequences may be greatly influenced by exercise parameters (i.e., type, duration, intensity, and frequency), by the duration of disuse (with longer disuse likely requiring extended recovery) (Nunes *et al.*, 2022), and the age of participants (Suetta *et al.*, 2009). Indeed, older participants may require more time to recover and may not fully regain their previous performance capacity (Hvid *et al.*, 2014; Rejc *et al.*, 2018). Therefore, there is a broad range of recovery protocols that could be designed and that have not been tested yet. For example, these protocols might aim at obtaining the best results when applied to different disuse models, to disuse periods of different duration, and for different populations.

## 7.2. Type 1 diabetes

Type 1 diabetes is a chronic disease which consequences are closely related to the quality of glycaemic control and the duration of the diseases (Pelletier *et al.*, 2012). Indeed, poor glycaemic control and disease duration are associated with an early onset of comorbidities and complications (Nathan *et al.*, 1993; Daneman, 2006). Consequently, it is plausible to believe that these above-mentioned factors, and age, may have a significant impact on the development of neuromuscular problems.

Our study showed, for the first time, that young people living with type 1 diabetes, with good fitness level, glycaemic control, and no clinical manifestation of neuropathy present different strategies of neural control compared to a matched healthy control group. This basic, but still novel finding highlights the importance of gaining a more comprehensive understanding of the neural condition in type 1 diabetes, and to become aware of how the aforementioned factors affect the progression of the disease from a neural perspective.

In light of this, many questions and considerations arise. In particular, how do age, diabetes duration, and glycaemic control influence the progression of neural degeneration in type 1 diabetes?

We could hypothesise that age, diabetes duration, and glycaemic control are interconnected factors that negatively impact the progression of neural degeneration in type 1 diabetes (Daneman, 2006). Also according to the available literature on the consequences of these factors on muscle health (Monaco *et al.*, 2021), we expect that older individuals with longer diabetes durations and poorer glycaemic control will exhibit more pronounced neural degeneration.

Building upon the previous hypothesis, we expect that neural degeneration in type 1 diabetes will not remain limited to a mild manifestation but will extend to functional and structural alterations. Specifically, we suggest that individuals with more advanced neural degeneration will experience reduced muscle force and mass.

If people with type 1 diabetes present various levels of neural degeneration across their lifespan and based on the quality of the management of the condition, it is also reasonable to hypothesise that that individuals with type 1 diabetes may exhibit blunted neural adaptations to exercise, as previously demonstrated for functional adaptations (Minnock *et al.*, 2022), with greater differences in the older cohort.

Finally, we postulate that males and females with type 1 diabetes may exhibit different responses to neural degeneration or experience varying magnitudes of manifestation, as previously demonstrated at muscle level (Monaco *et al.*, 2021; Dial *et al.*, 2021). Therefore, it would be of interest to examine whether sex-based differences in neural degeneration, and responses to exercise interventions exist in the context of type 1 diabetes.

## 7.3. openhdemg

Since the initial public release on July 2023, the *openhdemg* framework has been facing some challenges and obtained noticeable achievements. As for any community-based project, the greatest challenge is to gather people with similar or complementary expertise to contribute together to the development of new functionalities, to improve the existing ones and to improve the overall usability and accessibility of the framework.

A series of actions have been taken to achieve these goals, including:

- Website redesign: we performed a comprehensive website redesign to simplify site URLs and create direct links that connect users between the documentation and the source code. These changes improved the online resource navigation, making it more user-friendly.
- Tutorial articles: periodically, we publish tutorial articles aimed at guiding new users through the fundamental concepts necessary to take advantage of the library's capabilities. These tutorials aim to simplify the experience of newcomers to the library.
- Graphical user interface section: we dedicated a website section to cover all the use cases of our graphical user interface. This guide enables new users to exploit the library's functionalities without requiring coding skills.

- Contributor recruitment: To expand our community of contributors, we've introduced a dedicated website section that outlines the project's roadmap and provides information on how individuals can get involved and contribute to the development of the *openhdemg* framework.

All these actions simplified and favoured the approach of new users and increased the awareness of the public of what an open-source community-driven project means. Indeed, we received a number of feedback and suggestions that drove the second public release (September 11, 2023) and that opened discussions on the future necessities of the project.

Our outreach efforts, online and during international conferences, allowed us to establish connections with HD-EMG experts who have generously agreed to contribute to the ongoing development of the library's functionalities. Additionally, we are in the process of collaborating with these experts to create educational materials that will serve for the educational goals of the *openhdemg* framework in the near future.

In conclusion, the future development of the *openhdemg* framework will be driven by the objective necessities of open-source projects and by the feedback of the users, with the main goal of favouring a collaborative and friendly environment.

## Glossary

In alphabetical order:

| | |
|---|---|
| All-or-none principle | The concept that a neuron or muscle fibre either fully responds to a stimulus (fires) or does not respond at all. |
| Afterhyperpolarization phase | A brief period following an action potential during which the neuron's membrane potential becomes more negative than the resting potential. |
| Baseline Noise | The background noise present in the HD-EMG signal that is unrelated to MU action potentials. Accurate decomposition aims to distinguish MU spikes from this noise. |
| Computational Tools | These are software and algorithms used to process and analyse EMG data. Advances in computational tools have played a crucial role in the analysis of HD-EMG recordings, enabling the identification and mapping of MU action potentials. |
| Contrast Function | The contrast function is used in the iterative optimization procedure of independent component analysis. It's a mathematical function that guides the optimization algorithm to find the best estimates for the mixing matrix and original sources. |
| Convolutive Blind-Source Separation | A computational method used in HD-EMG decomposition to separate the mixed signals from multiple MUs. |
| Convolutive Sphering | Convolutive sphering is a signal processing technique used to transform signals so that they become more amenable to separation. In the context of HD-EMG decomposition, it involves extending and whitening the recorded signals to convert a convolutive model into an instantaneous one, making it easier to separate MU action potentials. |
| Current flow | The movement of electric charge (ions) through the neuron's membrane, which is responsible for changing the membrane potential. |
| End-Plate Potential | The depolarizing graded potential generated at the motor end plate in response to acetylcholine binding. It must reach a threshold for the muscle fibre to initiate an action potential. |
| Excitatory post-synaptic potential | The change in the membrane potential of a neuron that makes it more likely to generate an action potential. |
| Extension | In the context of HD-EMG signal processing, extension refers to incorporating delayed replicas of the original signals. This transformation helps convert the convolutive model into an instantaneous one. |
| Filters | Filters, in the context of HD-EMG decomposition, are sets of parameters or mathematical operations applied to the mixed signals during independent component analysis. These filters aim to produce statistically independent output signals, which are the estimated source signals representing MU activity. |

| | |
|---|---|
| Histochemical profiles | The staining patterns of muscle fibres that can be used to identify their type and characteristics. |
| Independent Component Analysis | A mathematical technique used in HD-EMG decomposition to estimate the mixing matrix and original source signals. It aims to find filters that produce statistically independent output signals, which represent the estimated MU action potentials. |
| Inhibitory post-synaptic potential | The change in the membrane potential of a neuron that makes it less likely to generate an action potential. |
| Innervation Zone | The innervation zone is the area of a muscle where the motoneuron's axon enters to innervate the muscle fibres. It's a critical location for EMG electrode placement. |
| Input Conductance | The size of the motoneuron soma and dendritic branches determines input conductance. Smaller motoneurons have higher input resistance and are easier to recruit. |
| Input resistance | The ease with which a neuron's membrane potential changes in response to incoming electrical signals. |
| Input-output function | Describes the relationship between the magnitude of synaptic input and the discharge rate (frequency of action potentials) of motoneurons. |
| Interference Electromyography Signal | This is the recorded electrical activity of a contracting muscle obtained using HD-EMG. It's characterized by the superimposition of action potentials from multiple MUs and is influenced by the volume conductor and muscle fibre geometry. |
| Ion channels | Proteins in a neuron's membrane that control the flow of ions (e.g., sodium, potassium, calcium) in and out of the cell. |
| Ionotropic synaptic channels | Ligand-gated channels that mediate synaptic transmission by responding to neurotransmitter binding. |
| Leak channels | Ion channels that allow the passage of ions, primarily potassium, and regulate the resting potential. |
| Man-Machine Interface | Man-machine interface refers to technologies or systems that allow direct communication or interaction between a human and a machine. In this context, HD-EMG can be used as an interface for controlling machines or devices based on muscle signals. |
| Mixing Matrix | In the context of independent component analysis (ICA) and source separation, the mixing matrix is a mathematical matrix that describes how the original source signals (in this case, MU action potentials) are linearly combined to create the observed mixed signals (recorded HD-EMG signals). The goal of ICA is to estimate this matrix, allowing the separation of the original sources. |
| Monoclonal antibodies | Antibodies that target specific isoforms of proteins, used in muscle fibre typing. |
| MU Decomposition | This is the process of separating the combined EMG signal from multiple MUs into individual MU action potentials. It's a complex task that requires advanced algorithms. |
| Muscle unit | A group of muscle fibres innervated by a single motoneuron, functioning as a coordinated unit. |

| | |
|---|---|
| Pulse Train | A series of discrete pulses or spikes in the decomposed HD-EMG signal that represent the firing times of individual MUs. |
| Random synaptic noise | Variability in the synaptic inputs to a motoneuron due to random factors. |
| Resting potential | The baseline electrical charge of a neuron's membrane when it's not transmitting signals |
| Sigmoidal relationship | A characteristic curve that describes the relationship between motoneuron discharge rate and muscle force, showing a threshold beyond which further increases in discharge rate do not result in higher contractile force. |
| Spatial Resolution | Spatial resolution refers to how finely the technique can detect and distinguish signals from different areas of the muscle surface. |
| Synaptic input | The current flow from dendrites to the soma, driving depolarisation and initiating action potentials. |
| Voltage-gated channels | Channels that open or close in response to changes in membrane potential and play a role in generating and propagating action potentials. |
| Voltage-gated Na+ channels | Channels that open in response to a depolarization of the membrane potential and are responsible for the rapid depolarization phase of an action potential. |
| Volume Conductor | This refers to the tissues between muscle fibres and the skin through which the EMG signal passes. It affects the filtering and propagation of muscle action potentials, leading to changes in their shape and synchrony. |
| Whitening | Whitening is a signal processing technique applied to the HD-EMG signals. It serves to decorrelate the extended measurements, reducing the impact of volume conductor filtering and improving the spatial-temporal representation of the signals. |

## References


Adrian ED & Bronk DW (1928). The discharge of impulses in motor nerve fibres: Part I. Impulses in single fibres of the phrenic nerve. *J Physiol* **66,** 81.

Adrian ED & Bronk DW (1929). The discharge of impulses in motor nerve fibres: Part II. The frequency of discharge in reflex and voluntary contractions. *J Physiol* **67,** i3.

Ahtiainen JP (2019). Physiological and Molecular Adaptations to Strength Training. In *Concurrent Aerobic and Strength Training: Scientific Basics and Practical Applications*, ed. Schumann M & Rønnestad BR, pp. 51–73. Springer International Publishing, Cham. Available at: https://doi.org/10.1007/978-3-319-75547-2_5.

Alvarado-Martel D, Velasco R, Sánchez-Hernández RM, Carrillo A, Nóvoa FJ & Wägner AM (2015). Quality of life and type 1 diabetes: a study assessing patients' perceptions and self-management needs. *Patient Prefer Adherence* **9,** 1315–1323.

Andreassen CS, Jensen JM, Jakobsen J, Ulhøj BP & Andersen H (2014). Striated muscle fiber size, composition, and capillary density in diabetes in relation to neuropathy and muscle strength. *J Diabetes* **6,** 462–471.

Andreassen S & Arendt-Nielsen L (1987). Muscle fibre conduction velocity in motor units of the human anterior tibial muscle: a new size principle parameter. *J Physiol* **391,** 561–571.

Appell HJ (1990). Muscular atrophy following immobilisation. A review. *Sports Med* **10,** 42–58.

Ariano MA, Armstrong RB & Edgerton VR (1973). Hindlimb muscle fiber populations of five mammals. *J Histochem Cytochem* **21,** 51–55.

Atherton PJ & Wilkinson DJ eds. (2023). *Neuromuscular Assessments of Form and Function*. Humana, New York, NY.

Bączyk M, Manuel M, Roselli F & Zytnicki D (2022). Diversity of Mammalian Motoneurons and Motor Units. In *Vertebrate Motoneurons*, ed. O'Donovan M. & Falgairolle M. Springer International Publishing, Cham.

Bagust J, Knott S, Lewis DM, Luck JC & Westerman RA (1973). Isometric contractions of motor units in a fast twitch muscle of the cat. *J Physiol* **231,** 87–104.

Bakdash JZ & Marusich LR (2017). Repeated measures correlation. *Front Psychol* **8,** 456.

Barrett EF, Barrett JN & Crill WE (1980). Voltage-sensitive outward currents in cat motoneurones. *J Physiol* **304,** 251.

Bates D, Mächler M, Bolker BM & Walker SC (2015). Fitting Linear Mixed-Effects Models Using lme4. *J Stat Softw* **67,** 1–48.

Beretta-piccoli M, Cescon C, Barbero M & Antona GD (2019). Reliability of surface electromyography in estimating muscle fiber conduction velocity : A systematic review. *J Electromyogr Kinesiol* **48,** 53–68.

Berg HE, Dudley GA, Haggmark T, Ohlsen H & Tesch PA (1991). Effects of lower limb unloading on skeletal muscle mass and function in humans. *J Appl Physiol* **70,** 1882–1885.

Besomi M et al. (2019). Consensus for experimental design in electromyography ( CEDE ) project :

Electrode selection matrix. *J Electromyogr Kinesiol* **48,** 128–144.

Binder M, Heckman C & Powers R (1996). The physiological control of motoneuron activity. In *Handbook of physiology exercise: regulation and integration of multiple systems*, ed. LB R & JT S, pp. 1–53. Oxford University Press, New York.

Binder MD (2003). Intrinsic dendritic currents make a major contribution to the control of motoneurone discharge. *J Physiol* **552,** 665.

Binder MD, Powers RK & Heckman CJ (2020). Nonlinear Input-Output Functions of Motoneurons. *Physiology* **35,** 31–39.

Biolo G, Pišot R, Mazzucco S, Di Girolamo FG, Situlin R, Lazzer S, Grassi B, Reggiani C, Passaro A, Rittweger J, Gasparini M, Šimunič B & Narici M (2017). Anabolic resistance assessed by oral stable isotope ingestion following bed rest in young and older adult volunteers: Relationships with changes in muscle mass. *Clin Nutr* **36,** 1420–1426.

Black JA, Kocsis JD & Waxman SG (1990). Ion channel organization of the myelinated fiber. *Trends Neurosci* **13,** 48–54.

Bleeker MWP, Hopman MTE, Rongen GA & Smits P (2004). Unilateral lower limb suspension can cause deep venous thrombosis. *Am J Physiol Regul Integr Comp Physiol*; DOI: 10.1152/AJPREGU.00718.2003.

Blijham PJ, Ter Laak HJ, Schelhaas HJ, Van Engelen BGM, Stegeman DF & Zwarts MJ (2006). Relation between muscle fiber conduction velocity and fiber size in neuromuscular disorders. *J Appl Physiol* **100,** 1837–1841.

Bloch-Gallego E (2015). Mechanisms controlling neuromuscular junction stability. *Cell Mol Life Sci* **72,** 1029–1043.

Blok JH, Van Dijk JP, Drost G, Zwarts MJ & Stegeman DF (2002). A high-density multichannel surface electromyography system for the characterization of single motor units. *Rev Sci Instrum* **73,** 1887–1897.

de Boer MD, Maganaris CN, Seynnes OR, Rennie MJ & Narici M V. (2007). Time course of muscular, neural and tendinous adaptations to 23 day unilateral lower-limb suspension in young men. *J Physiol* **583,** 1079–1091.

Botter A, Oprandi G, Lanfranco F, Allasia S, Maffiuletti NA & Minetto MA (2011*a*). Atlas of the muscle motor points for the lower limb: Implications for electrical stimulation procedures and electrode positioning. *Eur J Appl Physiol* **111,** 2461–2471.

Botter A, Oprandi G, Lanfranco F, Allasia S, Maffiuletti NA & Minetto MA (2011*b*). Atlas of the muscle motor points for the lower limb: implications for electrical stimulation procedures and electrode positioning. *Eur J Appl Physiol* **111,** 2461–2471.

Brocca L, Longa E, Cannavino J, Seynnes O, de Vito G, Mcphee J, Narici M, Pellegrino MA & Bottinelli R (2015). Human skeletal muscle fibre contractile properties and proteomic profile: adaptations to 3 weeks of unilateral lower limb suspension and active recovery. *J Physiol* **593,** 5361–5385.

Brooke M & Kaiser K (1970). Muscle fiber types: how many and what kind? *Arch Neurol* **23,** 369–379.

Brown MC & Matthews PBC (1960). An investigation into the possible existence of polyneuronal innervation of individual skeletal muscle fibres in certain hind-limb muscles of the cat. *J Physiol* **151,** 436.

Brzycki M (1993). Strength Testing—Predicting a One-Rep Max from Reps-to-Fatigue. *J Phys Educ Recreat Danc* **64,** 88–90.

Burke RE (1981). Motor Units: Anatomy, Physiology, and Functional Organization. *Compr Physiol*345–422.

Burke RE, Levine DN, Zajac FE, Tsairis P & Engel WK (1971). Mammalian motor units: physiological-histochemical correlation in three types in cat gastrocnemius. *Science* **174,** 709–712.

Campanini I, Merlo A & Farina D (2009). Motor unit discharge pattern and conduction velocity in patients with upper motor neuron syndrome. *J Electromyogr Kinesiol* **19,** 22–29.

Campbell EL, Seynnes OR, Bottinelli R, McPhee JS, Atherton PJ, Jones DA, Butler-Browne G & Narici M V. (2013). Skeletal muscle adaptations to physical inactivity and subsequent retraining in young men. *Biogerontology* **14,** 247–259.

Campbell M, Varley-Campbell J, Fulford J, Taylor B, Mileva KN & Bowtell JL (2019). Effect of Immobilisation on Neuromuscular Function In Vivo in Humans: A Systematic Review. *Sport Med* **49,** 931–950.

Casolo A, Farina D, Falla D, Bazzucchi I, Felici F & Del Vecchio A (2020). Strength Training Increases Conduction Velocity of High-Threshold Motor Units. *Med Sci Sports Exerc* **52,** 955–967.

Casolo A, Maeo S, Balshaw TG, Lanza MB, Martin NRW, Nuccio S, Moro T, Paoli A, Felici F, Maffulli N, Eskofier B, Kinfe TM, Folland JP, Farina D & Vecchio A Del (2023). Non-invasive estimation of muscle fibre size from high-density electromyography. *J Physiol* **601,** 1831–1850.

Casolo A, Del Vecchio A, Balshaw TG, Maeo S, Lanza MB, Felici F, Folland JP & Farina D (2021). Behavior of motor units during submaximal isometric contractions in chronically strength-trained individuals. *J Appl Physiol* **131,** 1584–1598.

Chalif JI & Mentis GZ (2022). Normal Development and Pathology of Motoneurons: Anatomy, Electrophysiological Properties, Firing Patterns and Circuit Connectivity. In *Vertebrate Motoneurons*, ed. O'Donovan MJ & Falgairolle M, pp. 63–85. Springer International Publishing, Cham. Available at: https://doi.org/10.1007/978-3-031-07167-6_3.

Chen M & Zhou P (2016). A novel framework based on FastICA for high density surface EMG decomposition. *IEEE Trans Neural Syst Rehabil Eng* **24,** 117–127.

Ciciliot S, Rossi AC, Dyar KA, Blaauw B & Schiaffino S (2013). Muscle type and fiber type specificity in muscle wasting. *Int J Biochem Cell Biol* **45,** 2191–2199.

Clancy EA, Morin EL & Merletti R (2002). Sampling, noise-reduction and amplitude estimation issues in surface electromyography. *J Electromyogr Kinesiol* **12,** 1–16.

Clark BC (2009). In vivo alterations in skeletal muscle form and function after disuse atrophy. *Med Sci Sports Exerc* **41,** 1869–1875.

Cohen JW, Vieira TM, Ivanova TD & Garland SJ (2023). Control of Movement Differential behavior of distinct motoneuron pools that innervate the triceps surae. 272–284.

Coombs JS, Eccles JC & Fatt P (1955). The specific ionic conductances and the ionic movements across the motoneuronal membrane that produce the inhibitory post-synaptic potential. *J Physiol* **130,** 326.

Cudicio A, Martinez-Valdes E, Cogliati M, Orizio C & Negro F (2022). The force-generation capacity of the tibialis anterior muscle at different muscle–tendon lengths depends on its motor unit contractile properties. *Eur J Appl Physiol* **122,** 317–330.

Cullheim S, Fleshman JW, Glenn LL & Burke RE (1987). Membrane area and dendritic structure in type-identified triceps surae alpha motoneurons. *J Comp Neurol* **255,** 68–81.

Cullheim S & Ulfhake B (1979). Relations between cell body size, axon diameter and axon conduction velocity of triceps surae alpha montoneurons during the postnatal development in the cat. *J Comp Neurol* **188,** 679–686.

Daneman D (2006). Type 1 diabetes. *Lancet* **367,** 847–858.

Del Vecchio A, Casolo A, Negro F, Scorcelletti M, Bazzucchi I, Enoka R, Felici F & Farina D (2019*a*). The increase in muscle force after 4 weeks of strength training is mediated by adaptations in motor unit recruitment and rate coding. *J Physiol* **597,** 1873–1887.

Del Vecchio A, Germer CM, Kinfe TM, Nuccio S, Hug F, Eskofier B, Farina D & Enoka RM (2023). The Forces Generated by Agonist Muscles during Isometric Contractions Arise from Motor Unit Synergies. *J Neurosci* **43,** 2860–2873.

Del Vecchio A, Holobar A, Falla D, Felici F, Enoka RM & Farina D (2020). Tutorial: Analysis of motor unit discharge characteristics from high-density surface EMG signals. *J Electromyogr Kinesiol*; DOI: 10.1016/J.JELEKIN.2020.102426.

Del Vecchio A, Negro F, Felici F & Farina D (2017). Associations between motor unit action potential parameters and surface EMG features. *J Appl Physiol* **123,** 835–843.

Del Vecchio A, Negro F, Holobar A, Casolo A, Folland JP, Felici F & Farina D (2019*b*). You are as fast as your motor neurons: speed of recruitment and maximal discharge of motor neurons determine the maximal rate of force development in humans. *J Physiol* **597,** 2445–2456.

Devendra D, Liu E & Eisenbarth GS (2004). Type 1 diabetes: recent developments. *BMJ* **328,** 750–754.

Dial AG, Monaco CMF, Grafham GK, Patel TP, Tarnopolsky MA & Hawke TJ (2021). Impaired Function and Altered Morphology in the Skeletal Muscles of Adult Men and Women with Type 1 Diabetes. *J Clin Endocrinol Metab*; DOI: 10.1210/clinem/dgab261.

Dideriksen J & Del Vecchio A (2023). Adaptations in motor unit properties underlying changes in recruitment, rate coding, and maximum force. *J Neurophysiol* **129,** 235–246.

Dideriksen JL, Negro F, Enoka RM & Farina D (2012). Motor unit recruitment strategies and muscle properties determine the influence of synaptic noise on force steadiness. *J Neurophysiol* **107,** 3357–3369.

Dideriksen JL, Negro F & Farina D (2015). The optimal neural strategy for a stable motor task requires a compromise between level of muscle cocontraction and synaptic gain of afferent feedback. *J Neurophysiol* **114,** 1895–1911.

Dorman JS, Laporte RE, Kuller LH, Cruickshanks KJ, Orchard TJ, Wagener DK, Becker DJ, Cavender

DE & Drash AL (1984). The Pittsburgh insulin-dependent diabetes mellitus (IDDM) morbidity and mortality study. Mortality results. *Diabetes* **33,** 271–276.

Drost G, Blok JH, Stegeman DF, Van Dijk JP, Van Engelen BGM & Zwarts MJ (2001). Propagation disturbance of motor unit action potentials during transient paresis in generalized myotoniaA high-density surface EMG study. *Brain* **124,** 352–360.

Duchateau J & Enoka RM (2011). Human motor unit recordings: Origins and insight into the integrated motor system. *Brain Res* **1409,** 42–61.

Duchateau J & Hainaut K (1990). Effects of immobilization on contractile properties, recruitment and firing rates of human motor units. *J Physiol* **422,** 55–65.

Edström L & Kugelberg E (1968). Properties of motor units in the rat anterior tibial muscle. *Acta Physiol Scand* **73,** 543–544.

ElSayed NA et al. (2023). 6. Glycemic Targets: Standards of Care in Diabetes-2023. *Diabetes Care* **46,** S97–S110.

Enoka RM (2019). Physiological validation of the decomposition of surface EMG signals. *J Electromyogr Kinesiol* **46,** 70–83.

Enoka RM & Duchateau J (2017). Rate coding and the control of muscle force. *Cold Spring Harb Perspect Med* **7,** 1–12.

Enoka RM & Farina D (2021). Force Steadiness: From Motor Units to Voluntary Actions. *Physiology (Bethesda)* **36,** 114–130.

Enoka RM & Fuglevand AJ (2001). Motor unit physiology: some unresolved issues. *Muscle Nerve* **24,** 4–17.

Erlanger J, Bishop GH & Gasser HS (1926). The action potential waves transmitted between the sciatic nerve and its spinal roots. *https://doi.org/101152/ajplegacy1926783574* **78,** 574–591.

Faisal AA, Selen LPJ & Wolpert DM (2008). Noise in the nervous system. *Nat Rev Neurosci* **9,** 292–303.

Farina D, Arendt-nielsen L, Merletti R & Graven-nielsen T (2002). Assessment of single motor unit conduction velocity during sustained contractions of the tibialis anterior muscle with advanced spike triggered averaging. **115,** 1–12.

Farina D, Cescon C, Negro F & Enoka RM (2008). Amplitude cancellation of motor-unit action potentials in the surface electromyogram can be estimated with spike-triggered averaging. *J Neurophysiol* **100,** 431–440.

Farina D & Enoka RM (2023). Evolution of surface electromyography: From muscle electrophysiology towards neural recording and interfacing. *J Electromyogr Kinesiol* **71,** 102796.

Farina D, Fortunato E & Merletti R (2000). Noninvasive Estimation of Motor Unit Conduction Velocity Distribution Using Linear Electrode Arrays. **47,** 380–388.

Farina D & Merletti R (2001). A novel approach for precise simulation of the EMG signal detected by surface electrodes. *IEEE Trans Biomed Eng* **48,** 637–646.

Farina D, Merletti R & Enoka RM (2004). The extraction of neural strategies from the surface EMG.

*J Appl Physiol* **96,** 1486–1495.

Farina D, Merletti R & Enoka RM (2014*a*). The extraction of neural strategies from the surface EMG: An update. *J Appl Physiol* **117,** 1215–1230.

Farina D, Muhammad W, Fortunato E, Meste O, Merletti R & Rix H (2001). Estimation of single motor unit conduction velocity from surface electromyogram signals detected with linear electrode arrays. *Med Biol Eng Comput* **39,** 225–236.

Farina D & Negro F (2015). Common Synaptic Input to Motor Neurons , Motor Unit Synchronization , and Force Control. 23–33.

Farina D, Negro F & Dideriksen JL (2014*b*). The effective neural drive to muscles is the common synaptic input to motor neurons. *J Physiol* **592,** 3427–3441.

Farina D, Negro F, Muceli S & Enoka RM (2016). Principles of motor unit physiology evolve with advances in technology. *Physiology* **31,** 83–94.

Farina D, Vujaklija I, Sartori M, Kapelner T, Negro F, Jiang N, Bergmeister K, Andalib A, Principe J & Aszmann OC (2017). Man/machine interface based on the discharge timings of spinal motor neurons after targeted muscle reinnervation. *Nat Biomed Eng*; DOI: 10.1038/s41551-016-0025.

Feher J (2017). *Quantitative Human Physiology*. Elsevier.

Feindel W, Hinshaw JR & Weddell G (1952). The pattern of motor innervation in mammalian striated muscle. *J Anat* **86,** 35.

Feldman EL, Nave KA, Jensen TS & Bennett DLH (2017). New Horizons in Diabetic Neuropathy: Mechanisms, Bioenergetics, and Pain. *Neuron* **93,** 1296–1313.

Felici F & Del Vecchio A (2020). Surface Electromyography: What Limits Its Use in Exercise and Sport Physiology? *Front Neurol* **11,** 1–6.

Freund H-J (1983). Motor unit and muscle activity in voluntary motor control. *Physiol Rev* **63,** 387–436.

Fritzsche K, Blüher M, Schering S, Buchwalow IB, Kern M, Linke A, Oberbach A, Adams V & Punkt K (2008). Metabolic profile and nitric oxide synthase expression of skeletal muscle fibers are altered in patients with type 1 diabetes. *Exp Clin Endocrinol Diabetes* **116,** 606–613.

Frontera WR & Ochala J (2015). Skeletal Muscle: A Brief Review of Structure and Function. *Behav Genet* **45,** 183–195.

Gallego JA, Dideriksen JL, Holobar A, Ibáñez J, Pons JL, Louis ED, Rocon E & Farina D (2015*a*). Influence of common synaptic input to motor neurons on the neural drive to muscle in essential tremor. *J Neurophysiol* **113,** 182–191.

Gallego JA, Dideriksen JL, Holobar A, Ibáñez J, Pons JL, Louis ED, Rocon E & Farina D (2015*b*). Influence of common synaptic input to motor neurons on the neural drive to muscle in essential tremor. *J Neurophysiol* **113,** 182–191.

Gallina A et al. (2022). Consensus for experimental design in electromyography (CEDE) project: High-density surface electromyography matrix. *J Electromyogr Kinesiol*; DOI: 10.1016/j.jelekin.2022.102656.

Gallina A & Botter A (2013). Spatial localization of electromyographic amplitude distributions associated to the activation of dorsal forearm muscles. *Front Physiol* **4,** 367–367.

Gandevia SC (2001). Spinal and supraspinal factors in human muscle fatigue. *Physiol Rev* **81,** 1725–1789.

Gazzoni M, Farina D & Merletti R (2004). A new method for the extraction and classification of single motor unit action potentials from surface EMG signals. **136,** 165–177.

Goodlich BI, Vecchio A Del, Horan SA & Kavanagh JJ (2023). Blockade of 5-HT 2 receptors suppresses motor unit firing and estimates of persistent inward currents during voluntary muscle contraction in humans. **6,** 1121–1138.

Gordon T, Hegedus J & Tam SL (2004). Adaptive and maladaptive motor axonal sprouting in aging and motoneuron disease. *Neurol Res* **26,** 174–185.

Grillner S (2003). The motor infrastructure: from ion channels to neuronal networks. *Nat Rev Neurosci* **4,** 573–586.

Guerrero-Hernandez A & Verkhratsky A (2014). Calcium signalling in diabetes. *Cell Calcium* **56,** 297–301.

Guo Y, Jones EJ, Inns TB, Ely IA, Stashuk DW, Wilkinson DJ, Smith K, Piasecki J, Phillips BE, Atherton PJ & Piasecki M (2022). Neuromuscular recruitment strategies of the vastus lateralis according to sex. *Acta Physiol (Oxf)* **235,** e13803.

Hassan AS, Fajardo ME, Cummings M, McPherson LM, Negro F, Dewald JPA, Heckman CJ & Pearcey GEP (2021*a*). Estimates of persistent inward currents are reduced in upper limb motor units of older adults. *J Physiol* **599,** 4865–4882.

Hassan AS, Fajardo ME, Cummings M, McPherson LM, Negro F, Dewald JPA, Heckman CJ & Pearcey GEP (2021*b*). Estimates of persistent inward currents are reduced in upper limb motor units of older adults. *J Physiol* **599,** 4865–4882.

Heckman CJ & Binder MD (1991). Computer simulation of the steady-state input-output function of the cat medial gastrocnemius motoneuron pool. *J Neurophysiol* **65,** 952–967.

Heckman CJ & Binder MD (1993). Computer simulations of the effects of different synaptic input systems on motor unit recruitment. *J Neurophysiol* **70,** 1827–1840.

Heckman CJ & Enoka RM (2004). Physiology of the motor neuron and the motor unit. *Handb Clin Neurophysiol* **4,** 119–147.

Heckman CJ & Enoka RM (2012). Motor Unit. *Compr Physiol* **2,** 2629–2682.

Heckman CJ, Gorassini MA & Bennett DJ (2005). Persistent inward currents in motoneuron dendrites: Implications for motor output. *Muscle Nerve* **31,** 135–156.

Heckman CJ, Johnson M, Mottram C & Schuster J (2008). Persistent Inward Currents in Spinal Motoneurons and Their Influence on Human Motoneuron Firing Patterns. *Neurosci* **14,** 264.

Heckman CJ, Mottram C, Quinlan K, Theiss R & Schuster J (2009). Motoneuron excitability: the importance of neuromodulatory inputs. *Clin Neurophysiol* **120,** 2040–2054.

Henneman E & Mendell LM (1981). Functional organization of motoneuron pool and its inputs. In *Handbook of physiology, the nervous system, motor control*, ed. Brooks VB, pp. 423–507.

American Physiological Society, Bethesda (MD).

Henneman E & Olson CB (1965). Relations between structure and function in the design of skeletal muscles. *J Neurophysiol* **28,** 581–598.

Henneman E, Somjen G & Carpenter DO (1965*a*). Functional significance of cell size in spinal motoneurons. *J Neurophysiol* **28,** 560–580.

Henneman E, Somjen G & Carpenter DO (1965*b*). Excitability and inhibitibility of motoneurons of different sizes. *J Neurophysiol* **28,** 599–620.

Hepple RT & Rice CL (2016). Innervation and neuromuscular control in ageing skeletal muscle. *J Physiol* **594,** 1965–1978.

Hille B (2001). *Ionic channels of excitable membranes. Bertil Hille. Sunderland, Ma: Sinauer Associates, 1984*, 3rd edn. Sinauer Assoc. Inc., Sunderland (MA). Available at: https://onlinelibrary.wiley.com/doi/full/10.1002/jnr.490130415.

Holobar A, Farina D, Gazzoni M, Merletti R & Zazula D (2009). Estimating motor unit discharge patterns from high-density surface electromyogram. *Clin Neurophysiol* **120,** 551–562.

Holobar A, Glaser V, Gallego JA, Dideriksen JL & Farina D (2012). Non-invasive characterization of motor unit behaviour in pathological tremor. *J Neural Eng*; DOI: 10.1088/1741-2560/9/5/056011.

Holobar A, Minetto MA & Farina D (2014). Accurate identification of motor unit discharge patterns from high-density surface EMG and validation with a novel signal-based performance metric. *J Neural Eng*; DOI: 10.1088/1741-2560/11/1/016008.

Holobar A & Zazula D (2007). Multichannel blind source separation using convolution Kernel compensation. *IEEE Trans Signal Process* **55,** 4487–4496.

Hortobágyi T, Dempsey L, Fraser D, Zheng D, Hamilton G, Lambert J & Dohm L (2000). Changes in muscle strength, muscle fibre size and myofibrillar gene expression after immobilization and retraining in humans. *J Physiol* **524 Pt 1,** 293–304.

Hu X, Suresh NL, Jeon B, Shin H & Rymer WZ (2014). Statistics of inter-spike intervals as a routine measure of accuracy in automatic decomposition of surface electromyogram. *2014 36th Annu Int Conf IEEE Eng Med Biol Soc EMBC 2014*3541–3544.

Hug F, Avrillon S, Ibáñez J & Farina D (2023). Common synaptic input, synergies and size principle: Control of spinal motor neurons for movement generation. *J Physiol* **601,** 11–20.

Hug F, Avrillon S, Del Vecchio A, Casolo A, Ibanez J, Nuccio S, Rossato J, Holobar A & Farina D (2021*a*). Analysis of motor unit spike trains estimated from high-density surface electromyography is highly reliable across operators. *J Electromyogr Kinesiol*; DOI: 10.1016/J.JELEKIN.2021.102548.

Hug F, Del Vecchio A, Avrillon S, Farina D & Tucker K (2021*b*). Muscles from the same muscle group do not necessarily share common drive: evidence from the human triceps surae. *J Appl Physiol* **130,** 342–354.

Hultborn H (2002). Plateau potentials and their role in regulating motoneuronal firing. *Adv Exp Med Biol* **508,** 213–218.

Hvid LG, Suetta C, Nielsen JH, Jensen MM, Frandsen U, Ørtenblad N, Kjaer M & Aagaard P (2014). Aging impairs the recovery in mechanical muscle function following 4 days of disuse. *Exp Gerontol* **52,** 1–8.

Inns TB, Bass JJ, Hardy EJO, Wilkinson DJ, Stashuk DW, Atherton PJ, Phillips BE & Piasecki M (2022). Motor unit dysregulation following 15 days of unilateral lower limb immobilisation. *J Physiol* **600,** 4537–4769.

Jones EJ, Chiou S-Y, Atherton PJ, Phillips BE & Piasecki M (2022). Ageing and exercise-induced motor unit remodelling. *J Physiol* **600,** 1839–1849.

Juhl OJ, Buettmann EG, Friedman MA, DeNapoli RC, Hoppock GA & Donahue HJ (2021). Update on the effects of microgravity on the musculoskeletal system. *npj Microgravity* **7,** 1–15.

Jurkat-Rott K & Lehmann-Horn F (2004). Ion Channels and Electrical Properties of Skeletal Muscle. In *Myology*, 3rd edn., ed. Engel AG & Franzini-Armstrong C, pp. 203–231. McGraw-Hill, New York.

Kandel ER, Schwartz JH, Jessell TM, Siegelbaum SA & Hudspeth AJ (2012). *Principles of Neural Science, Fifth Edition*. McGraw Hill LLC. Available at: https://books.google.it/books?id=Z2yVUTnlIQsC.

Kang D, Gho YS, Suh M & Kang C (2002). Highly sensitive and fast protein detection with Coomassie brilliant blue in sodium dodecyl sulfate-polyacrylamide gel electrophoresis [5]. *Bull Korean Chem Soc* **23,** 1511–1512.

Kavanagh JJ, Taylor JL, Kavanagh JJ & Taylor JL (2022). Voluntary activation of muscle in humans: does serotonergic neuromodulation matter? *J Physiol* **600,** 3657–3670.

Keenan KG, Farina D, Merletti R & Enoka RM (2006). Amplitude cancellation reduces the size of motor unit potentials averaged from the surface EMG. *J Appl Physiol* **100,** 1928–1937.

Kernell D (2006). *The Motoneurone and its Muscle Fibres*. Oxford University Press.

Kleine BU, Dijk JP Van, Lapatki BG, Zwarts MJ & Stegeman DF (2007). Using two-dimensional spatial information in decomposition of surface EMG signals. **17,** 535–548.

Kolliker A (1862). Untersuchungen über die letzten endigungen der nerven. *Z Wiss Zool* **12,** 149–164.

Kuhne W (1863). Die muskelspindeln. Ein beitrag zur lehre von der entwickelung der muskeln und nervenfasern. *Virchows Arch Path Anat Physiol* **28,** 528–538.

Kukulka CG & Clamann HP (1981). Comparison of the recruitment and discharge properties of motor units in human brachial biceps and adductor pollicis during isometric contractions. *Brain Res* **219,** 45–55.

Kuznetsova A, Brockhoff PB & Christensen RHB (2017). lmerTest Package: Tests in Linear Mixed Effects Models. *J Stat Softw* **82,** 1–26.

Laemmli UK (1970). Cleavage of structural proteins during the assembly of the head of bacteriophage T4. *Nature* **227,** 680–685.

Laidler P (1994). Neuromuscular plasticity. In *Stroke Rehabilitation: Structure and Strategy*, pp. 42–48. Springer US, Boston, MA. Available at: https://doi.org/10.1007/978-1-4899-3470-3_4.

Lapatki BG, Van Dijk JP, Jonas IE, Zwarts MJ & Stegeman DF (2004). A thin, flexible multielectrode grid for high-density surface EMG. *J Appl Physiol* **96,** 327–336.

Larsson L, Degens H, Li M, Salviati L, Lee Y Il, Thompson W, Kirkland JL & Sandri M (2019). Sarcopenia: Aging-Related Loss of Muscle Mass and Function. *Physiol Rev* **99,** 427–511.

LeFever RS & De Luca CJ (1982). A Procedure for Decomposing the Myoelectric Signal Into Its Constituent Action Potentials— Part I: Technique, Theory, and Implementation. *IEEE Trans Biomed Eng* **BME-29,** 149–157.

Leksell LGF (1945). The action potential and excitatory effects of the small ventral root fibres to skeletal muscle. *Acta Physiol Scand* **10,** 1–84.

Liddell EGT & Sherrington CS (1925). Recruitment and some Other Features o f Reflex Inhibition. *Proc R Soc B Biol Sci* **97,** 488–518.

LOWRY OH, ROSEBROUGH NJ, FARR AL & RANDALL RJ (1951). PROTEIN MEASUREMENT WITH THE FOLIN PHENOL REAGENT. *J Biol Chem* **193,** 265–275.

De Luca CJ (1985). Control properties of motor units. *J Exp Biol* **VOL. 115,** 125–136.

Luca CJ De (1997). The Use of Surface Electromyography in Biomechanics. *J Appl Biomech* **13,** 135–163.

De Luca CJ & Erim Z (1994). Common drive of motor units in regulation of muscle force. *Trends Neurosci* **17,** 299–305.

de Luca CJ, LeFever RS, McCue MP & Xenakis AP (1982). Behaviour of human motor units in different muscles during linearly varying contractions. *J Physiol* **329,** 113–128.

Lulic-Kuryllo T & Inglis JG (2022). Sex differences in motor unit behaviour: A review. *J Electromyogr Kinesiol* **66,** 102689.

Lulic-Kuryllo T, Negro F, Jiang N & Dickerson CR (2022). Differential regional pectoralis major activation indicates functional diversity in healthy females. *J Biomech* **133,** 110966.

Lulic-Kuryllo T, Thompson CK, Jiang N, Negro F & Dickerson CR (2021). Neural control of the healthy pectoralis major from low-to-moderate isometric contractions. *J Neurophysiol* **126,** 213–226.

Maathuis EM, Drenthen J, van Dijk JP, Visser GH & Blok JH (2008). Motor unit tracking with high-density surface EMG. *J Electromyogr Kinesiol* **18,** 920–930.

Mahmassani ZS, Reidy PT, McKenzie AI, Stubben C, Howard MT & Drummond MJ (2019). Age-dependent skeletal muscle transcriptome response to bed rest-induced atrophy. *J Appl Physiol* **126,** 894.

Mambrito B & De Luca CJ (1984). A technique for the detection, decomposition and analysis of the EMG signal. *Electroencephalogr Clin Neurophysiol* **58,** 175–188.

Manjarrez G, Herrera R, Leon M & Hernandez-R J (2006). A Low Brain Serotonergic Neurotransmission in Children With Type 1 Diabetes Detected Through the Intensity Dependence of Auditory-Evoked Potentials. *Diabetes Care* **29,** 73–77.

Manuel M, Meunier C, Donnet M & Zytnicki D (2007). Resonant or not, two amplification modes of proprioceptive inputs by persistent inward currents in spinal motoneurons. *J Neurosci* **27,**

12977–12988.

Manuel M & Zytnicki D (2011). Alpha, beta and gamma motoneurons: functional diversity in the motor system's final pathway. *J Integr Neurosci* **10,** 243–276.

Martin H, Bullich S, Guiard BP & Fioramonti X (2021). The impact of insulin on the serotonergic system and consequences on diabetes-associated mood disorders. *J Neuroendocrinol* **33,** e12928.

Martinez-Valdes E et al. (2023). Consensus for experimental design in electromyography (CEDE) project: Single motor unit matrix. *J Electromyogr Kinesiol* **68,** 102726.

Martinez-Valdes E, Farina D, Negro F, Del Vecchio A & Falla D (2018*a*). Early Motor Unit Conduction Velocity Changes to High-Intensity Interval Training versus Continuous Training. *Med Sci Sports Exerc* **50,** 2339–2350.

Martinez-Valdes E & Negro F (2023). Neuromuscular Function: High-Density Surface Electromyography. In *Neuromuscular Assessments of Form and Function*, ed. Atherton PJ & Wilkinson DJ. Humana, New York, NY.

Martinez-Valdes E, Negro F, Falla D, De Nunzio AM & Farina D (2018*b*). Surface electromyographic amplitude does not identify differences in neural drive to synergistic muscles. *J Appl Physiol* **124,** 1071–1079.

Martinez-Valdes E, Negro F, Laine CM, Falla D, Mayer F & Farina D (2017). Tracking motor units longitudinally across experimental sessions with high-density surface electromyography. *J Physiol* **595,** 1479–1496.

Matthews PB (1996). Relationship of firing intervals of human motor units to the trajectory of post-spike after-hyperpolarization and synaptic noise. *J Physiol* **492 ( Pt 2,** 597–628.

Mayer-Davis EJ, Lawrence JM, Dabelea D, Divers J, Isom S, Dolan L, Imperatore G, Linder B, Marcovina S, Pettitt DJ, Pihoker C, Saydah S & Wagenknecht L (2017). Incidence Trends of Type 1 and Type 2 Diabetes among Youths, 2002-2012. *N Engl J Med* **376,** 1419–1429.

Mcgill KC, Cummins KL & Dorfman LJ (1985). Automatic Decomposition of the Clinical Electromyogram. *IEEE Trans Biomed Eng* **BME-32,** 470–477.

McManus L et al. (2021). Consensus for experimental design in electromyography (CEDE) project: Terminology matrix. *J Electromyogr Kinesiol*; DOI: 10.1016/J.JELEKIN.2021.102565.

McManus L, De Vito G & Lowery MM (2020). Analysis and Biophysics of Surface EMG for Physiotherapists and Kinesiologists: Toward a Common Language With Rehabilitation Engineers. *Front Neurol* **11,** 1216.

Mcphedran AM, Wuerker RB & Henneman E (1965). Properties of motor units in a homogeneous red muscle (soleus) of the cat. *https://doi.org/101152/jn196528171* **28,** 71–84.

Mendell LM (2005*a*). The size principle: A rule describing the recruitment of motoneurons. *J Neurophysiol* **93,** 3024–3026.

Mendell LM (2005*b*). The size principle: a rule describing the recruitment of motoneurons. *J Neurophysiol* **93,** 3024–3026.

Merletti R & Cerone GL (2020). Tutorial. Surface EMG detection, conditioning and pre-processing:

Best practices. *J Electromyogr Kinesiol* **54,** 102440.

Merletti R & Farina A (2009). Analysis of intramuscular electromyogram signals. *Philos Trans A Math Phys Eng Sci* **367,** 357–368.

Merletti R & Farina D (2016). Surface Electromyography: Physiology, Engineering and Applications. *Surf Electromyogr Physiol Eng Appl*1–570.

Merletti R, Holobar A & Farina D (2008). Analysis of motor units with high-density surface electromyography. *J Electromyogr Kinesiol* **18,** 879–890.

Merletti R & Muceli S (2019). Tutorial. Surface EMG detection in space and time: Best practices. *J Electromyogr Kinesiol* **49,** 102363.

Mesin L, Damiano L & Farina D (2007). Estimation of average muscle fiber conduction velocity from simulated surface EMG in pinnate muscles. *J Neurosci Methods* **160,** 327–334.

Mesquita RM, Catavitello G, Willems PA & Dewolf AH (2023). Modification of the locomotor pattern when deviating from the characteristic heel-to-toe rolling pattern during walking. *Eur J Appl Physiol* **123,** 1455–1467.

Mesquita RNO, Taylor JL, Trajano GS, Škarabot J, Holobar A, Gonçalves BAM & Blazevich AJ (2022). Effects of reciprocal inhibition and whole-body relaxation on persistent inward currents estimated by two different methods. *J Physiol* **600,** 2765–2787.

Methenitis S, Karandreas N, Spengos K, Zaras N, Stasinaki AN & Terzis G (2016). Muscle Fiber Conduction Velocity, Muscle Fiber Composition, and Power Performance. *Med Sci Sports Exerc* **48,** 1761–1771.

Miller MS, Bedrin NG, Ades PA, Palmer BM & Toth MJ (2015). Molecular determinants of force production in human skeletal muscle fibers: effects of myosin isoform expression and cross-sectional area. *Am J Physiol - Cell Physiol* **308,** C473.

Milner-Brown HS & Stein RB (1975). The relation between the surface electromyogram and muscular force. *J Physiol* **246,** 549–569.

Milner-Brown HS, Stein RB & Yemm R (1973). The contractile properties of human motor units during voluntary isometric contractions. *J Physiol* **228,** 285–306.

Minnock D, Annibalini G, Le Roux CW, Contarelli S, Krause M, Saltarelli R, Valli G, Stocchi V, Barbieri E & De Vito G (2020). Effects of acute aerobic, resistance and combined exercises on 24-h glucose variability and skeletal muscle signalling responses in type 1 diabetics. *Eur J Appl Physiol* **120,** 2677–2691.

Minnock D, Annibalini G, Valli G, Saltarelli R, Krause M, Barbieri E & De Vito G (2022). Altered muscle mitochondrial, inflammatory and trophic markers, and reduced exercise training adaptations in type 1 diabetes. *J Physiol* **600,** 1405–1418.

Monaco CMF, Gingrich MA & Hawke TJ (2019). Considering Type 1 Diabetes as a Form of Accelerated Muscle Aging. *Exerc Sport Sci Rev* **47,** 98–107.

Monaco CMF, Hughes MC, Ramos S V., Varah NE, Lamberz C, Rahman FA, McGlory C, Tarnopolsky MA, Krause MP, Laham R, Hawke TJ & Perry CGR (2018). Altered mitochondrial bioenergetics and ultrastructure in the skeletal muscle of young adults with type 1 diabetes. *Diabetologia* **61,** 1411–1423.

Monaco CMF, Perry CGR & Hawke TJ (2017). Diabetic Myopathy: current molecular understanding of this novel neuromuscular disorder. *Curr Opin Neurol* **30,** 545–552.

Monaco CMF, Tarnopolsky MA, Dial AG, Nederveen JP, Rebalka IA, Nguyen M, Turner L V., Perry CGR, Ljubicic V & Hawke TJ (2021). Normal to enhanced intrinsic mitochondrial respiration in skeletal muscle of middle- to older-aged women and men with uncomplicated type 1 diabetes. *Diabetologia*; DOI: 10.1007/s00125-021-05540-1.

Monti E, Reggiani C, Franchi M V., Toniolo L, Sandri M, Armani A, Zampieri S, Giacomello E, Sarto F, Sirago G, Murgia M, Nogara L, Marcucci L, Ciciliot S, Šimunic B, Pišot R & Narici M V. (2021). Neuromuscular junction instability and altered intracellular calcium handling as early determinants of force loss during unloading in humans. *J Physiol* **599,** 3037–3061.

Murillo C, Martinez-Valdes E, Heneghan NR, Liew B, Rushton A, Sanderson A & Falla D (2019). High-Density Electromyography Provides New Insights into the Flexion Relaxation Phenomenon in Individuals with Low Back Pain. *Sci Rep*; DOI: 10.1038/S41598-019-52434-9.

Nathan DM, Genuth S, Lachin J, Cleary P, Crofford O, Davis M, Rand L & Siebert C (1993). The effect of intensive treatment of diabetes on the development and progression of long-term complications in insulin-dependent diabetes mellitus. *N Engl J Med* **329,** 977–986.

Needham DM (1926). Red and white muscle. *Physiol Rev* **6,** 1–27.

Negro F, Muceli S, Castronovo AM, Holobar A & Farina D (2016). Multi-channel intramuscular and surface EMG decomposition by convolutive blind source separation. *J Neural Eng*; DOI: 10.1088/1741-2560/13/2/026027.

Neuhoff V, Arold N, Taube D & Ehrhardt W (1988). Improved staining of proteins in polyacrylamide gels including isoelectric focusing gels with clear background at nanogram sensitivity using Coomassie Brilliant Blue G-250 and R-250. *Electrophoresis* **9,** 255–262.

Ning Y, Zhu X, Zhu S & Zhang Y (2015). Surface EMG decomposition based on K-means clustering and convolution kernel compensation. *IEEE J Biomed Heal Informatics* **19,** 471–477.

Nishikawa Y, Holobar A, Watanabe K, Takahashi T, Ueno H, Maeda N, Maruyama H, Tanaka S & Hyngstrom AS (2022). Detecting motor unit abnormalities in amyotrophic lateral sclerosis using high-density surface EMG. *Clin Neurophysiol* **142,** 262–272.

Nuccio S, Del Vecchio A, Casolo A, Labanca L, Rocchi JE, Felici F, Macaluso A, Mariani PP, Falla D, Farina D & Sbriccoli P (2021). Deficit in knee extension strength following anterior cruciate ligament reconstruction is explained by a reduced neural drive to the vasti muscles. *J Physiol* **599,** 5103–5120.

Nunes EA, Stokes T, McKendry J, Currier BS & Phillips SM (2022). Disuse-induced skeletal muscle atrophy in disease and nondisease states in humans: mechanisms, prevention, and recovery strategies. *Am J Physiol Cell Physiol* **322,** C1068–C1084.

Ohira Y, Yoshinaga T, Nomura T, Kawano F, Ishihara A, Nonaka I, Roy RR & Edgerton VR (2002). Gravitational unloading effects on muscle fiber size, phenotype and myonuclear number. *Adv Sp Res Off J Comm Sp Res* **30,** 777–781.

Okudaira M, Hirono T, Takeda R, Nishikawa T, Ueda S & Mita Y (2023). Longitudinal development of muscle strength and relationship with motor unit activity and muscle morphological characteristics in youth athletes. *Exp Brain Res* **241,** 1009–1019.

Oliveira AS & Negro F (2021). Neural control of matched motor units during muscle shortening and lengthening at increasing velocities. *J Appl Physiol* **130,** 1798–1813.

Oliveira DS de, Casolo A, Balshaw TG, Maeo S, Lanza MB, Martin NRW, Maffulli N, Kinfe TM, Eskofier BM, Folland JP, Farina D & Del Vecchio A (2022). Neural decoding from surface high-density EMG signals: influence of anatomy and synchronization on the number of identified motor units. *J Neural Eng* **19,** 046029.

Omar A, Marwaha K & Bollu P (2023). *Physiology, Neuromuscular Junction*. StatPearls, Treasure Island (FL).

Orssatto LBR, Borg DN, Blazevich AJ, Sakugawa RL, Shield AJ & Trajano GS (2021). Intrinsic motoneuron excitability is reduced in soleus and tibialis anterior of older adults. *GeroScience* **43,** 2719–2735.

Pascoe MA, Holmes MR, Stuart DG & Enoka RM (2014*a*). Discharge characteristics of motor units during long-duration contractions. *Exp Physiol* **99,** 1387–1398.

Pascoe MA, Holmes MR, Stuart DG & Enoka RM (2014*b*). Discharge characteristics of motor units during long-duration contractions. *Exp Physiol* **99,** 1387–1398.

Pelletier C, Dai S, Roberts KC, Bienek A, Onysko J & Pelletier L (2012). Report summary. Diabetes in Canada: facts and figures from a public health perspective. *Chronic Dis Inj Can* **33,** 53–54.

Periasamy M, Herrera JL & Reis FCG (2017). Skeletal Muscle Thermogenesis and Its Role in Whole Body Energy Metabolism. *Diabetes Metab J* **41,** 327.

Piasecki M, Garnés-Camarena O & Stashuk DW (2021). Near-fiber electromyography. *Clin Neurophysiol* **132,** 1089–1104.

Piasecki M, Ireland A, Stashuk D, Hamilton-Wright A, Jones DA & McPhee JS (2016). Age-related neuromuscular changes affecting human vastus lateralis. *J Physiol* **594,** 4525–4536.

Piotrkiewicz M, Kudina L & Mierzejewska J (2004). Recurrent inhibition of human firing motoneurons (experimental and modeling study). *Biol Cybern* **91,** 243–257.

Pope ZK, Hester GM, Benik FM & DeFreitas JM (2016). Action potential amplitude as a noninvasive indicator of motor unit-specific hypertrophy. *J Neurophysiol* **115,** 2608–2614.

Power KE, Lockyer EJ, Botter A, Vieira · Taian & Button DC (2022). Endurance-exercise training adaptations in spinal motoneurones: potential functional relevance to locomotor output and assessment in humans. *Eur J Appl Physiol* **122,** 1367–1381.

Powers RK & Binder MD (2001). Input-output functions of mammalian motoneurons. *Rev Physiol Biochem Pharmacol* **143,** 137–263.

Powers RK & Heckman CJ (2017). Synaptic control of the shape of the motoneuron pool input-output function. *J Neurophysiol* **117,** 1171–1184.

Purves D, Augustine GJ, Fitzpatrick D, Katz LC, LaMantia A-S, McNamara JO & Williams SM (2001*a*). The Motor Unit. In *Neuroscience*, 2nd edn. Sinauer Associates, Sunderland (MA). Available at: https://www.ncbi.nlm.nih.gov/books/NBK10874/.

Purves D, Augustine GJ, Fitzpatrick D, Katz LC, LaMantia A-S, McNamara JO & Williams SM (2001*b*). The Regulation of Muscle Force. In *Neuroscience*, 2nd edn. Sinauer Associates, Sunderland

(MA). Available at: https://www.ncbi.nlm.nih.gov/books/NBK11021/ [Accessed July 21, 2023].

Ranvier LA (1873). Propriétés et structures différentes des muscles rouges et des muscles blancs chez les lapins et chez les raies. *CR Acad Sci Paris* **77,** 1030–1034.

Rebbeck RT, Karunasekara Y, Board PG, Beard NA, Casarotto MG & Dulhunty AF (2014). Skeletal muscle excitation–contraction coupling: Who are the dancing partners? *Int J Biochem Cell Biol* **48,** 28–38.

Redfern PA (1970). Neuromuscular transmission in new-born rats. *J Physiol* **209,** 701–709.

Redondo MJ, Fain PR & Eisenbarth GS (2001). Genetics of type 1A diabetes. *Recent Prog Horm Res* **56,** 69–89.

Reggiani C (2015). Not all disuse protocols are equal: new insight into the signalling pathways to muscle atrophy. *J Physiol* **593,** 5227–5228.

Rejc E, Floreani M, Taboga P, Botter A, Toniolo L, Cancellara L, Narici M, Šimunič B, Pišot R, Biolo G, Passaro A, Rittweger J, Reggiani C & Lazzer S (2018). Loss of maximal explosive power of lower limbs after 2 weeks of disuse and incomplete recovery after retraining in older adults. *J Physiol* **596,** 647–665.

Rekling JC, Funk GD, Bayliss DA, Dong XW & Feldman JL (2000). Synaptic control of motoneuronal excitability. *Physiol Rev* **80,** 767–852.

Robbins N (1992). Compensatory plasticity of aging at the neuromuscular junction. *Exp Gerontol* **27,** 75–81.

Rosa-Caldwell ME & Greene NP (2019). Muscle metabolism and atrophy: Let's talk about sex. *Biol Sex Differ* **10,** 1–14.

Rosenblueth A (1935). The All-or-None Principle and the Nerve Effector Systems. *Q Rev Biol* **10,** 334–340.

Santuz A & Akay T (2023). Muscle spindles and their role in maintaining robust locomotion. *J Physiol* **601,** 275–285.

Sarto F, Bottinelli R, Franchi M V, Porcelli S, Simunič B, Pišot R & Narici M V (2023). Pathophysiological mechanisms of reduced physical activity: Insights from the human step reduction model and animal analogues. *Acta Physiol (Oxf)* **238,** e13986.

Sarto F, Stashuk DW, Franchi M V., Monti E, Zampieri S, Valli G, Sirago G, Candia J, Hartnell LM, Paganini M, McPhee JS, Vito G De, Ferrucci L, Reggiani C & Narici M V. (2022*a*). Effects of short-term unloading and active recovery on human motor unit properties, neuromuscular junction transmission and transcriptomic profile. *J Physiol*; DOI: 10.1113/JP283381.

Sarto F, Valli G & Monti E (2022*b*). Motor unit alterations with muscle disuse: what's new? *J Physiol* **0,** 1–3.

Schiaffino S, Gorza L, Sartore S, Saggin L, Ausoni S, Vianello M, Gundersen K & Lømo T (1989). Three myosin heavy chain isoforms in type 2 skeletal muscle fibres. *J Muscle Res Cell Motil* **10,** 197–205.

Schiaffino S & Reggiani C (2011). Fiber types in Mammalian skeletal muscles. *Physiol Rev* **91,** 1447–

1531.

von Scholten BJ, Kreiner FF, Gough SCL & von Herrath M (2021). Current and future therapies for type 1 diabetes. *Diabetologia* **64,** 1037–1048.

Schwiening CJ (2012). A brief historical perspective: Hodgkin and Huxley. *J Physiol* **590,** 2571.

Seki K, Kizuka T & Yamada H (2007). Reduction in maximal firing rate of motoneurons after 1-week immobilization of finger muscle in human subjects. *J Electromyogr Kinesiol* **17,** 113–120.

Seki K, Taniguchi Y & Narusawa M (2001). Effects of joint immobilization on firing rate modulation of human motor units. *J Physiol* **530,** 507.

Sherrington CS (1925). Remarks on some aspects of reflex inhibition. *Proc R Soc London Ser B, Contain Pap a Biol Character* **97,** 519–545.

Sherwood L (2010). *Human physiology*. Brooks/Cole-Cengage Learning, Belmont, CA.

Škarabot J, Brownstein CG, Casolo A, Del Vecchio A & Ansdell P (2021). The knowns and unknowns of neural adaptations to resistance training. *Eur J Appl Physiol* **121,** 675–685.

Škarabot J, Folland JP, Forsyth J, Vazoukis A, Holobar A & Del Vecchio A (2022). Motor Unit Discharge Characteristics and Conduction Velocity of the Vastii Muscles in Long-Term Resistance-Trained Men. *Med Sci Sports Exerc* **Publish Ah,** 824–836.

Slack JR, Hopkins WG & Williams MN (1979). Nerve sheaths and motoneurone collateral sprouting. *Nature* **282,** 506–507.

Smerdu V, Karsch-Mizrachi I, Campione M, Leinwand L & Schiaffino S (1994). Type IIx myosin heavy chain transcripts are expressed in type IIb fibers of human skeletal muscle. *Am J Physiol*; DOI: 10.1152/AJPCELL.1994.267.6.C1723.

Smith JAB, Murach KA, Dyar KA & Zierath JR (2023). Exercise metabolism and adaptation in skeletal muscle. *Nat Rev Mol Cell Biol*; DOI: 10.1038/s41580-023-00606-x.

Stashuk DW (1999). Decomposition and quantitative analysis of clinical electromyographic signals. **21,** 389–404.

Stein RB, French AS, Mannard A & Yemm R (1972). New methods for analysing motor function in man and animals. *Brain Res* **40,** 187–192.

Suetta C, Hvid LG, Justesen L, Christensen U, Neergaard K, Simonsen L, Ortenblad N, Magnusson SP, Kjaer M & Aagaard P (2009). Effects of aging on human skeletal muscle after immobilization and retraining. *J Appl Physiol* **107,** 1172–1180.

Tam SL & Gordon T (2003). Mechanisms controlling axonal sprouting at the neuromuscular junction. *J Neurocytol* **32,** 961–974.

Tam SL & Gordon T (2009). Axonal Sprouting in Health and Disease. In *Encyclopedia of Neuroscience*, ed. Binder MD, Hirokawa N & Windhorst U, pp. 322–328. Springer Berlin Heidelberg, Berlin, Heidelberg. Available at: https://doi.org/10.1007/978-3-540-29678-2_527.

Taylor AM, Steege JW, Enoka RM, Anna M, Steege JW & Motor- RME (2002). Motor-Unit Synchronization Alters Spike-Triggered Average Force in Simulated Contractions. 265–276.

Taylor JL, Amann M, Duchateau J, Meeusen R & Rice CL (2016). Neural Contributions to Muscle

Fatigue. *Med Sci Sport Exerc* **48,** 2294–2306.

Tesch PA, Lundberg TR & Fernandez-Gonzalo R (2016). Unilateral lower limb suspension: From subject selection to “omic” responses. *J Appl Physiol* **120,** 1207–1214.

Thomas J, Deville Y & Hosseini S (2006). Time-domain fast fixed-point algorithms for convolutive ICA. *IEEE Signal Process Lett* **13,** 228–231.

Tintignac LA, Brenner H & Rüegg MA (2015). Mechanisms Regulating Neuromuscular Junction Development and Function and Causes of Muscle Wasting. *Physiol Rev*809–852.

Udina E, Cobianchi S, Allodi I & Navarro X (2011). Annals of Anatomy Effects of activity-dependent strategies on regeneration and plasticity after peripheral nerve injuries. *Ann Anat* **193,** 347–353.

Vallat R (2018). Pingouin: statistics in Python. *J Open Source Softw* **3,** 1026.

Valli G, Minnock D, Tarantino G & Neville RD (2021). Delayed effect of different exercise modalities on glycaemic control in type 1 diabetes mellitus: A systematic review and meta-analysis. *Nutr Metab Cardiovasc Dis*; DOI: 10.1016/j.numecd.2020.12.006.

Valli G, Sarto F, Casolo A, Del Vecchio A, Franchi M V., Narici M V. & De Vito G (2023). Lower limb suspension induces threshold-specific alterations of motor units’ properties that are reversed by active recovery. *J Sport Heal Sci*(in press).

Vergès B (2020). Cardiovascular disease in type 1 diabetes: A review of epidemiological data and underlying mechanisms. *Diabetes Metab* **46,** 442–449.

Verkhratsky A & Fernyhough P (2014). Calcium signalling in sensory neurones and peripheral glia in the context of diabetic neuropathies. *Cell Calcium* **56,** 362–371.

Vieira TM, Botter A, Muceli S & Farina D (2017). Specificity of surface EMG recordings for gastrocnemius during upright standing. *Sci Rep* **7,** 13300.

Wachholder K (1928). Willkürliche Haltung und Bewegung. *Ergeb Physiol* **26,** 568–775.

Wen Y, Avrillon S, Hernandez-Pavon JC, Kim SJ, Hug F ois & Pons JL (2021). A convolutional neural network to identify motor units from high-density surface electromyography signals in real time. *J Neural Eng* **18,** 056003.

Widrick JJ, Trappe SW, Romatowski JG, Riley DA, Costill DL & Fitts RH (2002). Unilateral lower limb suspension does not mimic bed rest or spaceflight effects on human muscle fiber function. *J Appl Physiol* **93,** 354–360.

Winlow W & McCrohan CR (1987). *Growth and Plasticity of Neural Connections*. Manchester University Press. Available at: https://books.google.it/books?id=ReJRAQAAIAAJ.

Wood SJ & R. Slater C (2001). Safety factor at the neuromuscular junction. *Prog Neurobiol* **64,** 393–429.

Wood SJ & Slater CR (1997). The contribution of postsynaptic folds to the safety factor for neuromuscular transmission in rat fast- and slow-twitch muscles. *J Physiol* **500,** 165–176.

Wu R, Delahunt E, Ditroilo M, Ferri Marini C & De Vito G (2019). Torque steadiness and neuromuscular responses following fatiguing concentric exercise of the knee extensor and flexor muscles in young and older individuals. *Exp Gerontol*; DOI:

10.1016/J.EXGER.2019.110636.

Wuerker RB, Mcphedran AM & Henneman E (1965). Properties of motor units in a heterogeneous pale muscle (m. Gastrocnemius) of the cat. *J Neurophysiol* **28,** 85–99.

Yu Z, Guindani M, Grieco SF, Chen L, Holmes TC & Xu X (2022). Beyond t test and ANOVA: applications of mixed-effects models for more rigorous statistical analysis in neuroscience research. *Neuron* **110,** 21–35.